PSI-1206/
TR-1453

HYPERSONIC FLOW ULTRAVIOLET SIGNATURES

FINAL PROGRESS REPORT

G.E. CALEDONIA AND R.H. KRECH

JUNE 23, 1996

U.S. ARMY RESEARCH OFFICE

DAAH04-94-C-0014

PHYSICAL SCIENCES INC.
20 NEW ENGLAND BUSINESS CENTER
ANDOVER, MA 01810

APPROVED FOR PUBLIC RELEASE

DISTRIBUTION UNLIMITED

THE VIEWS, OPINIONS, AND/OR FINDINGS CONTAINED IN THIS REPORT ARE THOSE OF THE AUTHOR(S) AND SHOULD NOT BE CONSTRUED AS AN OFFICIAL DEPARTMENT OF THE ARMY POSITION, POLICY, OR DECISION, UNLESS SO DESIGNATED BY OTHER DOCUMENTATION.

REPORT DOCUMENTATION PAGE

Form Approved
OMB No. 0704-0188

Public reporting burden for this collection of information is estimated to average 1 hour per response, including the time for reviewing instructions, searching existing data sources, gathering and maintaining the data needed, and completing and reviewing the collection of information. Send comments regarding this burden estimate or any other aspect of this collection of information, including suggestions for reducing this burden, to Washington Headquarters Services, Directorate for Information Operations and Reports, 1215 Jefferson Davis Highway, Suite 1204, Arlington, VA 22202-4302, and to the Office of Management and Budget, Paperwork Reduction Project (0704-0188), Washington, DC 20503.

1. AGENCY USE ONLY *(Leave blank)*	2. REPORT DATE	3. REPORT TYPE AND DATES COVERED
	June 23, 1996	Final Progress Report 6/1/94 - 6/23/96

4. TITLE AND SUBTITLE

Hypersonic Flow Ultraviolet Signatures

5. FUNDING NUMBERS

DAAH04-94-C-0014

6. AUTHOR(S)

G.E. Caledonia and R.H. Krech

7. PERFORMING ORGANIZATION NAME(S) AND ADDRESS(ES)

Physical Sciences Inc.
20 New England Business Center
Andover, MA 01810

8. PERFORMING ORGANIZATION REPORT NUMBER

PSI-1206/TR-1453

9. SPONSORING/MONITORING AGENCY NAME(S) AND ADDRESS(ES)

U.S. Army Research Office
P.O. Box 12211
Research Triangle Park, NC 27709-2211

10. SPONSORING/MONITORING AGENCY REPORT NUMBER

ARO 32947.2-EG-SDI

11. SUPPLEMENTARY NOTES

The views, opinions and/or findings contained in this report are those of the author(s) and should not be construed as an official Department of the Army position, policy or decision, unless so designated by other documentation.

12a. DISTRIBUTION/AVAILABILITY STATEMENT

Approved for public release; distribution unlimited.

12b. DISTRIBUTION CODE

13. ABSTRACT *(Maximum 200 words)*

We have investigated the kinetic aspects of the shuttle glow. This work includes a review of previous experimental studies and recent flight data, an evaluation of thermal accommodation and desorption of NO on an engineering surface, a suggested glow mechanism, glow intensity predictions for the Skipper Mission and a Monte Carlo analysis of the flow environment.

14. SUBJECT TERMS

Shuttle glow, surface kinetics, DSMC, Skipper

15. NUMBER OF PAGES 129

16. PRICE CODE

17. SECURITY CLASSIFICATION OF REPORT	18. SECURITY CLASSIFICATION OF THIS PAGE	19. SECURITY CLASSIFICATION OF ABSTRACT	20. LIMITATION OF ABSTRACT
Unclassified	Unclassified	Unclassified	UL

NSN 7540-01-280-5500

Standard Form 298 (Rev. 2-89)
Prescribed by ANSI Sta. Z39-18
298-102

19960909 043

TABLE OF CONTENTS

LIST OF FIGURES

1. FORWARD

Continuum visible emission (the visible shuttle glow) is observed around Space Shuttle and other satellites operating in low earth orbit. The emission is found to be proportional to the local O-atom concentration and is apparently the result of reaction between ambient oxygen atoms and surface adsorbed NO. The detailed kinetic process by which this occurs is not yet well established. The SKIPPER mission, designed to monitor the bow region emissions of a blunt vehicle as it re-enters from low earth orbit, provided an exceptional opportunity to amass critical data on this phenomenon which could have been used to validate a proposed mechanism.

The potential kinetic processes which could contribute to this process are manifold. They include both O and NO surface accommodation and chemical reactivity, collisional and thermal desorption, and various non-Maxwellian gas phase kinetic interactions. In an earlier effort, a detailed glow model was developed and the available literature reviewed to provide estimates of the various required kinetic parameters. Limited experimental evaluation of NO accommodation and collisional desorption coefficients were also provided.

The present research effort was directed towards understanding and evaluating the kinetic mechanisms responsible for the visible shuttle glow. The technical work is provided in three sections as described below.

- An evaluation of adsorption/desorption behavior of NO on engineering surfaces.

  It is believed that collisions between ambient oxygen atoms and surface adsorbed NO produce the visible "shuttle glow." We have provided measurements which can be interpreted in terms of the NO surface accommodation coefficient and the thermal desorption coefficient. These are key parameters in the kinetic model for the surface glow.

- A critical review of laboratory measurements of visible shuttle glow.

  A variety of papers, some seemingly inconsistent, have been published on laboratory studies of the glow. These were critically reviewed and it was found that the weight of data suggests that the glow occurs through a combined Eley-Rideal, Langmuir-Hinshelwood kinetic mechanism. An interesting data collection on the temperature dependence of the glow was also developed. This work was presented as an invited paper at the December 1994 AGU meeting.

- A collaboration with Iain Boyd, Cornell University, on a Monte Carlo model for the glow.

  We conclude that the observed altitude dependence of the glow in part results from transition flow effects. A DSMC model for this phenomena has been assembled and exercised.

Several reports, publications and presentations are included as appendices.

2. TECHNICAL STUDIES

2.1 NO Adsorption/Desorption Study

The surface kinetics responsible for the shuttle glow can be quite complex. Knowledge is required on the surface accommodation, thermal and collisional desorption and chemical reaction of chemical species such as N, O and NO.

A few years ago, we reported a preliminary study of NO surface accommodation and thermal desorption (Caledonia and Krech, 1994). There was some uncertainty in those earlier results, and in the present program we have repeated and expanded the study.

Basically, we developed a simple model for the NO surface coverage history of an initially clean material in vacuum which is "instantaneously" subjected to a constant background pressure of NO. The model is limited to monolayer coverage; the experiment was performed at room temperature where the NO vapor pressure is sufficiently high to preclude formation of a deeper NO surface layer. We described this model in the 1994 report. It is summarized again below.

Let f be the fractional coverage of NO on the surface, S_{NO} be the sticking coefficient, and τ_{NO} be the characteristic time for thermal desorption. Then

$$\frac{df}{dt} = \frac{(NO)}{N_s}\frac{\bar{c}}{4} S_{NO} (1-f) - \frac{f}{\tau_{NO}} \qquad (2.1.1)$$

where N_s is the previously defined monolayer surface coverage, (NO) is the local NO concentration in cm^{-3}, and $\bar{c}$ is the mean NO molecular speed.

This has the steady state solution

$$f_s = \frac{S_{NO}(NO)\bar{c}/4}{S_{NO}(NO)\bar{c}/4 + \tau_{NO}^{-1} N_s} \qquad (2.1.2)$$

which can be recast as

$$\frac{f_s}{1-f_s} = \frac{S_{NO}(NO)}{N_s}(\bar{c}/4)\tau_{NO} \quad . \qquad (2.1.3)$$

Thus, if one can measure f_s versus NO concentration, one could measure the product $S_{NO}\,\tau_{NO}$. This is a straightforward steady-state measurement.

The time dependent solution of Eq. (2.1.1) provides additional information. This is

$$f = f_s\left(1 - e^{-\left(\frac{(NO)}{N_s}\frac{\bar{c}}{4}S_{NO} + \tau_{NO}^{-1}\right)t}\right) \quad . \tag{2.1.4}$$

Thus, by monitoring f at early times, after the NO flow is turned on, one can back out the overall characteristic time, whichever dominates.

In our experiment, we subjected the surface to a controlled NO pressure and then bombarded the surface with 8 km/s oxygen atoms at various times after NO exposure. The O-bombardment results in NO_2 fluorescence where the fluorescence intensity is necessarily proportional to the surface coverage of NO. The experimental procedure was described in our 1994 report and is again summarized below.

The experimental measurements were performed within our O-atom facility on a target plate 15.2 cm high by 35.6 cm long. A schematic of the experiment is shown in Figure 2.1.1. The plate was placed some 72.5 cm from the nozzle throat and was completely engulfed by the O-beam which was typically pulsed at 2 Hz. A typical O-beam fluence per pulse at the plate was 3.6×10^{14} cm^{-2}, a fraction of a monolayer. The plate temperature was held at 290 K.

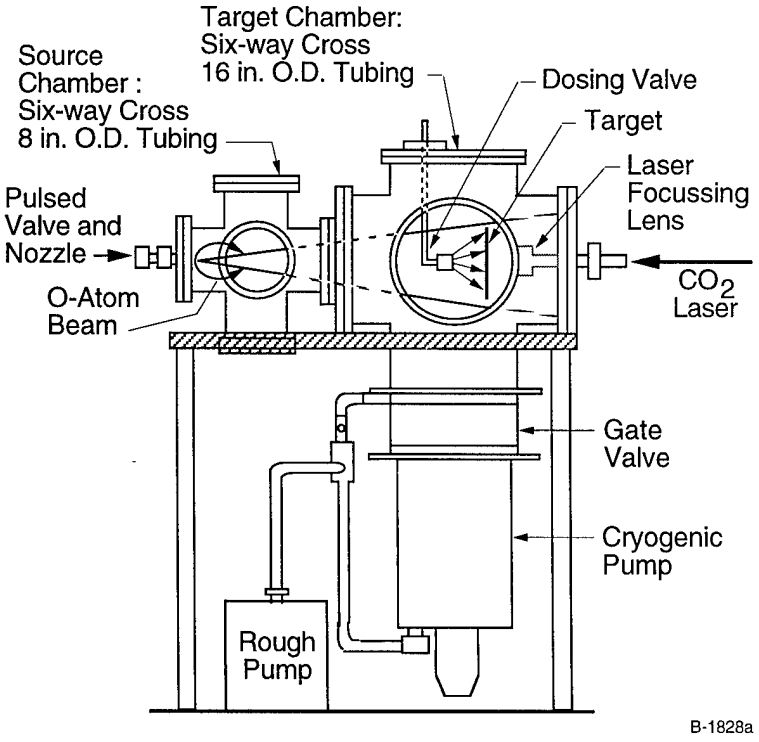

Figure 2.1.1 Schematic of experimental apparatus.

The glow intensity was measured just above the plate at a central wavelength of 630 nm with a 10 nm bandpass. This wavelength is just to the blue of peak glow intensity. The optical field of view was cylindrical with a 3.2 cm diameter.

The O-beam exhibits a small intrinsic radiation level at this wavelength. Furthermore the beam interacts with the gaseous NO to produce a continuum glow. This gas phase glow is blue-shifted related to the surface glow, and most likely results from energetic oxygen atom interactions with dimers. The measurements of glow intensity above the surface will necessarily include a contribution from this gas phase glow as well as from the surface glow. These relative contributions are distinguished by performing the intensity measurements with and without the target in place. The difference in intensities between these two measurements is taken to be the contribution of the surface glow. An example of such measurement is shown in Figure 2.1.2 for an NO pressure of 3.7×10^{-5} torr. As can be seen, the gas glow intensity is small compared to that of the surface glow. Note that the initial NO exposure occurred at slightly different times for the two traces shown in Figure 2.1.2.

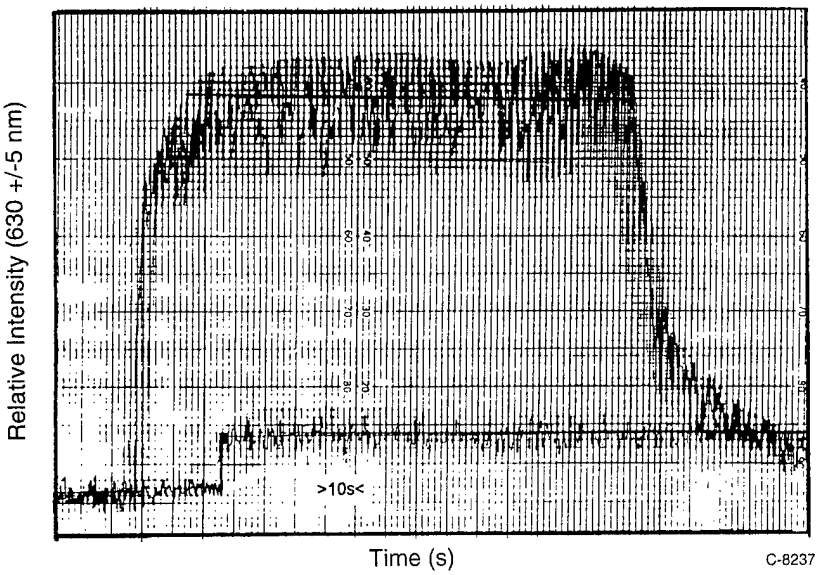

Figure 2.1.2 Pulse rate 2 Hz, measured O + NO surface and gas glow. $P_{NO} = 3.7 \times 10^{-5}$ torr, Top: O + NO surface glow, Bottom: O + NO gas glow

The summary of "steady" intensity data reported in 1994 is shown in Figure 2.1.3, which is taken from that source. The data shown versus pressure is the saturated surface glow, concomitant gas phase glow and the difference between the two signals.

As pointed out earlier, the 50% saturation point in the data occurs at ~10^{-5} torr and thus from Eq. (2.1.3)

$$1 = 3.3 \times 10^{11} \frac{S_{NO}\, \bar{c}\, \tau_{NO}}{4\, N_s} \qquad (2.1.5)$$

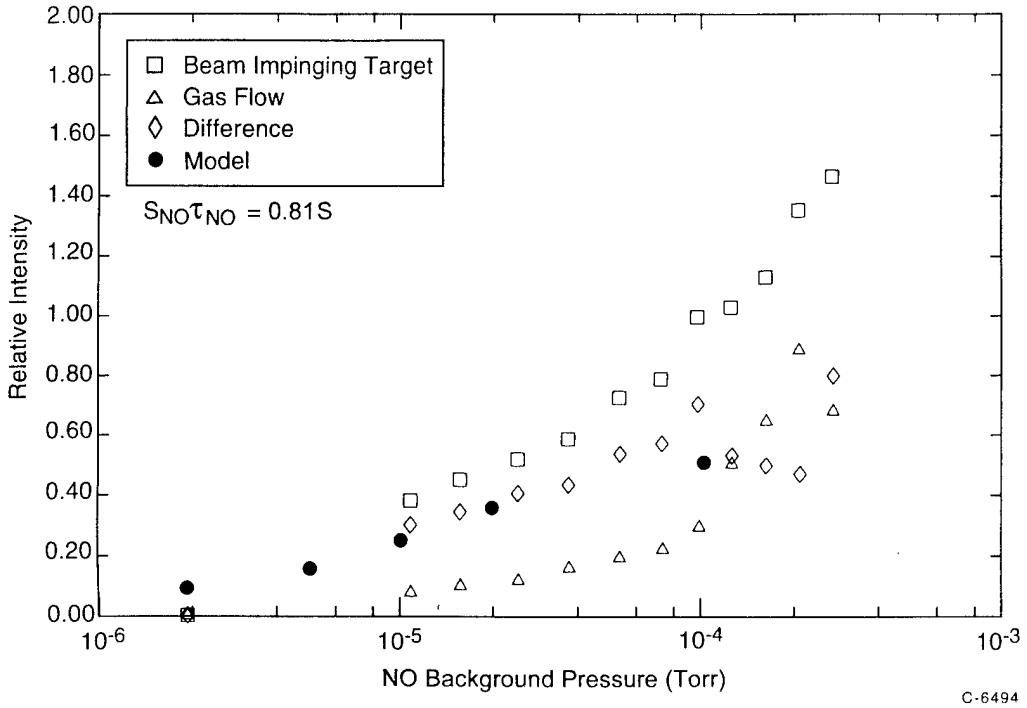

Figure 2.1.3 Observed steady glow intensity at 630 nm and 290 K versus no pressure, 8 km/s O-atom at 2 Hz on anodized Al.

where we have substituted in the NO concentration at P = 10^{-5} torr. ∴ for $\bar{c}$ = 4.5 x 10^4 and N_s ~ 3 x 10^{15} cm^{-2} we have then

$$S_{NO}\tau_{NO} = 0.81s \qquad (2.1.6)$$

and, since S_{NO} cannot exceed unity, this implies that at 290 K

$$\tau_{NO} \geq 0.81s \quad .$$

We have included Eq. (2.1.2), evaluated with Expression (2.1.6) on Figure 2.1.3. As can be seen, the comparison is reasonable. Nonetheless, this evaluation is uncertain to at least a factor of two given the scatter in the data and the arbitrariness in the specification of N_s (more properly, Eq. (2.1.3) should be used to define the quantity $S_{NO}\ \tau_{NO}/N_s$).

We have now extended this work to exploit additional information which can be found in the time variation of the glow intensity. More specifically, we monitored the characteristic e-fold time of the intensity at NO pressures of 1.4 x 10^{-5}, 2.3 x 10^{-5} and 3.7 x 10^{-5} torr. These measurements were made several times and the results were highly repeatable. Furthermore at these pressures, the gas phase glow intensity never exceeded 20% of the total observed intensity.

In all cases, we found that the characteristic e-fold time varied inversely with pressure as expected from Eq. (2.1.5). Indeed, the characteristic e-fold time dropped from 4.5 to 2 s over the aforementioned pressure range. This temporal variation is slightly less than linear with pressure presuming reflecting the contribution of the τ_{NO}^{-1} term in the exponential of Eq. (2.1.5). We can use the lowest measured e-fold time of 2 s to make a lower bound estimate for S_{NO} using the same values mentioned previously for $\bar{c}$ and N_s. From this, we deduce that $S_{NO} \geq 0.1$ whence $\tau_{NO} < 8.1$ s. These values are of course consistent with the 50% saturation point occurring at an NO pressure of 10^{-5} torr.

Note that the additional measurements of the e-fold time for steady coverage allows the uncertainty in specifying N_s to only affect the uncertainty in S_{NO}, i.e., a factor of two increase in N_s will produce a factor of two increase in S_{NO}. The remaining uncertainty in τ_{NO} is only that resulting from the scatter in the data.

We have found no measurements in the literature for comparison with the present results.

2.2 A Review of Laboratory Studies of the Visible Shuttle Glow

2.2.1 Introduction

There have been many studies of the visible Shuttle glow both in flight (see the review by Garrett et al. (1988), as well as more recent measurements by Viereck et al. (1991), Viereck et al. (1992), and Swenson et al. (1995)), and in the laboratory (Arnold and Coleman, 1988, 1991; Caledonia et al., 1990, 1993; Orient et al., 1990, 1992; Swenson et al., 1991; Ardebili et al., 1991; and Greer et al., 1993). It is now well established that the visible Shuttle glow arises from the surface catalyzed recombination of NO and O forming electronically excited NO_2. The mechanism by which this occurs remains elusive, however. In this work we will review the available laboratory data on surface catalytic recombination of NO_2 and identify those key observations which can lead to a consistent interpretation of the glow mechanism.

2.2.2 Review of Experimental Data

The three-body gas phase recombination reaction between thermal O and NO has been well studied. The electronically excited NO_2 produced in the reaction emits a yellow-green continuum spectrum known as the air afterglow. A representative spectral measurement (Fontijn et al., 1964), among many, is shown in Figure 2.2.1. When similar measurements are performed in a flow of O and NO directed over a nickel surface, an orange glow is observed, see Figure 2.2.1 (Kenner and Ogryzlo, 1984; Chu et al., 1986; and references therein).

The red shift of the spectrum is usually presumed to be due to energy loss to the surface in the heterogeneous reaction. Nonetheless, although this reaction has been studied since the 1960's, the kinetic interpretation of these spectra is still uncertain due to the possible occurrence of simultaneous gas and surface phase processes. Specifically, these measurements are made in

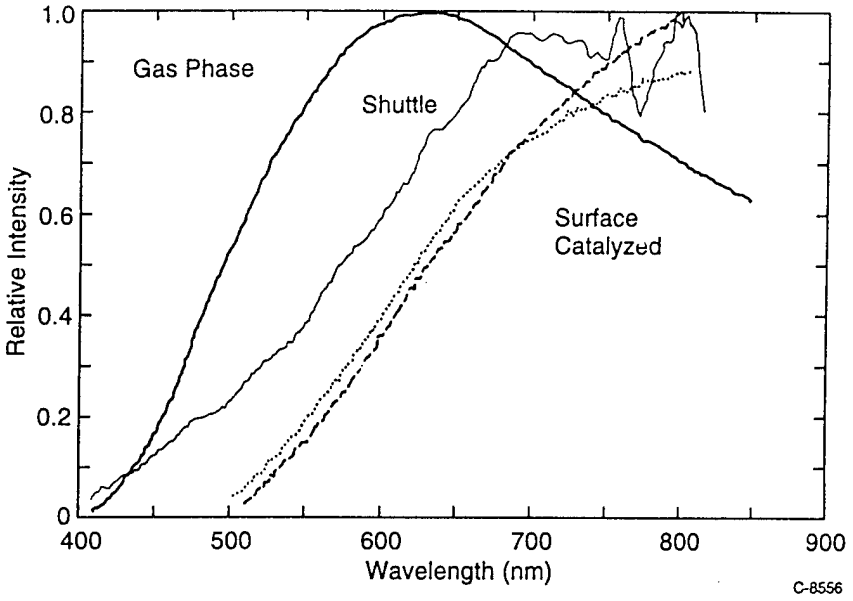

Figure 2.2.1 Thermal studies of O + NO recombination glow contrasted with the shuttle glow, ——— gas phase glow, Fontijn et al. (1964); ——— shuttle glow, Viereck et al. (1992); surface catalyzed glows; .... Kenner and Ogryzlo (1984); -----, Chu et al. (1986).

mixed streams of O and NO at pressures exceeding 0.02 torr. While surface catalyzed recombination reactions such as:

$$NO + O \xrightarrow{S} NO_2^* \qquad (2.2.1)$$

$$O + O \xrightarrow{S} O_2(A\,^3\Sigma_u^+),\ O_2^* \qquad (2.2.2)$$

will occur, the pressures are sufficiently high such that subsequent gas phase reactions such as:

$$O_3^* + NO \rightarrow NO_2^* + O_2 \qquad (2.2.3)$$

$$O_2(A) + O_2 \rightarrow O_3^* + O \qquad (2.2.4)$$

can also contribute to the observed glows (Kenner and Ogryzlo, 1984; and Chu et al., 1986). Indeed, Chu et al. (1986) demonstrated that the effective lifetime of the glow, as determined by

its spatial extent, decreased by an order of magnitude when O_2 was eliminated from the flow, clearly demonstrating the importance of gas phase reactions subsequent to surface recombination.

Shown for comparison with the results of these thermal studies is a representative measurement of the Shuttle glow (Viereck et al., 1992). This glow is clearly red-shifted relative to the gas phase continuum yet is to the blue of the thermal surface catalytic glows.

There have now been several measurements of the visible glow performed with beams of atomic oxygen at pressures low enough to eliminate the possibility of significant gas phase reaction. Three such studies (Arnold and Coleman, 1990, 1992; Ardebili et al., 1991; Greer et al., 1993) have been performed at O-beam energies of $\lesssim$1 eV, typical of arc-type oxygen atom sources. In these works a fast O-beam (diluted in a rare gas), flux $<3 \times 10^{15}$ $cm^{-2} \bullet s^{-1}$, was mixed with an effusive source of NO above a surface (nickel, metals, Z306) with total pressures below 10^{-5} torr.

The results of these measurements, contrasted with the Shuttle glow, are shown in Figure 2.2.2. Note the comparison between the three sets of measurement is quite good (although the spectral resolution of the data of Greer et al. (1993) is quite coarse, 150 nm FWHM). No significant variations in spectral shape were observed as the target material was changed.

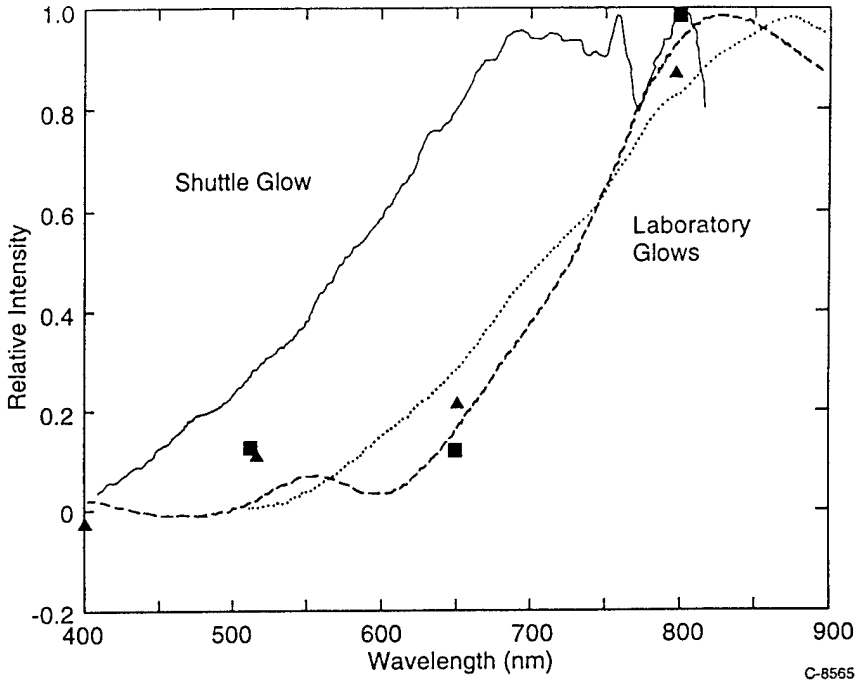

Figure 2.2.2 Low velocity O beam recombination glows contrasted with shuttle glow. _____, Shuttle glow, Viereck et al. (1992); .... Ardebili et al. (1991), V_O = 1.85 km/s; ----- Arnold and Coleman (1990), V_O = 1.4 km/s; symbols, Greer et al. (1993), ■ $-V_O$ = 1.5 km/s, ▲ - V_O = 3.3 km/s.

There are at least three significant aspects to these measurements:

1. the pressures are so low that only surface reactions should pertain

2. the measurements of Greer et al. (1993) show no O-atom velocity dependence on the glow intensity

3. the observed spectrum is red-shifted relative to the thermal atom surface catalyzed glows.

This last point is particularly interesting in that, if anything, one might have conjectured a blue shift to result from the increased O-atom velocity. Perhaps this suggests that a different kinetic mechanism is operative in the free molecular regime. We will return to this point.

Two studies of the surface catalyzed O + NO recombination glow have been performed under free molecular conditions with an oxygen beam velocity of ~ 8 km/s, or orbital velocity. In both instances the beams were formed from pure O_2 without a rare gas diluent. In the first of these (Caledonia et al., 1990; Swenson et al., 1991), a pulsed O-beam was used to irradiate a surface which had previously been dosed with less than a mono-layer of NO. The O-beam flux was $< 10^{15}$ $cm^{-2} \bullet s^{-1}$ and the operating pressure $< 10^{-5}$ torr. In the second experiment (Orient et al., 1990, 1992), a CW O-beam with flux $< 10^{13}$ cm^{-2} s^{-1}, and an NO gas jet were directed onto surfaces at total pressures $< 2 \times 10^{-7}$ torr. In both experiments targets of several different materials were used with no significant change observed in the spectral shape of the glow.

The results of these two measurements, again contrasted with the Shuttle glow, are shown in Figure 2.2.3. The disparity between the two measurements is not understood, however it is clear that the glow induced by 8 km/s oxygen atoms is significantly blue shifted relative to that observed with lower velocity O-beams, as shown in Figure 2.2.2. Furthermore, the measurement of Caledonia et al. (1990) is in excellent agreement with the observed Shuttle glow spectra, demonstrating that the Shuttle glow can be simulated in the laboratory by the interaction of 8 km/s oxygen atoms with absorbed NO. It was further demonstrated (Swenson et al., 1991) that a similar simulation relative to the spatial extent of the glow was also achieved.

There have also been several laboratory observations on the temperature dependence of the glow. The low velocity beam measurements (Arnold and Coleman 1988, 1990; Ardebili et al., 1991) report confusing variations of glow intensity with temperature. These include one hundred-fold changes in intensity, apparently due to surface passivation effects, and convoluted temperature variations. No attempt will be made to rationalize these observations here. On the other hand, measurements performed with the 8 km/s beams provide an interesting and unexpected comparison with each other and with flight data as described below.

Swenson et al. (1986) examined glow intensities from several shuttle flights and concluded that the glow intensity exhibited a temperature dependence. They proposed an Arrhenius type dependence, exp $\Delta E/kT$, with characteristic energy ΔE ~0.12 eV. More recently,

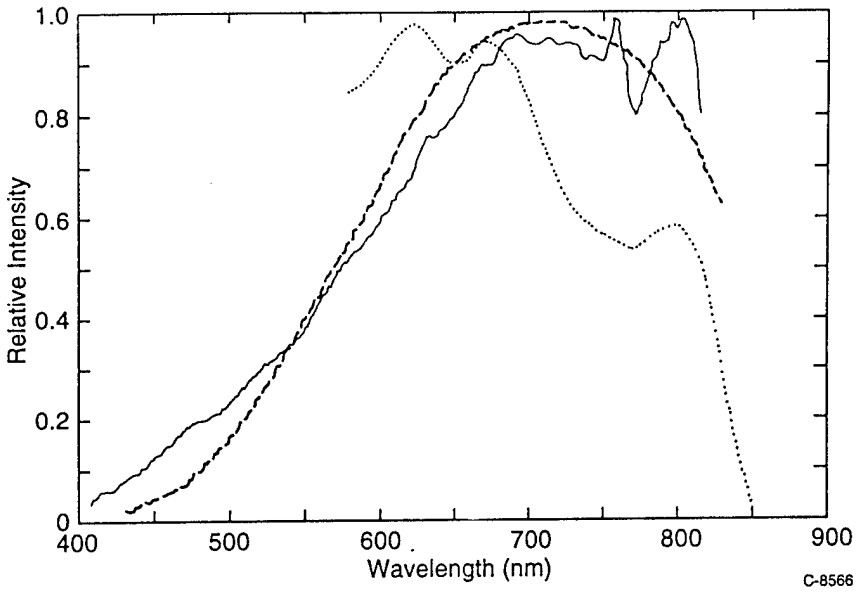

Figure 2.2.3 8 km/s O-beam recombination glows contrasted with the shuttle glow, ... Orient et al. (1992); ------ Caledonia et al. (1990); Shuttle glow, Viereck et al. (1992).

Orient et al. (1992) reported laboratory measurements of the temperature dependent glow intensity above MgF_2, Ni and Ti substrates using their CW 8 km/s O-beam source. Their results which cover the temperature range of 240 to 340 K are shown in Figure 2.2.4. They also fit their data to an Arrhenius expression, deducing values of $\Delta E \approx 0.11$ to 0.12 eV in apparent agreement with the suggestion of Swenson et al. (1986).

The temperature variation of the glow intensity was also observed with a pulsed 8 km/s O-beam (Oakes et al., 1992). These results are also shown in Figure 2.2.4. These measurements were performed with a constant NO background pressure of 10^{-5} torr while the target temperature was varied. (The data may be suspect below 150 K because of condensation on the substrate.) Clearly, the observed variation in glow intensity with temperature, does not correlate with a simple Arrhenius behavior. Nevertheless, both sets of data are in remarkably good agreement over the common temperature range of the measurements.

This comparison suggests that an Arrhenius expression is not appropriate for modeling the glow intensity. Indeed, as can be seen in Figure 2.2.4, an Arrhenius expression would require a temperature variation which would strongly diverge from the measurement of Oakes et al. (1992) at lower temperatures. The good comparison between the two sets of data suggest that the glow intensity temperature dependence is more complex than a simple activation energy. Most compelling, very recent flight data reported by Swenson et al. (1995) arbitrarily normalized in Figure 2.2.4, exhibit a weaker temperature dependence than predicted by the earlier Arrhenius expression and are in reasonable agreement with the laboratory data.

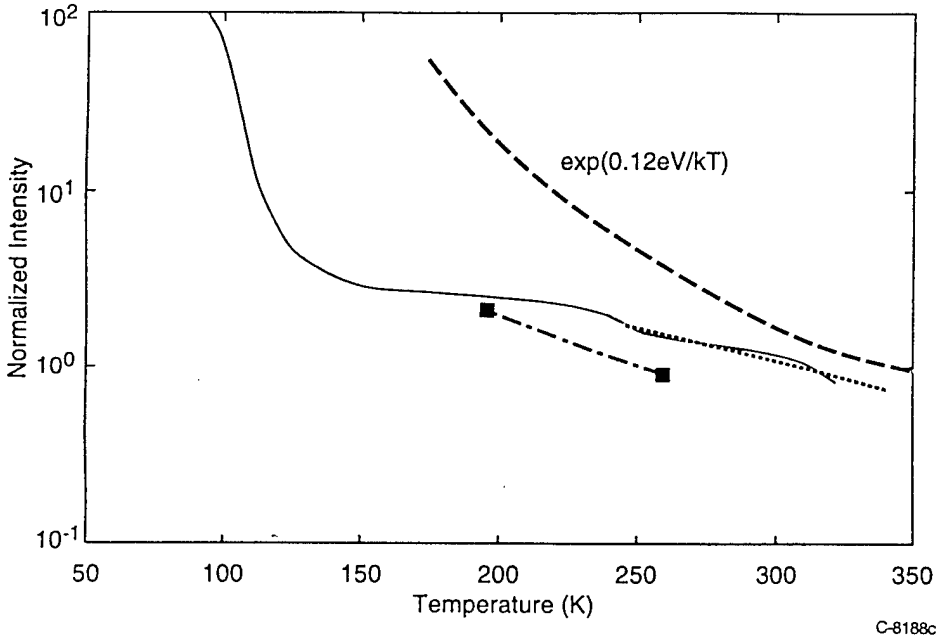

Figure 2.2.4 Observed temperature dependence of O + NO surface glow intensity, 5 eV O-atoms. _____ Oakes et al. (1992), λ = 400 to 800 nm, Al; .... Orient et al. (1992), λ = 625 nm, MgF_2, Ni, Ti; contrasted with recent shuttle observation -·-·-·- Swenson et al. (1995). Also shown for comparison is the Arrhenius expression exp (0.12 eV/kT) arbitrarily normalized, ---------.

A last point with regard to the laboratory measurements concerns the production of NO. Various mechanisms have been proposed for NO production around shuttle (e.g., see Swenson et al., 1985; Green et al., 1986; Kofsky and Barrett, 1986). These include surface recombination of ambient N and O, surface dissociation of ram N_2 producing N which can ultimately form NO, ambient NO, and the gas phase atom exchange reaction:

$$O + N_2 \rightarrow NO + N \qquad (2.2.5)$$

which is thermoneutral at O-atom ram velocities. Although the specific NO formation mechanism remains to be defined, this last reaction has been studied in the laboratory for O-atom velocities of 7 to 12 km/s (Upschulte et al., 1992) and its cross section has been shown to be large enough to produce NO densities consistent with observed flight NO_2* emission levels. The NO formation mechanism is particularly important in that it helps determine the scaling of glow intensity with atmospheric species concentration.

Analysis

We are in the process of developing a detailed kinetic mechanism for the visible glow which will allow us to scale the glow observations to other flight conditions. In this section we will review the status of that analysis and the impact of the laboratory observations on mechanistic interpretation.

Surface catalyzed recombination is usually considered in terms of two limiting mechanisms. The first of these is the Langmuir-Hinshelwood (L-H) where recombination is assumed to occur between two adsorbed species with subsequent release of the recombined species into the gas phase, e.g.

$$A(S) + B(S) \xrightarrow{S} AB^{*} \qquad (2.2.6)$$

where the symbol S refers to surface bound species. Alternatively the Eley-Rideal mechanism proposes recombination occurring in the collision between an incident gaseous species and an absorbed species with ultimate release of the recombined species in the gas phase, e.g.

$$A + B(S) \xrightarrow{S} AB^{*} \quad . \qquad (2.2.7)$$

In the past, either one or the other of these mechanisms has been proposed to interpret the visible shuttle glow. Ardebili et al. (1991) has suggested a two step process involving both mechanisms to explain the complex temperature dependence of their laboratory observations.

Assuming that the source of NO is in the gas phase, e.g. the exchange reaction (2.2.5), or even ambient NO, then a number of kinetic steps could be involved in the glow process. These are summarized in Table 2.2.1. One must consider surface adsorption and collisional and thermal desorption reactions for both O and NO as well as the ultimate surface recombination reactions. If the Eley-Rideal mechanism pertains, the NO_2 collisional formation mechanisms become important as well. Note furthermore that the NO_2 production reactions will not necessarily produce NO_2 in the excited state with unit efficiency. The inclusion of all these mechanisms along with the NO production mechanism produces a necessarily complex relationship for the glow intensity. This is particularly true since all these kinetic quantities can depend on both temperature and material (thus the importance of the data in Figure 2.2.4). Some limited data on the individual mechanisms is available for engineering material surfaces. For instance collisional desorption efficiencies of adsorbed NO impacted by 8 km/s oxygen atoms have been reported (Krech at al., 1993) as 0.05 to 0.01 for selected materials. As noted in Section 2.1, we have found room temperature NO sticking coefficients $\gtrsim 0.1$ with thermal desorption times of less than 8 seconds. Ultimately, the available visible laboratory and flight data provide the critical test for mechanistic assumptions/interpretations.

As a specific example let us review the implications of the wavelength dependence of the glow observations reported in the previous section. The glow from lower energy ($\lesssim 1$ eV) beam measurements (Arnold and Coleman (1990; 1992), Ardebili et al (1991), Greer et al. (1993)) are shifted to the red of those from thermal measurements performed at higher pressures even though, in at least one instance, the free molecular directed velocity was close to thermal. One interpretation of this observation is that the free molecular measurements represent the true surface reaction between O and NO while the higher pressure results reflect contributions from other species and/or gas phase reactions.

Table 2.2.1 Suggested Kinetic Processes of Relevance to the Visible Shuttle Glow Mechanism

Reaction Type	Process	Kinetic Quantity
Adsorption	$O(g) \longrightarrow O(S)$ $NO(g) \longrightarrow NO(S)$	Sticking coefficient
Thermal Desorption	$O(S) \longrightarrow O(g)$ $NO(S) \longrightarrow NO(g)$	Thermal desorption rate
Collisional desorption or reaction	$O(g)+O(S) \longrightarrow 2O(g)$ $\longrightarrow O_2(g)$ $X(g)+O(S) \longrightarrow X(g)+O(g)$ $O(g)+NO(S) \longrightarrow O(g)+NO(g)$ $\longrightarrow NO_2(g)$ $O(g)+NO_2(S) \rightarrow O(g)+NO_2(g)$ $NO(g)+O(S) \rightarrow NO(g)+O(g)$ $\rightarrow NO_2(g)$ $X(g)+NO(S) \longrightarrow X(g)+NO(g)$	Collisional desorption or reaction efficiency
Surface Reaction	$O(S)+NO(S) \longrightarrow NO_2(g), NO_2(S)$ $O(S)+O(S) \longrightarrow O_2(g), O_2(S)$	Reaction rate

*g ⇒ Gas Phase Species
*S ⇒ Surace Adsorbed Species

T-19970a

On the other hand the blue shift observed in the higher energy (~5 eV) beam measurements (Orient et al. (1990; 1992), Caledonia et al. (1990), Swenson et al. (1991)) is difficult to reconciliate with an L-H mechanism. It is certainly not consistent with complete surface accommodation of the oxygen atoms prior to recombination, although presumably a quasi-L-H type recombination process could occur with partial accommodation.

Furthermore Oakes et al. (1992) have observed a velocity squared dependence of the glow intensity on O-atom velocity over the velocity range of 6 to 12 km/s. Again this observation is more consistent with an Eley-Rideal mechanism than an L-H mechanism. Recall however, that Greer et al. (1993) did not observe a velocity dependence in glow intensity at the lower O-atom velocities of 1.5 to 3.3 km/s.

These observations collectively suggest that the visible shuttle glow results either from a Eley-Rideal mechanism or more likely a combination mechanism. One possibility would be L-H recombination to produce free and bound NO_2, e.g.

$$O(S) + NO(S) \rightarrow NO_2(g),\ NO_2(S) \qquad (2.2.8)$$

both with some efficiency for producing electronically excited NO_2, followed by a knockoff or exchange reaction with incoming oxygen atoms, e.g.

$$O(g) + NO_2(S) \rightarrow O(g) + NO_2(g) \qquad (2.2.9)$$

again with some efficiency for releasing electronically excited gaseous NO_2.

A similar mechanism was previously proposed by Ardebili et al. (1991) to rationalize their experimental observations.

One additional measurement which supports this latter hypothesis has been reported by Caledonia et al. (1993). In this work surfaces in vacuum were dosed with NO_2 and then irradiated with 8 km/s oxygen atoms. The resulting glow was spectrally similar to that observed when surfaces were dosed with NO. Although this observation is consistent with reaction (2.2.9) it must be cautioned that potential effects due to dissociative chemisorption of NO_2 cannot be ruled out.

Summary

In summary, the data base on laboratory studies of surface catalyzed recombination of O + NO has been reviewed and analyzed in terms of the visible shuttle glow. Observed trends in the laboratory data have led to the suggestion of a combined Eley-Rideal, Langmuir-Hinshelwood kinetic mechanism for production of the laboratory glow. The scaling behavior of this mechanism is presently being examined in the light of flight observations.

It should be noted (Gelb, 1995) that all laboratory studies to date have involved energetic oxygen atoms impacting adsorbed NO. In flight the inverse reaction, energetic NO impacting adsorbed O, can also occur and this could result in different glow observations.

2.3 Altitude Dependence of the Glow and DSMC Modeling

There have only been two measurements of the altitude variation in the shuttle glow intensities taken during an individual flight where all other experimental parameters are held fixed. The first of these is from the Atmosphere Explorer series of the 1970's and was reported by Yee and Abreu in 1983. Their results, at a wavelength of 732 nm, are shown in Figure 2.3.1. The glow data span the altitude range of 140 to 270 km and as can be seen, the intensity scales linearly with the oxygen atom density (simultaneously measured) from 270 to 160 km and then begins to increase more rapidly with decreasing altitude, approximately trailing the N_2 density variation.

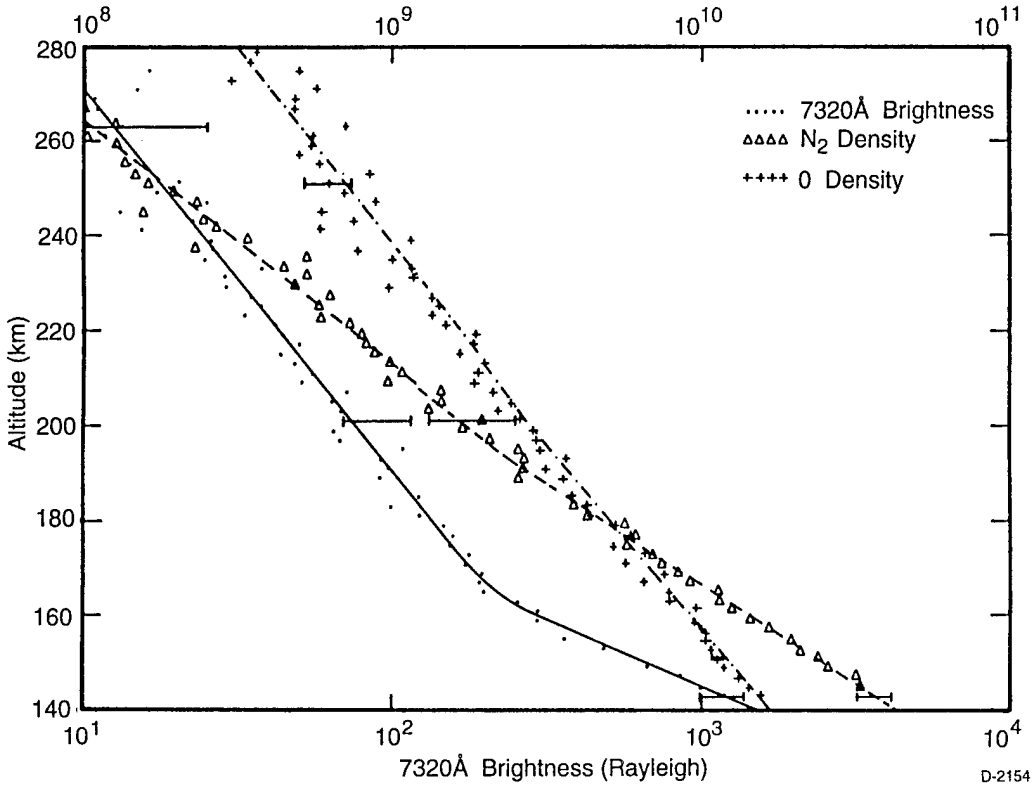

Figure 2.3.1 Visible glow intensity at 7320 Å as observed on Atmospheric Explorer contrasted with measured oxygen atom and nitrogen molecule concentrations (Yee and Abreu, 1983).

For many years, this was the only altitude dependent data available and the change in slope had been largely interpreted in terms of a change in the dominating chemical kinetic mechanism. Very recent measurements reported by Swenson et al. (1996) and shown in Figure 2.3.2 may change this interpretation. This data, all taken in one shuttle flight, STS-62, shows glow intensity tracking the O-atom density down to an altitude of ~220 km and then increasing less steeply than the O-atom density at lower altitude, i.e., opposite from the Atmospheric Explorer observation.

Swenson et al. (1996) suggest this falloff may be the result of density buildup on the ram side of shuttle where the measurement was made. Interestingly, the AE satellite is approximately an order of magnitude smaller than shuttle. Since the atmospheric scale height is ≈ 60 km at these altitudes, the Knudsen number for the shuttle at 220 km is the same as that for Atmospheric Explorer at 140 km, i.e., the observed change in slope of glow intensity occurs at the same Knudsen number (or for that matter, Reynolds number) on both flights. This observation of aerodynamic scaling strongly suggests that the glow slope "kink" results from transitional flow rather than chemical kinetic effects.

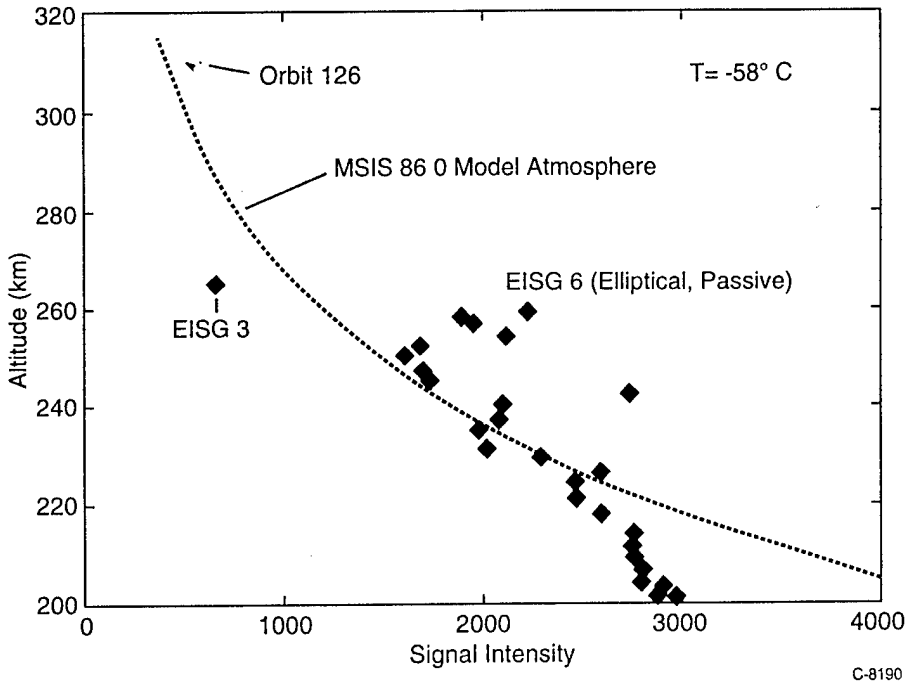

Figure 2.3.2 Observed variation of glow intensity on the Experimental Investigation of Shuttle Glow (EISG) experiment on space shuttle (Swenson et al., 1996).

The Knudsen number, which is the ratio of the mean free path to characteristic body dimension, is ~25 at the glow intensity "kink" altitude. Although this magnitude Knudsen number is generally considered to be well into the free molecular limit, Probstein (1961) pointed out that for hypersonic flow, it is more appropriate to apply the hyperthermal mean free path

$$\lambda_H \approx \lambda_\infty / M_\infty \qquad (2.3.1)$$

where M_∞ is the flow Mach number, ≈25 for our interest. The hyperthermal mean free path so defined reflects the collision mean free path between incident and surface reflected molecules.

Indeed, Bird (1990) recently studied space shuttle data on lift over drag, L/D, with his Direct Simulation Monte Carlo (DSMC) model and deduced that the shuttle data was most consistent with diffuse reflection of ambient molecules off of shuttle surfaces. A comparison of shuttle data to Bird's DSMC calculations is shown in Figure 2.3.3 contrasted with the free molecular limit. Bird states that transition regime effects on space shuttle persist to about 300 km. More recently, Dogra and Moss (1991) also predict significant transition flow effects on space shuttle above 200 km.

Thus, there is strong evidence that the aforementioned glow observations are impacted by transitional flow effects and that a simple free molecular model is insufficient for flight predictions. The fact that the two flights show differing trends for glow intensity variation at the

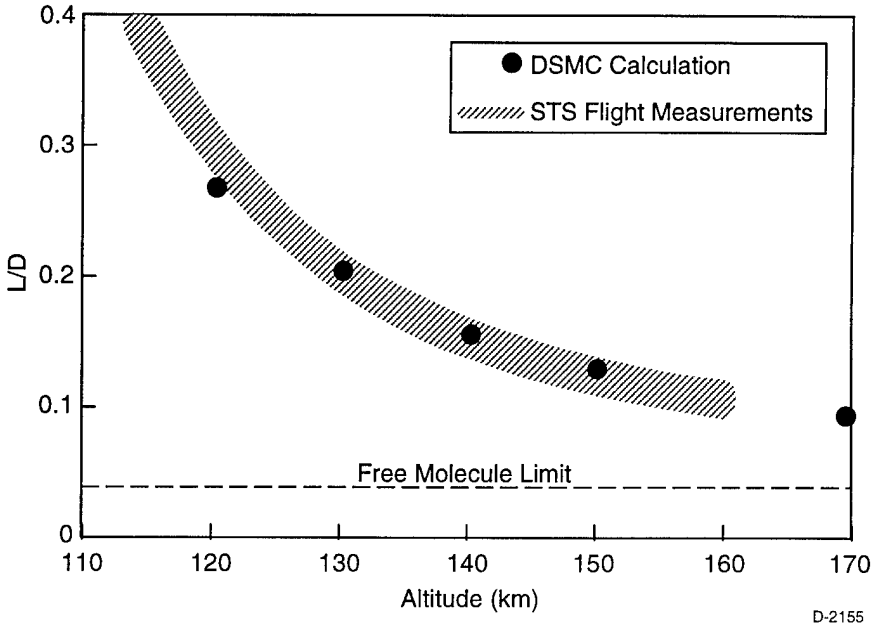

Figure 2.3.3 Comparison of shuttle measurements of lift over drag with DSMC calculations assuming diffuse reflection (Bird, 1990).

lower altitudes is intriguing. Recall that the glow results from a surface-catalyzed reaction. Surface properties of course will not scale with Knudsen number and will be altitude dependent. The surface coverages at the glow "kink" points of the two flights should be significantly different and this may provide for the difference in the two observations. Again, this may be addressed in a more sophisticated model.

We have entered into a collaborative effort with Prof. Iain Boyd, Cornell University, to develop transition flow predictions of visible glow intensity. The object is to have Prof. Boyd exercise his DSMC model to provide surface fluxes and velocity distributions of the key species O, N, NO and N_2. These four species are all present in the ambient atmosphere, but N and NO can also be produced by chemical reaction between incident and scattered O and N_2, as described below. These flux predictions will be vehicle specific, i.e., scale with Knudsen number, and can be used with a separate surface model employing relevant kinetic mechanisms to predict the altitude dependent glow intensity behavior.

The key to the DSMC model is the proper calculation of the impinging flux incorporating effects due to surface scattered primary ambient species O and N_2 undergoing secondary collisions with incoming species, including chemical reaction. We assume the key chemical reaction to be between impinging and scattered O and N_2, i.e.,

$$\vec{O} + \overleftarrow{N_2} \rightarrow \vec{NO} + N \qquad (2.3.2a)$$

$$\overleftarrow{O} + \vec{N_2} \rightarrow \vec{NO} + N \qquad (2.3.2b)$$

Note that this reaction also forms N atoms which can also reach the surface and ultimately form NO_2*.

Reaction 2.3.2 is thermoneutral at an O-atom velocity of ~8 km/s, orbital velocity, so for the reaction to have an appreciable rate constant, the scattered species must have a finite velocity. Specifically, the center of mass energy of the collision pair must exceed the reaction endothermicity of 3.26 eV. The reduced mass, M, of the collision pair is 10.2 gms/mole. The collision pair energy in the center of mass system (which automatically conserves momentum) is

$$E_{cm} = \frac{1}{2}\mu \ (V_{rel})^2$$

where V_{rel} is the magnitude of the relative velocity between the two particles, $\vec{V}_1 + \vec{V}_2$. At 8 km/s relative velocity E_{cm} is 3.38 eV for the O,N_2 collision pair. The cross section for reaction increases dramatically with V_{rel}. (We have an approximate measurement as described below.) Thus, the velocity at which the O,N_2 scatters from the surface is critical to predict the NO production rate. Unfortunately, there is very little data on this subject. We have some very preliminary data on scattering of 8 km/s O-atoms from engineering surfaces. We find the scattering is isotropic, but that the scattered velocity is not thermal but of order 1 km/s with a broad spread. Limited data on N_2 suggest a scattered velocity <1.6 km/s at low energies. This is all for normal incidence. This subject is a research area in itself. We have suggested that for our present calculations we assume isotropic scattering and scattered velocities of 1 and 2 km/s. These values of scattered velocity are sufficiently slow that the center of mass velocity of the collision pair is towards the scattered surface (recall this discussion is limited to ram flow).

For simplicity, we assume the NO,N created in the process moves towards the surface at the center of mass velocity (and direction) of the collision pair

$$\vec{V}_{cm} = \frac{M_1\vec{V}_i + M_2\vec{V}_s}{M_1 + M_2}$$

when i and s signify incident and scattered and once again 1 and 2 can signify either O or N_2. We will neglect an angular spread on the reaction products for the present. This can be included at a later date.

There are no data on the cross section for Reaction (2.3.2). Upschulte et al. (1992) report results for production of vibrationally excited NO by this reaction. These measurements are for a ~1000 K O-atom collision partner. We've extrapolated total cross sections for Reaction (2.3.2) from this data to be 2, 4, 6 and 15 x 10^{-18} cm^2 for relative collision velocities of 8, 9, 10 and 11 km/s respectively.

The remaining quantities needed are spacecraft dimensions. The AE satellite diameter is 1.35 m. The shuttle is more problematic. The experiment of Swenson et al. (1996) involved measurement across a 1 x 1 m structure. Nonetheless, the structure itself was in the bay and that general environment is defined by the orbiter itself. The shuttle body is ≈ 5 x 30 m with a rear wing spread of approximately 20 m.

The DSMC modeling is in process. Preliminary results were presented at the June 1996 AIAA Thermophysics Conference. See Appendix A.

Since this modeling was not completed in time for the Skipper launch, pre-flight predictions were provided by extrapolating the AE data. These results were presented in Boyd et al. (1995) and are included as Figure 2.3.4.

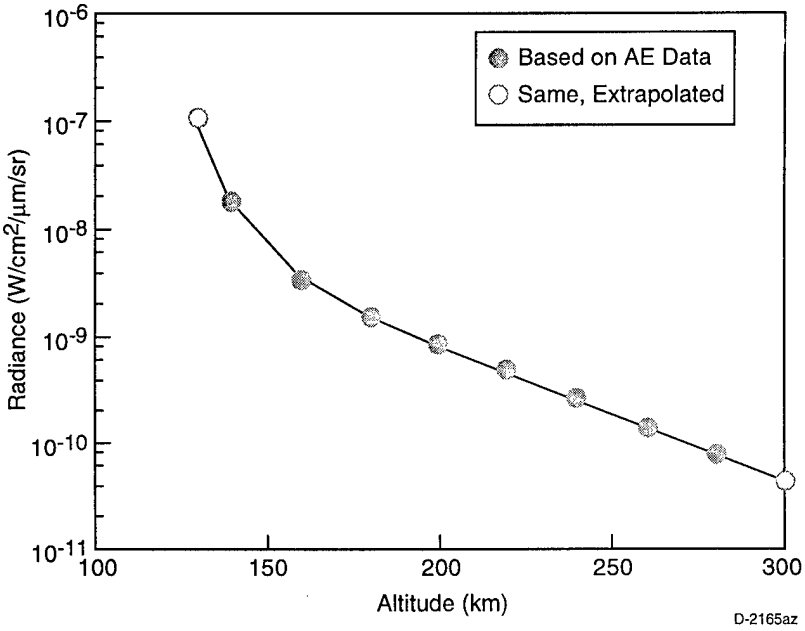

Figure 2.3.4 Skipper glow intensity predictions at 732 nm.

3. SUMMARY OF REPORTS, PARTICIPANTS, AND INVENTIONS

A. Reports

1. G.E. Caledonia and R.H. Krech, Technical Progress Report for 1 June through 31 December 1994, January 27, 1995.

2. I.D. Boyd, D.P. Karipides, D.A. Levin, and G.E. Caledonia, "Pre-Flight Predictions of Ultraviolet and Visible Emissions for the Skipper Flight Experiment," Cornell Univ. Report FDA-95-09, December 1995.

3. D.P. Karipides, I.D. Boyd, and G.E. Caledonia, "Development of a Monte Carlo Overlay Method with Application to Spacecraft Glow," AIAA-96-1847, 31st AIAA Thermophysics Conf., June 17-20, 1996, New Orleans, LA.

4. G.E. Caledonia, R.H. Krech and A. Leone, "A Review of Laboratory Studies of Spacecraft Atmospheric Interaction Glows," invited paper at the Fall American Geophysical Union Meeting, 9 December 1994 (VG only).

B. Participants

Participants in this research at Physical Sciences Inc. were George E. Caledonia and Robert H. Krech.

C. Inventions

None.

4. REFERENCES

Ardebili, M.N.P., R. Grice, C.J. Hughes, and J.C. Whitehead, "Time Dependent Chemiluminescence from the Surface Catalyzed Recombination of O and NO on Polycrystalline Ni", J. Chem. Soc. Faraday Transactions, 87, 2877, 1991.

Arnold, G.S. and D.J. Coleman, "Surface-Mediated Chemiluminescent Reaction of O with NO", Chem. Phys. Lett. 177, 279, 1991.

Arnold, G.S., and D.J. Coleman, "Surface Mediated Radical Recombination Luminescence: O + NO + Ni", J. Chem. Phys., 88, 7147, 1988.

Bird, G.A., "Applications of the Direct Simulation Monte Carlo Method to the Full Shuttle Geometry," AIAA-90-1692, AIAA/ASME 5th Joint Thermophysics and Heat Transfer Conference, June 18-20, 1990, Seattle, WA.

Boyd, I.D., Karipides, D.P., Levin, D.A., and Caledonia, G.E., "Pre-flight Predictions of Ultra-violet and Visible Emissions for the Skipper Flight Experiment," Cornell University report FDA-95-09, December, 1995.

Caledonia, G.E. and Krech, R.H. "Ultraviolet Emissions Occurring about Hypersonic Vehicles in Rarefied Flows," Physical Sciences Inc. TR-1305, April 1994.

Caledonia, G.E., K.W. Holtzclaw, R.H. Krech, D.M. Sonnenfroh, A. Leone, and W.A.M. Blumberg, "Mechanistic Investigations of Shuttle Glow", J. Geophys. Res., 98, 3725, 1993.

Caledonia, G.E., K.W. Holtzclaw, B.D. Green, R.H. Krech, A. Leone and G.R. Swenson, "Laboratory Investigation of Shuttle Glow Mechanism", Geophys. Res. Lett., 17, 1881, 1990.

Caledonia, G.E., R.H. Krech, and B.D. Green, "A High Flux Source of Energetic Atoms for Material Degradation Studies", AIAA, J., 25, 59, 1987.

Chu, A-L, R.R. Reeves, and J.A. Halstead, "Surface-Catalyzed Formation of Electronically Excited Nitrogen Dioxide and Oxygen", J. Phys. Chem., 90, 446, 1986.

Dogra, V.K. and J.H. Moss, AIAA J., 29, 1250, 1991.

Fontijn, A., C.B. Meyer and H.I. Schiff, "Absolute Quantum Yield Measurements of the NO-O Reaction and its Use as a Standard for Chemiluminescent Reactions", J. Chem. Phys., 40, 64, 1964.

Garrett, H.B., A. Chutjian, and S. Gabriel, "Space Vehicle Glow and its Impact on Spacecraft Systems", J. Spacecraft, 25, 321, 1988.

Gelb, A., Private communication, 1995.

Green, B.D., W.T. Rawlins, and W.J. Marinelli, "Chemiluminescent Processes Occurring Above Shuttle Surfaces", Planet. Space Sci., 34, 879, 1986.

Greer, W.A.D., N.H. Pratt, and J.P.W. Stark, "Spacecraft Glows and Laboratory Luminescence, Evidence for a Common Reaction Mechanism", Geophys. Res. Lett, 20, 731, 1993.

Kenner, R.D. and E.A. Ogryzlo, "Orange Chemiluminescence from NO_2", J. Chem. Phys., 80, 1, 1984.

Kofsky, I.L. and J.I. Barrett, "Spacecraft Glows from Surface-Catalyzed Reactions", Planet. Space Sci., 34, 665, 1986.

Krech, R.H., M.J. Gauthier and G.E. Caledonia, "High Velocity Atomic Oxygen/Surface Accommodation Studies", J. Spacecraft, 30, 509, 1993.

Oakes, D.B., M.E. Fraser, M. Gauthier, K.W. Holtzclaw, M. Malonson, and A. Gelb, "Optical Emissions from Oxygen Atom Reactions with Adsorbates", in, ed. P. Glassford, Vol. 1754, Proceedings of the "Optical Systems Contamination Effects, Measurements, and Control, III" session of the SPIE Conf., San Diego, CA, 23-24 July, 1993, p. 136.

Orient, O.J., K.E. Martus, A. Chutjian and E. Murad, "Recombination of 5 eV $O(^3P)$ Atoms with Surface-Adsorbed NO: Spectra and Their Dependence on Surface Material and Temperature," Phys. Rev. A, 45, 2998, 1992.

Orient, O.J., A. Chutjian and E. Murad, "Recombination Reactions of 5 eV $O(^3P)$ Atoms on a MgF_2 Surface," Phys. Rev. A 41, 4106, 1990.

Probstein, R.F., Amer. Rock. Soc. J., 31, 185, 1961.

Swenson, G.R., Rairden, R.L., Jennings, D.E., and Ahmadjian, M., Spacecraft and Rockets, 33, 240, 1996.

Swenson, G.R., S.B. Mende, and K.S. Clifton, "Ram Vehicle Glow Spectrum; Implication of NO Recombination Continuum", Geophys. Res. Lett., 12, 97, 1995.

Swenson, G.R., R. Rairden, D. Jennings, and M. Ahmadjian, "Visible Glow Measurements on STS-62", AIAA 95-0491, 33rd Aerospace Sciences Meeting, Reno, NV, Jan 9-12, 1995.

Swenson, G.R., A. Leone, K.W. Holtzclaw and G.E. Caledonia, "Spatial and Spectral Characterization of Laboratory Shuttle Glow Simulations", J. Geophys. Res., 96, 7603, 1991.

Swenson, G.R., S.B. Mende and E.J. Llewellyn, "The Effect of Temperature on Shuttle Glow", Nature, 323, 519, 1986.

Upschulte, B.L., D.B. Oakes, G.E. Caledonia, and W.A.M. Blumberg, Geophys. Res. Lett. 19, 993, 1992.

Upschulte, B.L., D.B. Oakes, G.E. Caledonia, and W.A.M. Blumberg, "Infrared Emissions Arising from the Reaction of Fast O/O^+ with N_2", Geophys. Res. Lett., 19, 993, 1992.

Viereck, R., E. Murad, C. Pike, S. Mende, G. Swenson, S.L. Culberston, and R.C. Springer, "Spectral Characteristics of the Shuttle Glow", Geophys. Res. Lett., 19, 1219, 1992.

Viereck, R.B., E. Murad, B.D. Green, P. Joshi, C.P. Pike, R. Hieb and G. Harbaugh, "Origin of the Shuttle Glow", Nature, 354, 48, 1991.

Yee, J.H. and V.J. Abreu, Geophys. Res. Lett., 10, 126, 1983.

APPENDIX A

Development of a Monte Carlo Overlay Method
with Application to Spacecraft Glow

AIAA Paper No. 96-1847

31st AIAAThermophysics Conference
June 17-20, 1996/New Orleans, LA

AIAA-96-1847

Development of a Monte Carlo Overlay Method With Application to Spacecraft Glow

Daniel P. Karipides and Iain D. Boyd
Cornell University
Ithaca, NY 14853

George E. Caledonia
Physical Sciences Inc.
Andover, MA 01810

31st AIAA Thermophysics Conference
June 17-20, 1996 / New Orleans, LA

For permission to copy or republish, contact the American Institute of Aeronautics and Astronautics
370 L'Enfant Promenade, S.W., Washington, D.C. 20024

Development of a Monte Carlo Overlay Method With Application to Spacecraft Glow

Daniel P. Karipides* and Iain D. Boyd†
Department of Mechanical & Aerospace Engineering
Cornell University, Ithaca NY 14853

George E. Caledonia‡
Physical Sciences Inc.
Andover, MA 01810

Abstract

Glow brightness calculations for the Atmospheric Explorer satellite are made. A simple model for glow is proposed, identifying nitric oxide as the important species in the gas phase controlling glow brightness. The flow field is determined using the direct simulation Monte Carlo method. A novel overlay technique is used to capture the microscopic behavior of rare atmospheric species, in particular nitric oxide. Sensitivity to altitude and to different chemical cross-sections for nitric oxide production is assessed. The importance of nitric oxide production is found to be greatest at lower altitudes. At higher altitudes, the ambient concentration of nitric oxide is the critical factor in determining glow brightness.

Introduction

Ram surfaces in low earth orbit are known to exhibit visible and ultraviolet glow. Such glows have been detected during space shuttle missions[1,2] and satellite flights of the Atmospheric Explorer (AE).[3] In proposed models of this phenomenon, species produced through chemistry are assumed to travel through the flow field without undergoing collisions and gas-surface reactions are entirely responsible for glow production.[4-9] These models neglect two important effects that are critical in the production of glow. At the lower, more dense altitudes, a weak shock forms in front of the ram surface. In this region, the assumption of a collisionless flow is inappropriate. At the higher altitudes, production through chemical reactions becomes negligible and the inclusion of free stream concentrations is critical. From data taken by the AE satellite, it is evident that the rate at which the brightness at 6563 Å changes with altitude, and therefore with free stream density, is dramatically different below 160 km compared to that above 160 km.[3] This experimental evidence suggests that gas-gas collisions become important below 160 km, indicating that the flow is collisional. Therefore, to predict glow brightness accurately, a method that includes the effects of gas-gas collisions in the weak shock, ambient species concentrations and chemical production throughout the flow field is required.

The free stream conditions at altitudes around 160 km are extremely rarefied and a high degree of both thermal and chemical non-equilibrium is to be expected throughout the flow field. The direct simulation Monte Carlo (DSMC) technique is ideal for simulating rarefied flows and has been successfully applied to hypersonic, non-equilibrium aerothermochemistry in previous work. Production of the chemical species critical to the formation of glow in this regime is controlled by rare collisions and rare chemical events. Proper modeling of such rare events using the DSMC technique requires modifications to the standard technique. These changes are outlined in this paper. In particular, procedures for handling the interaction of rare particles with a more dense background flow field and for calculating the production of particles due to rare chemical events are described. Results are presented for simulation of

*Graduate Student, Member AIAA
E-mail: karipid@mae.cornell.edu
†Associate Professor, Member AIAA
‡President, Associate Fellow AIAA

Copyright ©1996 by the American Institute of Aeronautics and Astronautics, Inc. All rights reserved.

the Atmospheric Explorer satellite over the range of altitudes from 140 km to 180 km. General flow field structure, various velocity distributions and calculations for glow brightness are discussed.

Glow Production Model

A simple model for the glow mechanism is proposed. The production of glow is assumed to be entirely due to the gas-surface reaction:

$$\begin{aligned} NO(g) + O(a) &\rightarrow NO_2^*(g) \\ NO_2^* &\rightarrow NO_2 + h\nu \end{aligned}$$

where (g) indicates a molecule in the gas state and (a) indicates a surface adsorbed particle. The NO_2^* is formed in an excited state and then spontaneously decays to the ground state, emitting a photon. These photons comprise the glow. The molecular surface coverage of a satellite results from a complex balance of atmospheric and flow properties, surface accommodation, thermal desorption, collisional desorption and chemical reactions. In the present study the simplifying approximation is made that the surface is saturated with oxygen atoms, one of the dominant ambient species at the altitudes of interest. Obviously, the flux of nitric oxide striking the surface will be crucial to determining the brightness of the glow. Where the flow is collisional, gas-gas collisions and reactions will be important in determining the nitric oxide flux.

A number of simplifying assumptions are made in implementing this model. Without data to suggest otherwise, every NO molecule that strikes the surface is assumed to interact with an adsorbed oxygen atom and the probability of a reaction forming NO_2^* is set to unity. Clearly, the probability of reaction should be less then one. Additional modeling is possible that would account for more detailed behavior of the surface chemistry and production of NO_2^*. Examples of such potential additions to the model include a dependence of the reaction probability on the incident energy of the NO molecule and a variation of the surface coverage of atomic oxygen with altitude. Given the microscopic detail available in a DSMC simulation, the framework exists to readily incorporate these affects.

Atmospheric Considerations

For the lower range of altitudes where glow brightness data was taken on the Atmospheric Explorer (less than 180 km), the ambient concentrations of NO and N are less than the concentrations of N_2, O_2 and O by several orders of magnitude. Furthermore, the rates of the relevant chemical reactions are such that NO and N are not produced in quantity throughout the flow field. Using the definition that any species with a mole fraction less than 10^{-2} is considered *rare* and is otherwise considered *common*, then in all the cases considered, NO and N can be considered rare species, while N_2, O_2 and O are common species. Given that the ratio of the number density of the common species to that of the rare species is so great, it is a reasonable assumption that the collisions and reactions of the rare species do not significantly affect the common species flow field.

Flow of air against a ram surface at orbital speeds (8 km/s) is primarily a five species gas mixture, consisting of N_2, O_2, NO, N and O. Atmospheric concentrations for all of these species excluding NO are determined using the MSIS-90 model.[10] A robust atmospheric model, dependent on a wide variety of specific input conditions, the MSIS model is used here to generate a generic atmosphere. Unfortunately, the number density of nitric oxide is not included in the atmospheric structure produced by the model. Determining accurate NO number densities is a difficult problem. The formation and destruction of nitric oxide is a key component of the odd-nitrogen cycle that occurs in the Earth's atmosphere. Many different factors determine the concentration of NO at any particular time and the concentration is highly sensitive to many of these factors. In this study, estimates for nitric oxide number densities are taken from experimental rocket measurements.[11] When analyzing the simulation results, it should be kept in mind that only estimates of the NO concentrations have been used. These estimates are likely different from the actual atmospheric NO concentrations experienced during the AE flights.

DSMC Resolution Difficulties

Simulating rare species and low probability events using the DSMC technique causes a number of resolution difficulties. When simulating a flow field with one or more rare species, there is often no acceptable choice for the value of the particle weight, W_p, defined as the ratio of the number of real particles to the number of simulated particles. A relatively low value of W_p is required in order for a statistically significant number of particles representing the rare species to be generated. However, with the particle weight set at such a value, inordinate num-

bers of particles representing the common species will also be generated. This results in unacceptably high numbers of simulated particles in each cell, requiring massive amounts of computational effort to calculate the flow field. Alternatively, the value of W_p can be set relatively high, so that reasonable numbers of common species particles are produced. In this case, however, very few, if any, rare species particles are then produced and the simulation no longer generates meaningful statistics for the rare species. Prior experience with rare species and resolution difficulties are discussed in Refs. 12 and 13.

Previous attempts to handle these resolution difficulties have used a continuum-based overlay method.[12,13] A two step procedure is used to calculate the flow field. In the first step, a DSMC simulation is performed to determine the properties of the common species throughout the flow domain. The particle weight in this simulation is set so that essentially no rare species particles are created. The second step involves a continuum-based calculation, where mass conservation equations are solved for the rare species using the underlying DSMC flow field solution. The assumption is made that the behavior of the rare species does not have an appreciable effect on the common species flow field. This continuum-based approach suffers from two problems. The procedure used to solve the mass conservation equations makes use of the temperature calculated for the common species in each computational cell. However, in the range of altitudes relevant for spacecraft glow, the flow field is sufficiently rarefied and in such a degree of non-equilibrium that thermodynamic variables such as temperature are not valid representations of the state of the gas. The velocity distribution of the molecules is very often bimodal and certainly not Maxwellian. It is therefore incorrect to use temperature to characterize the underlying flow field. In addition to this, the use of a continuum-based overlay also results in a loss of microscopic detail of the rare species. Such detail, particularly velocity distributions, may have a significant impact on chemical rates and glow production. It is important that this microscopic information is retained throughout the simulation.

DSMC Overlay Method

In this study, a DSMC-based overlay technique is developed. Conceptually, this is very similar to the continuum overlay approach, where two separate simulations are performed except that in this case both simulations use the DSMC technique. In the first (*base*) simulation, the particle weight is set so that the common species are represented at an appropriate level. In the second (*overlay*) simulation, the particle weight is reduced so that the rare species are represented. Generation of the common species is suppressed during the overlay simulation. In essence, the overlay simulation can be considered to be a magnified simulation, focusing only on the rare species. As a particle method, DSMC is ideal for handling the non-equilibrium nature of the flow field and for determining the microscopic behavior of the particles. Thus, the DSMC overlay approach overcomes the two main disadvantages of the continuum overlay method.

Coupling Between Rare and Common Species

The main challenge of performing a DSMC overlay simulation lies in achieving a detailed coupling between the two distinct simulations. This is not a concern in the base simulation as it is assumed that the flow field of the common particles is unaffected by the behavior of the rare particles. It is a significant concern, however, when performing the overlay simulation. The overlay simulation cannot simply be assumed to be a regular DSMC simulation at a lower density. The rare particles are moving through and colliding with a background of much denser common species. In addition, rare chemical events in the base simulation that did not noticeably affect the common species flow field may have a pronounced affect on the rare species flow field.

In order to achieve this coupling, the particle properties are binned in every cell during the sampling period of the base simulation. Five different properties are binned: the three components of velocity, the rotational energy and the vibrational energy. During the overlay simulation, a temporary common particle is created to act as a collision partner for each rare particle in every cell. These temporary particles have their properties determined through sampling of the bins stored during the base simulation. From these pairs, the appropriate number of common-rare collisions is determined. After standard DSMC collision mechanics is performed, the temporary particles are discarded. Thus, the particles of the overlay simulation interact with the background flow field at the microscopic level. It is important to note that given the assumption that the rare species have a number density that is several orders of magnitude lower than the common species, the probability of common-rare collisions is much greater than rare-rare collisions. In the cases considered here, rare-rare collisions are neglected in the

overlay simulation.

Chemistry in DSMC Overlay

Applying the DSMC overlay procedure outlined above to chemically reacting flows is somewhat more involved. It is important to determine what classes of collisions will lead to chemical reactions that affect the rare species. The three possible candidates are common-common collisions, common-rare collisions and rare-rare collisions. As was previously mentioned, rare-rare collision are neglected, so no reactions stemming from these types of collision are considered. Common-rare collisions are handled using the bins and temporary particles. Standard DSMC reaction routines are used to handle the probability and mechanics of common-rare reactions. However, consideration must be given to the relative importance of common-rare reactions compared to the common-common reactions. Since the probability of a common-rare collision is several orders of magnitude lower than a common-common collision, the reaction probability must be very high in order for the common-rare reaction to be important relative to the common-common reaction. In the cases considered here, the reaction probabilities for the reactions of interest are not sufficiently high, and the inclusion of common-rare reaction has no quantitative effect on the rare species flow field. This leaves only common-common reactions as the important reactions in terms of the production of rare species.

Common-common reactions cannot be handled during the overlay simulation using standard DSMC techniques as no common-common collision pairs are processed. Regardless of the technique used to determine the concentration and properties of the rare particles created via these reactions, their introduction into the overlay simulation will take the form of a source term for the different rare species in every cell. A completely general scheme for accomplishing this would require binning more detailed information during the base simulation. For the work presented here, a more approximate method of determining both the rate of production and the properties of the rare species due to common-common reactions is used. The predominant reaction considered is:

$$N_2 + O \rightarrow NO + N$$

It is assumed that only the most energetic collisions lead to chemical reaction. In the Atmospheric Explorer flows, this occurs when a free stream particle collides with a particle that has rebounded from the ram surface of the satellite. Thus, there are two different types of collisions leading to the formation of nitric oxide:

$$\vec{N_2} + \overleftarrow{O} \rightarrow \overleftarrow{NO} + \vec{N} \quad \text{(I)}$$

$$\overleftarrow{N_2} + \vec{O} \rightarrow \vec{NO} + \overleftarrow{N} \quad \text{(II)}$$

where the arrows indicate the direction in which the molecule is moving. Thus, reaction I represents a free stream nitrogen molecule, moving at orbital speed, colliding with an atomic oxygen molecule that has reflected from the surface. Reaction II represents free stream atomic oxygen reacting with reflected N_2.

Data on the velocity distributions of surface scattered 8 km/s O and N_2 is limited. Examination of the collision of 8 km/s oxygen atoms with engineering surfaces indicates that the scattering is largely diffuse, although the scattered atoms have a broad velocity distribution centered around 1 km/s.[14] Limited measurements of high velocity N_2 scattering suggest that the scattered velocity is approximately 2 km/s.[15] Using a value of 8 km/s for orbital speed, this results in a relative velocity of 9 km/s or 10 km/s for Reactions I and II, respectively. Using these approximations and appropriate values for the cross-section of the reaction at these speeds, the rate of production of NO and N can be determined in each cell using the equation:

$$\frac{dn(NO)}{dt} = \frac{dn(N)}{dt} = n(N_2)n(O)g\sigma$$

Note that the value for the number density used for nitrogen and atomic oxygen must be modified to account for the assumptions that lead to the choice of values for the relative velocity. An appropriate value for σ is found from consideration of other sources.

In each cell at each time step, a number of NO and N particles are generated according to the production term evaluated using number densities from the base simulation. For the non-flow direction components of velocity, the properties of the NO and N particles created can be approximated from the velocity distributions of N_2 and O, respectively. The velocity component in the direction of the flow for the newly formed NO and N is approximated by the center of mass velocity of the collision, with a thermal spread obtained by sampling the azimuthal distribution in that cell.

Results

Simulations are performed at 10 km intervals over the altitude range of 140 km to 180 km for flow over the Atmospheric Explorer satellite. The geometry of the satellite is a 0.7 m radius cylinder,

h [km]	Kn	n(NO) [m^{-3}]	n(N) [m^{-3}]
140	27.5	7.0e12	7.54e12
150	47.7	5.5e12	1.39e13
160	75.9	4.0e12	2.17e13
170	114.0	3.0e12	2.90e13
180	164.5	2.0e12	3.44e14

Table 1: Summary of Free Stream Condition

1.0 m in length. At each altitude, three different simulations are made. The first of these is a base DSMC simulation, where the flow field of the common species is determined and particle properties are binned. Two overlay DSMC simulations are then run using the base simulation for the background conditions. These simulations differ in the choice of cross-sections for the source term chemical reactions for NO and N. In the first overlay simulation, cross-sections of $\sigma_I = 4 \times 10^{-22}$ m^2 for Reaction I and $\sigma_{II} = 6 \times 10^{-22}$ m^2 for Reaction II are used.[16] In the other overlay simulation, values for σ_I and σ_{II} obtained from a molecular dynamics trajectory analysis are used[17] and are five times greater than the values used in the first overlay simulation. A summary of free stream values is given in Table 1.

Computational Performance

The simulations presented here are performed using a highly modified version of MONACO, a parallel, object-oriented DSMC code developed at Cornell University.[18] The code is run on eight nodes of an IBM SP-2. The total number of particles used during the simulation varies from 150,000 to 1,000,000, depending on the altitude. For the base simulations, the flow takes 6,000 time steps to reach steady state and the flow field is sampled for 2,000 time steps. The transient period for overlay simulations also takes 6,000 times steps. For overlay simulations, 5,000 sampling steps are used in order to accurately resolve wall distributions. The computational effort required also varies significantly between the various runs. Base simulations are runs with a computational cost of 10 μs/particle/time step. The additional overhead of sampling the velocity distributions increases the cost to 24 μs/particle/time step in the overlay simulation. This variation in computational cost coupled with the varying number of particles results in a range of CPU times from 2 to 10 hours.

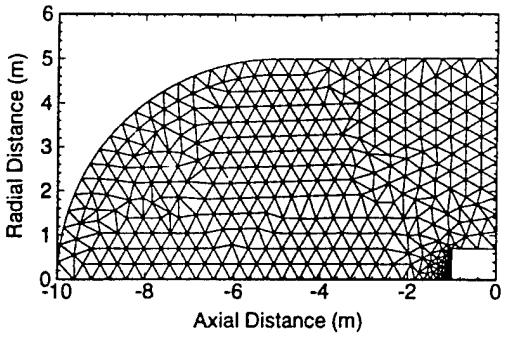

Figure 1: Computational Grid Used At All Altitudes

General Flow Field Structure

A grid consisting of 722 computational cells is used for all altitudes and is shown in Figure 1. Cells of a typical DSMC grid scale in size with the mean free path of the flow. For the altitudes considered the mean free path varies from about 3 m to 200 m and thus is not a useful scaling parameter. Instead, cell sizes are scaled in order to achieve useful resolutions during sampling. This permits the same grid to be used for all the altitudes and cases considered.

The overall structure of the flow field is given in Figure 2, which shows the translational temperature at 140 km. A diffuse bow shock can be seen in front of the body of the Atmospheric Explorer, consistent with rarefied, hypersonic flow. No quantitative conclusions should be drawn from plots such as this, as the relevance of thermodynamic variables in this rarefied regime is questionable. It is provided more for a qualitative overview of the structure of the flow field.

Plots of the number density for all five species along the axis at 140 km and using the first set of cross-sections are shown in Figure 3. The data for these density profiles is obtained from both the base and overlay simulations. Immediately clear is the large difference in the number density between the common species and the rare species.

Sensitivity to Altitude

Effects of varying the altitude on the form of the velocity distributions is now considered. For the distributions presented, the comparison is made between cases at 140 km and 180 km, using the first cross-section. Above this altitude range, the concentration of atomic nitrogen has increased to such a level

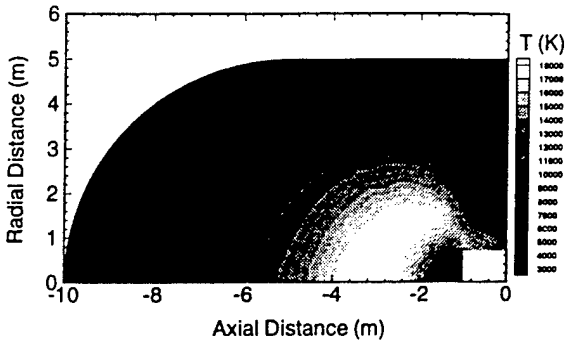

Figure 2: Common Species Translational Temperature at 140 km

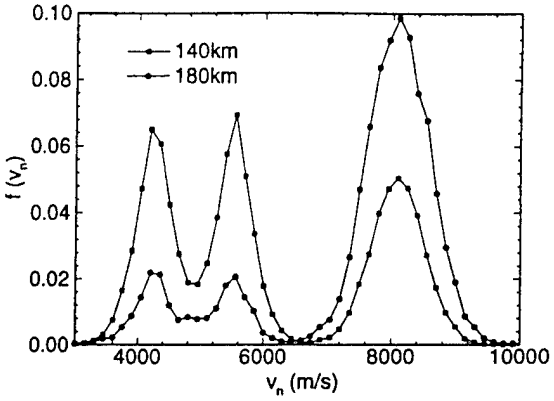

Figure 4: Variation of the Normal Velocity Distribution Functions at the Wall with Altitude

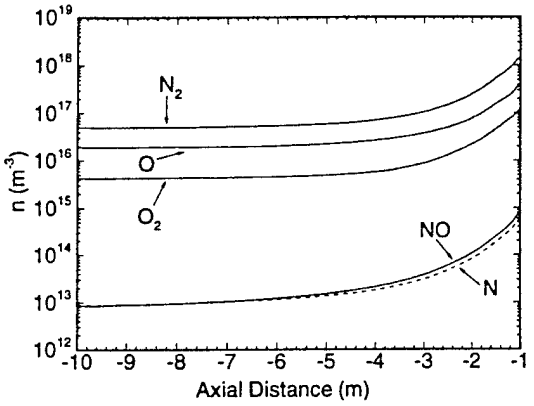

Figure 3: Number Density Profiles Along the Axis at 140 km

that it can no longer be considered a rare species. Due to the affects this would have on the source term chemistry, simulations above this altitude were not performed. Unless otherwise stated, the distributions from the intermediate altitudes follow the trends from lower to higher altitude described in the plots. Note that in all cases, the distributions are normalized. Thus, an increase in one area of the distributions must lead to a corresponding decrease in other areas.

Figure 4 illustrates the normal velocity distributions of nitric oxide particles impacting the surface. At 180 km, the majority of the particles striking the surface have a velocity centered around 8 km/s with a thermal spread corresponding to free stream conditions. This peak represents free stream particles that have reached the surface of the satellite without undergoing any collisions. The two other peaks in the 180 km distribution are representative of the nitric oxide particles created from source term reactions. The two distinct peaks are due to the different center of mass velocities of the two production reactions. The velocity distribution at 140 km shows a similar form. The main distinction lies in the relative importance of the source term NO to free stream NO. At 140 km, the majority of NO particles striking the surface are created in the flow field, as opposed to those present in the ambient atmosphere.

Some further comments about the normal velocity distributions are warranted. The distributions have not been plotted for the lower range of velocities ($v_n < 3$ km/s) because the distributions are identically zero in this range. This indicates that the number of rare-common collisions in the flow field is extremely limited, even at the lowest of the altitudes considered. If there were a substantial number of rare-common collisions, a discernible number of NO particles striking the surface would have a low normal velocity. It should also be noted that, due to the importance of the source term chemistry at the lower altitudes, the average velocity of the NO particles hitting the surface is comparatively lower than at the higher altitudes. This is important in interpreting the effects of using the larger cross-sections.

Sensitivity to Reaction Cross-Sections

Comparison of the effects of the two reaction cross-sections tested is most appropriately studied at the lowest altitude considered, 140 km. At this altitude the base flow field density is the highest, and therefore the effects of changing the cross-section are the most noticeable. Figures 5 – 8 compare the nitric

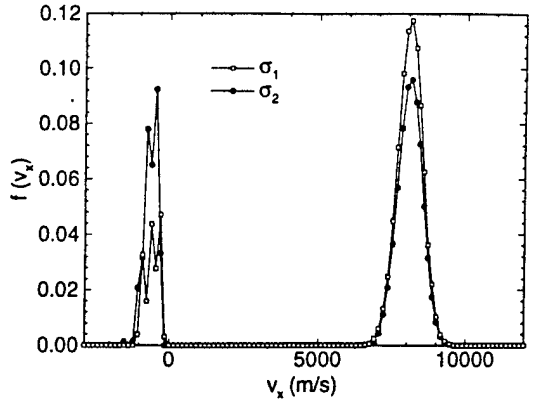

Figure 5: Variation of the X-Velocity Distribution Functions with Cross-section in an Inflow Cell

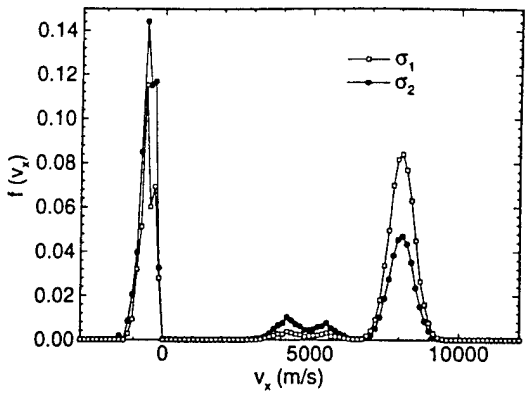

Figure 6: Variation of the X-Velocity Distribution Functions with Cross-section in an Mid-Flow Field Cell

oxide x-velocity distributions for cases using the two cross-sections at 140 km at four points in the flow field. The four points chosen are the inflow cell along the axis approximately 10 m from the the front of the satellite, a mid-flow field cell approximately 3 m from the surface on the axis, the last cell before the wall on the axis and on the ram surface of the satellite itself.

Figures 5 compares the x-velocity distribution in the inflow cell along the axis. In both cases, two distinct groups of particles are evident. The group with the high, positive x-velocity represents free stream particles moving towards the satellite at orbital speeds. The other represents particles that have collided with the front face of the satellite and are moving away with a negative x-velocity. Given the extremely rarefied conditions, these particles travel throughout the entire flow field without undergoing collisions. Note that the relative frequency of particles in the rebounded group is larger with the second, larger cross-sections (σ_2). With the larger cross-sections, more particles have been created throughout the flow field due to the source chemistry. These particles also collide with the surface, rebound and are sampled in the inflow cell with a negative x-velocity.

A comparison of the x-velocity distributions in the mid-flow field cell on the axis is presented in Figure 6. The two groups evident in the inflow cell are also seen here. The relative increase of the negative x-velocity group with the second cross-section is also apparent. In addition to these groups, two smaller groups are distinguishable. Noticeably smaller in magnitude than the first two groups, these can be seen at an x-velocity of about 5 km/s. These groups represent the particles created through the source term chemistry that have yet to collide with the AE satellite. The two peaks in this grouping show the difference in the center of mass velocity in the two source term reactions. When an N_2 molecule traveling at orbital speeds collides with a reflected oxygen atom, the center of mass velocity is larger than when the atomic oxygen is traveling at orbital speeds.

Near the wall, the comparison between the distributions is noticeably different. In both cases shown in Figure 7, the distribution is dominated by a group of reflected particles, moving in the negative x-direction with a relatively slow speed. The form of these distributions is consistent with the number density profiles. The magnitude of the velocity of the rebounding particles is relatively small, so that it will take a much longer time for these particles to leave the cell than it will for the high speed free stream particles in the opposite direction. Consequently, at any time there are many more reflected particles than free stream particles in cells near the surface.

The final comparison of the effects of changing the cross-section is given in Figure 8, which shows normal velocity distributions along the wall. In both distributions, the presence of source term NO as well as free stream NO is evident. Also distinguishable is the bimodal behavior of the source term particles. Once again, the increased importance of the source term chemistry is visible; the distribution in the second cross-section case is heavily weighted towards these particles. Note that the predominance of source term particles is so large that it greatly overshadows the free stream peak.

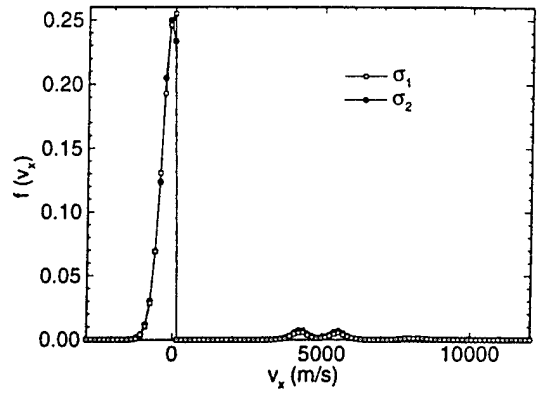

Figure 7: Variation of the X-Velocity Distribution Functions with Cross-section in a Near Wall Cell

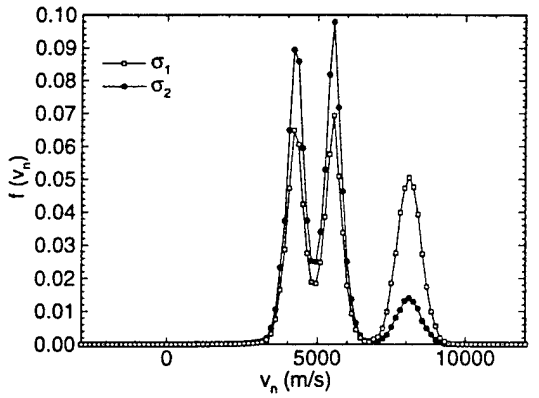

Figure 8: Variation of the Normal Velocity Distribution Functions with Cross-section at the Wall

Glow Brightness Predictions

Figures 9 and 10 show a comparison between experimental AE data for the glow brightness at 6563 $\AA$ at varying altitudes[3] and predictions based on the DSMC overlay simulations using the cross-sections sets σ_1 and σ_2. In both cases, the results have been scaled to units of Rayleighs, where 1 Rayleigh is defined as 10^6 photons/cm^2/s. The DSMC overlay prediction of the glow brightness is based on the average nitric oxide flux hitting the surface. It is assumed that each NO molecule striking the surface interacts with an adsorbed oxygen atom, forms a NO_2^* molecule in the gas phase that spontaneously decays, emitting a photon. The NO_2^* molecule is assumed to emit the photon in a random direction, with all directions being equally probable. The DSMC prediction of the brightness is further scaled so that the prediction agrees with experiment at an altitude of 160 km. The magnitude of this scaling is substantial, on the order of 10^4, and is larger for the second cross-section cases. This scaling is required for the most part to correct for the unit probability assumption for the gas-surface interaction. A true reaction probability is likely to be significantly less than one, so that the true production rate of NO_2^* is much less than the incident NO flux striking the surface. In each case, a prediction of the glow brightness based solely on free stream nitric oxide is included for comparison. At a particular altitude, the magnitude of the difference between the DSMC overlay prediction and the free stream estimate is an indication of the importance of gas-gas collisions and chemistry.

DSMC predictions for the first cross-sections are presented in Figure 9. In general, the predictions show good agreement over the range of altitudes considered. The deviation from the free stream reference is greatest at the lowest altitude. This is consistent with the input conditions and the previous results. At the lower altitudes, the density is higher so the production from source term chemistry is greater. This results in a higher overall NO flux which in turn leads to increased glow production. As altitude increases, the DSMC predictions approach the free stream reference predictions. At the highest altitude considered, 180 km, the two predictions almost coincide. This is an indication that production of nitric oxide in the flow field is unimportant at greater altitudes and that the glow is almost entirely due to free stream nitric oxide. In addition, it demonstrates the importance of the initial estimates of the nitric oxide densities, as the DSMC predictions will inevitably match the free stream predictions at higher altitudes. Error in the nitric oxide number density directly translates into error in the glow production.

Figure 10 gives the predictions based on the second cross-sections. The DSMC simulations are seen to overpredict the brightness at the lower altitudes, where the source term production of NO is more important. Larger predicted brightness using the second cross-sections is certainly to be expected, as the larger magnitude of the second cross-sections results in an increase in the production of NO. It is not entirely clear, however, that the first cross-section should be preferred over the second simply on the basis of the superior agreement with the experimental data. The effects of the normal velocity distributions along the wall for the incident nitric oxide is neglected in the simulations presented here. For the lower altitude case, as seen in Figure 4, a larger

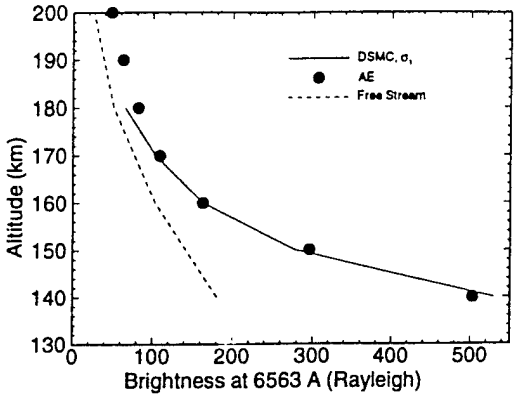

Figure 9: Comparison of Predicted Glow Brightness Using σ_1 with AE Experimental Data

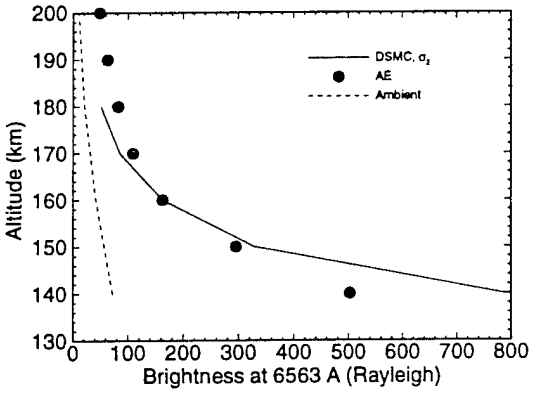

Figure 10: Comparison of Predicted Glow Brightness Using σ_2 with AE Experimental Data

fraction of the NO striking the surface is produced through the source term chemistry. This results in the NO striking the surface having a lower average velocity at the lower altitudes. If the simple assumption is made that the higher the incident energy, the higher the probability of reaction, then the predicted brightness at the lower altitudes would be reduced. So, taking into account the effect of the normal velocity distribution may result in the second cross-section giving better agreement with experiment.

Conclusions

A DSMC overlay technique suitable for simulating rare species has been developed. This method was applied to the flow around the Atmospheric Explorer satellite in order to predict the NO_2 glow brightness.

Feasibility of the DSMC overlay technique has been demonstrated. Recall the number density profiles shown in Figure 3 indicate that the relative difference between the densities of the common and rare species is three orders of magnitude. Thus, the DSMC overlay method can clearly resolve the behavior of rare species. Numerous velocity distributions for nitric oxide have also been presented, showing the ability of the method to maintain microscopic detail for the rare species throughout the simulation.

Prediction of the glow brightness over a range of altitudes has been made. For the reaction cross-sections based on measurement, the qualitative agreement of the scaled predictions with the experiment data was quite good. For the cross-sections based on computational chemistry, the agreement was not as good at the lower altitudes where the prediction was significantly larger than experiment. This overprediction could be tempered by the inclusion of collisional energy effects in the formation of NO_2^*. In both cases, the importance of source term chemistry was seen to diminish at higher altitudes. At altitudes greater than 200 km, the results suggest that the glow production is entire due to ambient nitric oxide. This highlights the importance of accurately determining the ambient concentrations of the rare species.

Acknowledgements

Funding for this work has been provided by the Ballistic Missile Defense Organization under AASERT award DAAH04-95-1-0204. Computational resources were provided on an IBM SP-2 by the Cornell Theory Center.

References

[1] Ahmadjian, M., Jennings, D.E., "Analysis of STS-39 Space Shuttle Glow Measurements," *Journal of Spacecraft and Rockets*, Vol. 32, No. 3, 1995, pp. 507–513.

[2] Swenson, G.R., Rairden, R.L., Jennings, D.E. and Ahmadjian, M., "Vehicle Glow Measurements on Space Shuttle Transportation System Flight 62," *Journal of Spacecraft and Rockets*, Vol. 33, No. 2, pp. 240–249.

[3] Yee, J.H., Abreu, V.J., "Visible Glow Induced by Spacecraft-Environment Interaction," *Geophysical Research Letters*, Vol. 10, No. 2, 1983, pp. 126–129.

[4] Swenson, G.R., Mende, S.B. and Clifton, K.S., "Ram Vehicle Glow Spectrum; Implications of NO Recombination Continuum," *Geophysical Research Letters*, Vol. 12, No. 97, 1985.

[5] Kofsky, I.L. and Barrett, J.I., "Spacecraft Glows From Surface-Catalyzed Reactions," *Planetary Space Science*, Vol. 34, No. 8, 1986, pp. 665–681.

[6] Meyerott, R.E. and Swenson, G.R., "N_2 Spacecraft Glows From N(^{4}S) Recombination," *Planetary Space Science*, Vol. 39, No. 3, 1991, pp. 469–478.

[7] Greer, W.A.D., Pratt, N.H. and Stark, J.P.W., "Spacecraft Glows and Laboratory Luminescence: Evidence For a Common Reaction Mechanism," *Geophysical Research Letters*, Vol. 20, No. 8, 1993, pp. 731–734.

[8] Green, B.D., Rawlins, W.T. and Marinelli, W.J., "Chemiluminescent Processes Occurring Above Shuttle Surfaces," *Planetary Space Science*, Vol. 34, No. 9, 1986, pp. 879-887.

[9] Caledonia, G.E., Holtzclaw, K.W., Krech, R.H. and Sonnenfroh, D.M., "Mechanistic Investigations of Shuttle Glow," *Journal of Geophysical Research*, Vol. 98, No. A3, 1993m pp. 3725–3730.

[10] Hedin, A.E., "The Atmospheric Model in the Region 90 to 2000km," *Adv. Space Res, 8(5-6)*, 9, 1988.

[11] McCoy, R.P., "Thermospheric Odd Nitrogen 1. NO, N(^4S), and O(^3P) Densities from Rocket Measurements of the NO δ and γ Bands and the O_2 Herzberg I Bands," *Journal of Geophysical Research*, Vol. 88, No. A4, 1983, pp. 3197-3205.

[12] Boyd, I.D., Karipides, D.P., Candler, G.V., Levin, D.A., "Effect of Dissociation Modeling in Strongly Nonequilibrium Flows at High Altitude," AIAA Paper 95-0709, January 1995.

[13] Karipides, D.P., Boyd, I.D, Levin, D.A., "Prediction of Ultraviolet Emissions in Rarefied Hypersonic Flow," AIAA Paper 95-2091, June 1995

[14] Caledonia, G.E., Krech, R.H. and Oakes, D.B., "Laboratory Studies of Fast Oxygen Atom Interactions With Materials," Proceedings of the Sixth International Symposium on Materials in a Space Environment, The Netherlands, 1994.

[15] Hurlbut, F.C., "Particle Surface Interaction in the Orbital Context: A Survey," *Rarefied Gas Dynamics: Progress in Aeronautics and Astronautics*, Vol. 116, 1989.

[16] Upschulte, B.L., Oakes, D.B., Caledonia, G.E. and Blumberg, W.A.M., "Infrared Emissions Arising From the Reactions of Fast $0/0^+$ With N_2," *Geophysical Research Letters*, Vol. 19, No. 10, 1992.

[17] Boyd, I.D., Bose, D. and Candler, G.V., "Monte Carlo Modeling of Nirtic Oxide Formation Based on Quasi-Classical Trajectory Calculations," AIAA Paper 96-1845, June 1996.

[18] Dietrich, S., and Boyd, I. D., "Scalar and Parallel Optimized Implementation of the Direct Simulation Monte Carlo Method," accepted for publication in *Journal of Computational Physics.*

APPENDIX B

Pre-Flight Predictions of Ultraviolet and Visible Emissions for the Skipper Flight Experiment

Cornell University Report

Pre-Flight Predictions of Ultraviolet and Visible Emissions for the Skipper Flight Experiment

Iain D. Boyd and Daniel P. Karipides
Department of Mechanical & Aerospace Engineering
Cornell University, Ithaca, NY 14853

Deborah A. Levin
Institute for Defense Analyses, Alexandria, VA 22311

George E. Caledonia
Physical Sciences, Inc., Andover, MA 01810

FDA-95-09 December 1995

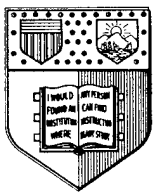

Fluid Dynamics and Aerodynamics Program

Sibley School of
Mechanical and Aerospace Engineering

Cornell University Ithaca, New York 14853

Pre-Flight Predictions of Ultraviolet and Visible Emissions for the Skipper Flight Experiment

Iain D. Boyd and Daniel P. Karipides
Department of Mechanical & Aerospace Engineering
Cornell University, Ithaca NY 14853

Deborah A. Levin
Institute for Defense Analyses, Alexandria, VA 22311

George E. Caledonia
Physical Sciences, Inc., Andover, MA 01810

Abstract

The Skipper flight experiment is due for launch in December 1995. The experiment is designed to make measurements of visible and ultra-violet emissions caused by the interaction of a hypersonic vehicle with the atmosphere at very high altitudes. The mission consists of two distinct phases: (1) measurement of spacecraft glow emission during orbit of the earth over the altitude range of 300 down to about 130 km; and (2) measurement of bow-shock generated radiation during reentry over the altitude range of 180 to about 100 km. This document provides pre-flight predictions for emission generated in both phases of the flight. The purpose of these predictions is to assist during the execution of the Skipper flight. The results should be regarded as preliminary. It is anticipated that more detailed modeling will be performed after the flight based on the data provided by Skipper.

Introduction

The Skipper flight experiment is designed to characterize the aerothermochemistry experienced by a spacecraft traveling at hypersonic speeds during low earth orbit and atmospheric reentry. The flight is composed of two distinct stages. The first stage consists of a number of elliptical, low-earth orbits, during which spacecraft glow measurements will be taken. In the second stage, the satellite will take radiation measurements during reentry.

Earlier flight experiments have successfully gathered data for use in refining air-chemistry modeling. One of these experiments (BSUV-1) operated at a velocity of about 3.5 km/s and covered an altitude range of 40 km to 70 km.[2] While initial calculations of the ultraviolet emissions were low by several orders of magnitude, improvements to the air radiation models give good agreement between the measured and calculated emissions. A second flight experiment (BSUV-2) operated at a velocity of 5.1 km/s over the altitude range of 65 km to 100 km.[3] Due to the rarefied nature of the atmosphere at the higher altitudes, direct simulation Monte Carlo (DSMC) calculations give better agreement with measured emissions of NO than CFD predictions. Under these conditions, simulation is required both of species present in extremely low concentrations and of extremely rare collision events. Initial DSMC calculations lacking the particle resolution to simulate such rare species and events grossly underpredicted the NO emission. Use of an overlay technique in conjunction with a standard DSMC calculation allowed both common and rare species and events to be modeled correctly, bringing the predictions much closer to the measured values.[4]

This report presents preflight predictions of radiation measurements. These predictions are not meant to be definitive, but rather are intended for assistance during the operation of the Skipper spacecraft. It is anticipated that the predictions discussed here will give only qualitative agreement with the actual data set. Predictions are provided for both the orbital and reentry portions of the Skipper mission.

The results and the methods employed are presented in the following sections.

UV and VUV Emissions Observed During Reentry

In this section predictions are provided of ultraviolet and vacuum-ultra-violet radiative emissions for nitric oxide (NO), and atomic oxygen (O). Results are presented over the altitude range from 160 down to 100 km. We describe the solution procedure for computation of the flow fields around the Skipper vehicle, the chemistry models, and the radiation models.

Solution Procedure

A multistep procedure is used to calculate radiative emission predictions, consisting of a DSMC calculation, an overlay calculation, and a radiance calculation. The DSMC simulation takes as input free-stream conditions corresponding to the altitude in question. Due to limitations in particle resolution, this calculation only simulates the major species, N_2, O_2 and O, to determine macroscopic properties such as temperature and mass density in the flow field. The resulting solution serves as input to the overlay code. The overlay calculation determines the concentrations of the trace species, NO and N. As with previous use of the overlay technique, the trace species are assumed to be present in such low concentrations that reactions involving these species have no effect on the overall temperature and density of the flow field, nor on the concentrations of the major species. Finally, the complete flow field solution, including both major and trace species, is used in the NEQAIR code[5] [6] to compute the radiative emissions.

Atmospheric Model

Two separate atmospheric models are used. The first uses the MSISE-90 model[7] to predict the atmospheric structure. Inputs to the model include date, time, latitude, longitude, solar flux indices and the geomagnetic index. Predictions of atmospheric structure are obtained for latitude 23°N and longitude 164°E, an approximate location for reentry. The second atmosphere used is simply a standard atmosphere taken from the Handbook of Geophysics and the Space Environment.[8] While not specific to the reentry point or any of the other parameters that determine atmospheric composition, the standard atmosphere does form a good baseline to compare with the MSIS atmosphere.

Determination of the concentrations of N and NO is somewhat more complicated. While the MSIS model gives variation of N number density with altitude, the standard atmosphere does not include trace species. The MSIS value for the number density of N is used as the standard atmosphere value as well. Because the concentration of the trace species is much smaller than the major species, estimating the N concentration in this manner does not affect the DSMC simulation. The concentration of NO is so low compared to the major species that the MSIS atmosphere does not predict NO number density. Nitric oxide number density for both atmospheres is estimated from data presented by McCoy.[9] At all altitudes in question, the amount of NO produced through chemical reaction far outweighs the amount present in the free-stream. Therefore, reasonable errors in these estimates should not affect the emission predictions.

DSMC Calculations

The code employed for the DSMC calculations is based on that described by Boyd and Gokcen.[10] The satellite is assumed to be roughly cylindrical, with a diameter of 0.8 m and an axial length of 1.25 m. For all simulations, the base of the cylinder is positioned at the origin, with the body set in the negative x-direction. Due to the extreme change in atmospheric density over the altitude range in question, a different grid is used at each altitude. Grid sizes range from 89 x 36 cells, covering an actual domain of approximately 2 m x 1 m, for the 100 km case, to 19 x 45 cells, covering a physical domain of approximately 20 m x 15 m, for the 160 km case. Due to the large difference in the concentrations of the major species (N_2, O_2, O) to the trace species (NO, N), which varies from 4 to 6 orders of magnitude in the cases considered, only reactions involving the major species are simulated in the DSMC code. Output of the DSMC simulation gives concentrations for the major species, as well as temperatures and mass density values for each cell. While reactions involving the trace species are not simulated due to lack of particle resolution, it is assumed that these species are indeed rare enough that including them later in the overlay calculation will not change the macroscopic flow field values.

Overlay Calculations

Following the method that was successful in simulating trace species reactions for the BSUV-2 flight,[4]

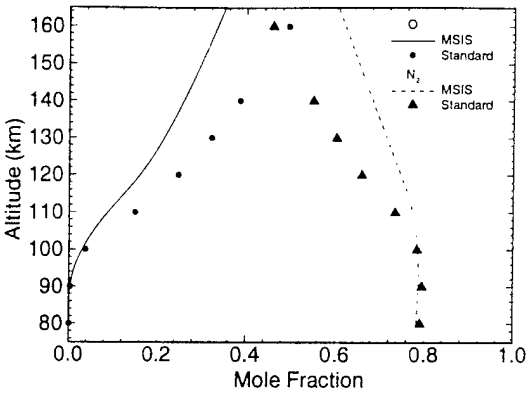

Figure 1: N_2 and Atomic O Concentration with Altitude for the MSIS and Standard Atmospheres

an overlay code is employed using the output flow field from the DSMC simulation. The overlay code was written by Candler, with minor modifications made for the present study. As mentioned above, the overlay method assumes that the trace species are present in such small amounts that they do not affect the overall flow field. The DSMC calculated flow field serves as the unvarying flow field. Mass conservation is then solved using the following conservation equation:

$$\frac{\partial \rho_s}{\partial t} + \frac{\partial}{\partial x_j}(\rho_s u_j + \rho_s v_{sj}) = w_s, \quad \text{for } s = 1, \ldots, n$$

for each of the n trace species. ρ_s is the trace species density, v_{sj} is the diffusion velocity and w_s is the chemical source term for species s. The mass-averaged velocity, u_j, is determined from the DSMC solution.

Chemical Reactions

One of the primary measurements on the Skipper flight is the 230 nm ultraviolet emission of nitric oxide. Accordingly, it is possible that the modeling of any reactions resulting in the production of NO could have a great effect on the NO emission predictions. For rarefied air, the two most important NO formation reactions are the Zeldovich exchange reactions:

$$\begin{aligned} NO + O &\rightleftharpoons O_2 + N \\ N_2 + O &\rightleftharpoons NO + N \end{aligned}$$

With the first of these two reactions, the backwards reaction is controlled by the concentration of atomic nitrogen. At high altitude, the dissociation of N_2 is extremely rare and N is present only as a trace species in the free-stream, so there is generally very little atomic N available to drive this reaction. Therefore, the second of the listed exchange reactions is much more important in controlling the production of NO. While the first exchange reaction is modeled, the corresponding rate coefficient is not varied in this study. In the second exchange reaction, the concentration of atomic O controls the production of NO. In the BSUV-2 case, it was found that the dissociation rate of O_2 had to be modeled very carefully in order to accurately predict the amount of NO produced. In the higher altitude range being considered here, dissociation modeling is less important as there is already a significant amount of atomic O present in the ambient atmosphere; solar radiation results in a large amount of photodissociation of O_2. It is therefore important that the forward rate of the second exchange reaction be modeled accurately. Two different reaction rates are used in making the predictions. The first of these is the rate proposed by Park,[11] which assumes an Arrhenius form of:

$$k_f = 6.40 \times 10^{14}\, T^{-1} \exp(-38,370/T) \quad \frac{\text{cm}^3}{\text{mol sec}}$$

In the high temperature range, the exponent on the temperature term should be a nonpositive value. It was arbitrarily set to -1 and the coefficient was determined via a curve fit to existing experimental data. The second rate is one determined by Monat,[12] which is of the form:

$$k_f = 1.84 \times 10^{11} \exp(-38,370/T) \quad \frac{\text{cm}^3}{\text{mol sec}}$$

This second formulation is the result of shock-tube studies that covered a temperature range of 2,000 K to 4,000 K. The temperatures of the weak bow-shock in the flow are of the order of 10,000 K; however, the Monat rate is at least derived directly from experiment. The different temperature dependence of the two rates, especially at high temperatures, is shown in Figure 2. For these reasons, the Monat rate is a good second choice to determine the sensitivity of the predictions to the exchange reaction rate.

Radiance Calculations

In the final step of the solution procedure, the flow field solution, with correct concentrations of both the major and trace species, is analyzed with the NEQAIR code. This code uses input from a calculated flow field and can be used to compute emission predictions at particular wavelength for a given

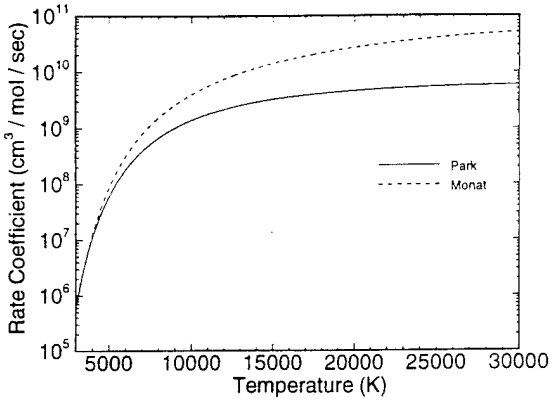

Figure 2: Comparison of the Park and Monat Reaction Rate Coefficients for the $N_2 + O \rightarrow NO + N$ Exchange Reaction

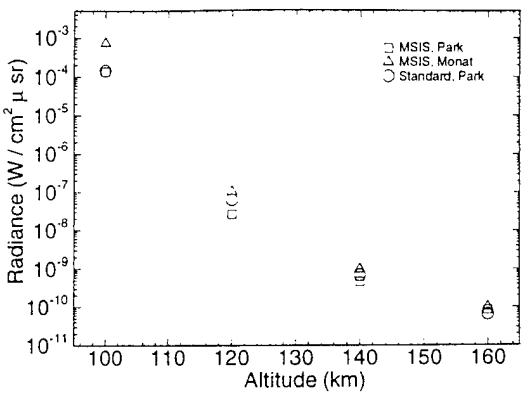

Figure 3: Nitric Oxide 230 nm ± 5 nm Radiance Emission Predictions

species. Corresponding to the data that will be taken during the Skipper flight experiment, 230 nm ± 5 nm NO emissions are integrated along the axis and 131.0 nm atomic O emissions are integrated along a line off the axis.

Results

At all altitudes, three separate simulations are performed. The first uses the MSIS generated atmosphere and the Park reaction rate for the second exchange reaction. Given that the MSIS atmosphere is likely the more accurate prediction of the actual atmospheric structure that will be present during reentry and that the Park reaction rate is applicable over the entire temperature range, this first calculation is considered the baseline solution for each altitude. In order to investigate the effects of changing the reaction rate, the second calculation made at each altitude uses the same atmosphere, but employs the Monat rate for the second exchange reaction. Calculations of this type will be referred to as Monat results. The third calculation at each altitude uses the Park reaction rate, but employs the standard atmosphere as the free-stream conditions. These calculations will be referred to as standard atmosphere results.

Nitric Oxide Radiance Predictions

The 230 nm ± 5 nm ultraviolet radiance predictions for NO at all altitudes are given in Figure 3. The radiance predictions are most sensitive to the NO number density along the stagnation streamline at the point of the peak translational temperature.

At 100 km, there is very little difference between the radiance predictions for the baseline result and the standard atmosphere result. This is expected as the NO number density profiles for the two cases are very similar along the entire stagnation streamline. The locations of the peaks in translational temperature for both cases is relatively unimportant; regardless of where the individual peaks are located, there is little difference between the NO number densities computed at those points. An order of magnitude difference exists between the baseline result and Monat result. This difference arises directly from the NO number density profiles for which there is a large difference at the point of peak translational temperature.

At 120 km, the radiance prediction of the standard atmosphere calculation is about a factor of four higher than the baseline radiance prediction. This follows directly from the NO number density profiles. A difference is still notable between the baseline predictions and the Monat predictions. Again, this is expected from examination of the NO number density profiles. The overall magnitude of the difference is less than is the case for the 100 km case. This can be attributed to the reduced magnitude of the difference between the NO number densities as compared to the 100 km results.

Relations between the predictions obtained from the various 140 km and 160 km calculations are qualitatively similar, with the actual differences between cases being much less pronounced at these higher altitudes than is the case at the lower altitudes. At 140 km, the difference between the baseline prediction and Monat prediction is relatively small, due to the reduced effect of chemistry in the extremely

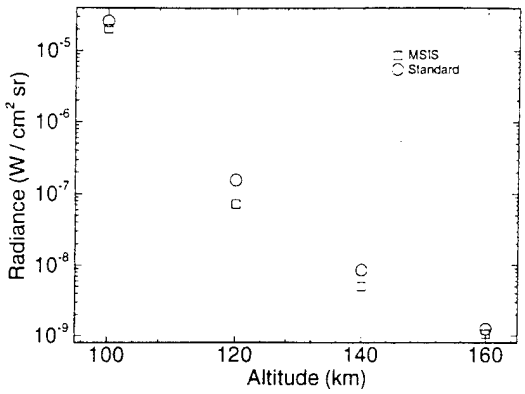

Figure 4: Atomic Oxygen 131 nm Radiance Emission Predictions

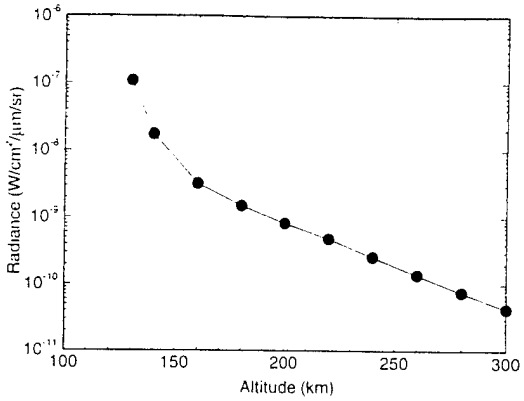

Figure 5: NO_2 732 nm Radiance Emission Estimates

rarefied flow field. At 160 km, the insensitivity to changes in the reaction rate is even more pronounced. This insensitivity at both altitudes carries over to the standard atmosphere results. Despite the relatively large difference between the MSIS atmosphere and the standard atmosphere at the higher altitudes, little difference exists between the predictions for these two conditions.

Atomic Oxygen Radiance Predictions

Atomic oxygen 131.0 nm vacuum ultraviolet radiance predictions are shown in Figure 4. At each altitude only the results from the baseline and standard atmosphere calculations are plotted. Since the overlay technique only changes the concentrations in the trace species, the concentration of O cannot be affected by an overlay calculation. Since the only difference between the procedure used to generate Monat results from the procedure used to generate baseline results is different input parameters to the overlay calculation, there can be no difference in the concentration of O between the two cases. Thus, the atomic oxygen radiance predictions of the Monat results must be identical to the baseline predictions.

Overall trends in the atomic O predictions at the various altitudes are consistent with previous results. The difference at 100 km is relatively small, again due to the similarity of the two atmospheres at this altitude. There is a notable difference at 120 km, where the two atmospheres start to deviate. At the higher altitudes, the difference between predictions is not as large as the difference between the two atmospheres in this range would suggest. Use of the different atmospheres results in differences in the temperature and atomic O density profiles along the line of integration. These differences are such that they counteract each other to some extent, resulting in the reduced sensitivity of the predictions at the higher altitudes.

Visible Emissions Observed During Orbit

In this section we provide estimates of visible glow that has been observed previously on the Atmospheric Explorer (AE) satellite and on the Space Shuttle. Orange in color, this glow has been attributed to an excited state of NO_2. The glow model as it stands has too many undetermined parameters to allow a high-confidence pre-flight prediction for the Skipper mission. Therefore we have estimated Skipper intensities using an extrapolation of the data measured by the Atmospheric Explorer satellite.[13]

The extrapolation is shown in Fig. 5. It has been assumed that the Skipper surface temperature is similar to that of AE at 293 K. The dimensions of the AE and Skipper spacecraft are also similar. The data is for ram measurement; AE measurements were at an angle of 10°. A cosine scaling law is recommended.

The peak glow intensity is anticipated to occur around the wavelength of 732 nm for which the data is presented. Estimated scaling factors for other wavelengths are 0.35, 0.6, and 0.70 for 550 nm, 600 nm, and 800 nm respectively.

Note that the extrapolation to 130 km is highly uncertain. Skipper measurements in this lower altitude range will provide a major contribuion to our understanding of visible glow phenomena.

Acknowledgements

The work at Cornell is supported by the Army Research Office (grant DAAH04-93-G-0089). Work performed at the Institute for Defense Analyses was carried out under contract number DASW01-94-C-0054 for the Innovative Science and Technology Office of the Ballistic Missile Defense Organization.

References

[1] Levin, D.A., Candler, G.V., Boyd, I.D., Howlett, L.C. and Erdman, P.W., "In-Situ Measurements of Translational and Continuum Flow and UV Radiation from Small Satellite Platforms," AIAA Paper 94-0248, January 1994.

[2] Levin, D.A., Candler, G.V., Collins, R., Erdman, P.W., Zipf, E., Epsy, P. and Howlett, L.C., "Comparison of Theory and Experiment for the Bow Shock Ultraviolet Rocket Flight," *Journal of Thermophysics and Heat Transfer*, Vol. 7, 1993, p. 30.

[3] Levin, D.A., Candler, G.V.,Collins, R., Erdman, P.W., Zipf, E. and Howlett, L.C., "Examination of Ultraviolet Radiation Theory for Bow Shock Rocket Experiments," *Journal of Thermophysics and Heat Transfer*, Vol. 8, 1994, p. 447.

[4] Boyd, I.D., Candler, G.V., and Levin, D.A., "Dissociation Modeling in Low Density Hypersonic Flows of Air," *Physics of Fluids*, Vol. 7, 1995, pp. 1757-1763.

[5] Park, C., "Calculation of Nonequilibrium Radiation in the Flight Regimes of the Aero-Assisted Orbital Transfer Vehicles," *Thermal Design of Aeroassisted Orbital Transfer Vehicles*, edited by H. F. Nelson, Vol. 96, Progress in Astronautics and Aeronautics, AIAA, New York, 1985.

[6] Levin, D., Candler, G., Howlett, C. and Whiting, E., "Comparison of Theory with Atomic Oxygen 130.4 nm Radiation from the Bow Shock Ultraviolet 2 Rocket Experiment," *Journal of Thermophysics and Heat Transfer*, (in press)

[7] Hedin, A.E., "The Atmospheric Model in the Region 90 to 2000 km," *Adv. Space Res. 8(5-6)*, 9, 1988.

[8] *Handbook of Geophysics and the Space Environment*, edited by A.S. Jurda, Air Force Geophysics Laboratory, Air Force Systems Command, United States Air Force, 1985.

[9] McCoy, R.P., "Thermospheric Odd Nitrogen 1. NO, $N(^4S)$, and $O(^3P)$ Densities from Rocket Measurements of the NO δ and γ Bands and the O_2 Herzberg I Bands," *Journal of Geophysical Research*, Vol. 88, No. A4, 1983, pp. 3197-3205.

[10] Boyd, I.D. and Gokcen, T. "Computation of Axisymmetric and Ionized Hypersonic Flows Using Particle and Continuum Methods," *AIAA Journal*, Vol. 32, 1994, pp. 1828-1837.

[11] Park, C., *Nonequilibrium Hypersonic Aerothermodynamics*, John Wiley & Sons, New York, 1990.

[12] Monat, J.P., Hanson, R.K., and Kruger, C.H., "Shock Tube Determination of the Rate Coefficient for the reaction $N_2 + O \rightarrow NO + N$", *Proceedings of the 17th Symposium (International) on Combustion*, 1978, pp. 543-552.

[13] Yee, J. H., et al., *Geophysical Review Letters*, Vol. 12, 1985, p. 651.

APPENDIX C

A Review of Laboratory Studies of
Spacecraft-Atmosphere Interaction Glows

Presented at Fall AGU Meeting, 9 December 1994

PSI
PHYSICAL SCIENCES INC.

A REVIEW OF LABORATORY STUDIES OF SPACECRAFT-ATMOSPHERIC INTERACTION GLOWS

G.E. Caledonia and R.H. Krech
Physical Sciences Inc.
20 New England Business Center
Andover, MA 01810

A. Leone
Lockheed Corp., Calabasas, CA

Presented at Fall AGU Meeting, 9 December 1994

OVERVIEW

T-22561

- Clear Shuttle and Satellite evidence of glows due to surface-catalyzed reactions occurring in low earth orbit

  — $NO + O \xrightarrow{S} NO_2^*$

  $N + N \xrightarrow{S} N_2^*$

  Others ?

- Laboratory studies appropriate to elucidate mechanisms
  - — long history of surface catalyzed glow studies
  - — ability to vary key parameters
  - — simulation always an issue

PSI

PHYSICAL SCIENCES INC.

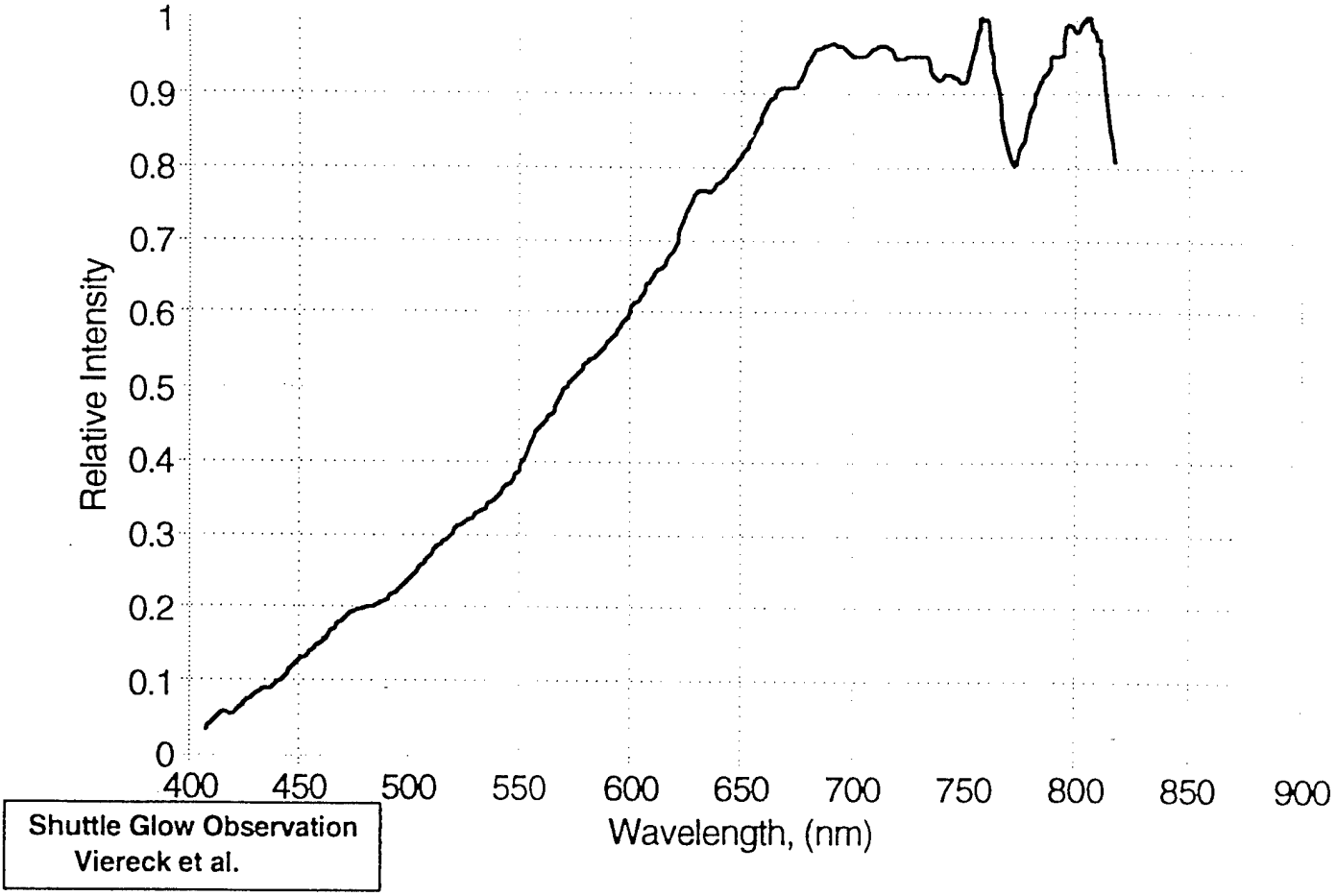
Relative Intensity
1
0.9
0.8
0.7
0.6
0.5
0.4
0.3
0.2
0.1
0
400
450
500
550
600
650
700
750
800
850
900
Wavelength, (nm)
Shuttle Glow Observation
Viereck et al.

NO_2^* CONTINUUM GLOW - THERMAL MEASUREMENTS

T-22562

- $NO + O + M \rightarrow NO_2^* + M$, the air afterglow, a yellow-green emission well studied and understood
- $NO + O \xrightarrow{S} NO_2^*$ produces red shifted continuum emission
  - — several studies since early 1960's
  - — measurements performed at 0.01 to 1 Torr
  - — kinetics confusing, competing processes, e.g.,
    - $NO + O \xrightarrow{S} NO_2^*$
    - $O + O \xrightarrow{S} O_2^*, O_2(A)$

      $O_2(A) + O_2 \rightarrow O_3^* + O$

      $O_3^* + NO \rightarrow NO_2^* + O_2$

PSI

PHYSICAL SCIENCES INC.

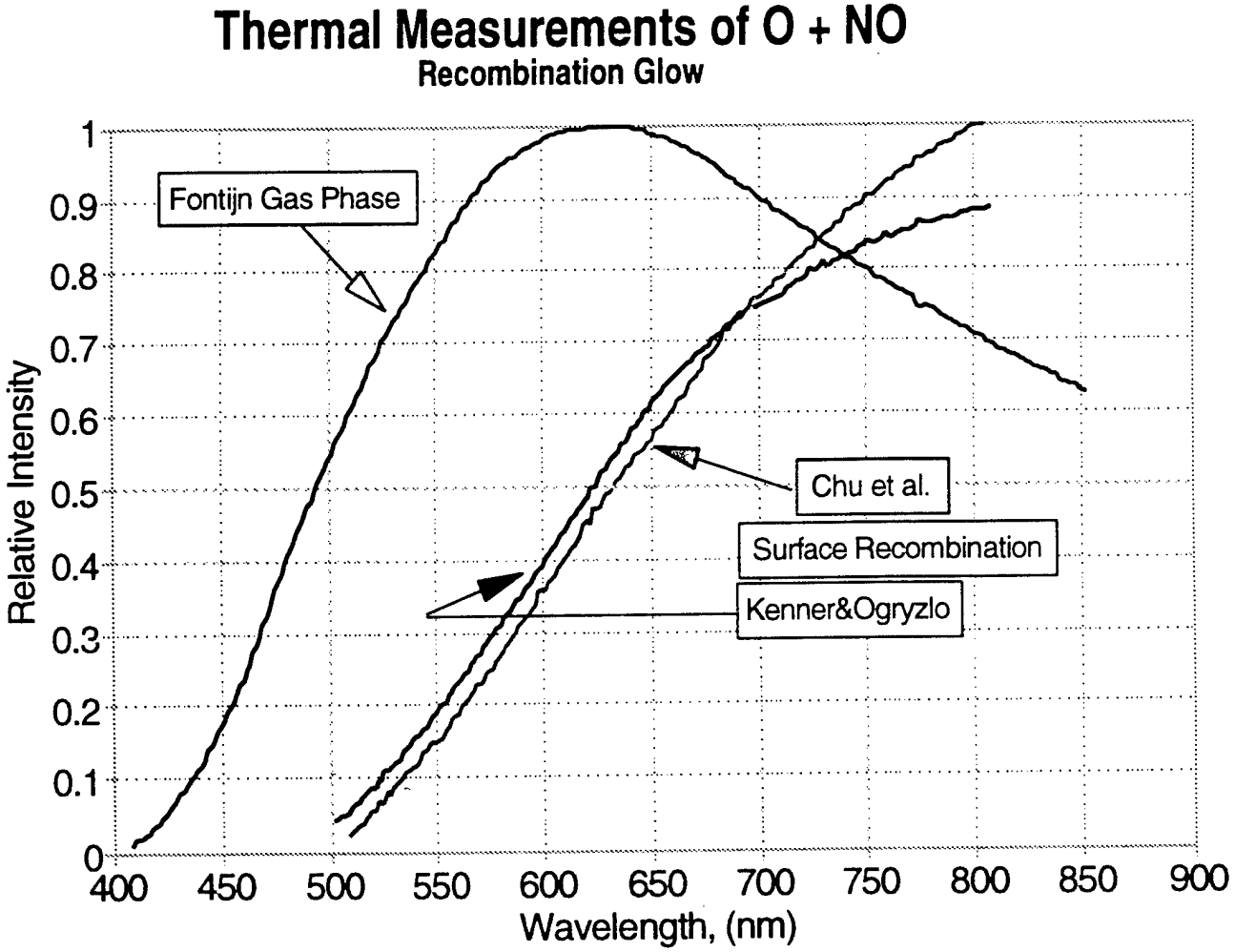
Thermal Measurements of O + NO
Recombination Glow
Fontijn Gas Phase
Chu et al.
Surface Recombination
Kenner&Ogryzlo
Relative Intensity
Wavelength, (nm)
0
0.1
0.2
0.3
0.4
0.5
0.6
0.7
0.8
0.9
1
400
450
500
550
600
650
700
750
800
850
900

NO_2^* CONTINUUM GLOW - ~ 1 eV O-ATOM MEASUREMENTS

T-22563

- Typical maximum energy for discharge excited O_2/rare gas fast oxygen atom sources
- Directed O-atom source and effluent thermal NO source directed onto target
- Continuous fluxes $\lesssim 3 \times 10^{15}$ cm^{-2} s^{-1} at very low pressure, some V variation
- At least three recent studies in reasonable agreement
  - Arnold + Coleman (1988, 1991)
  - Ardebili et al. (1991)
  - Greer et al. (1993)

PSI

PHYSICAL SCIENCES INC.

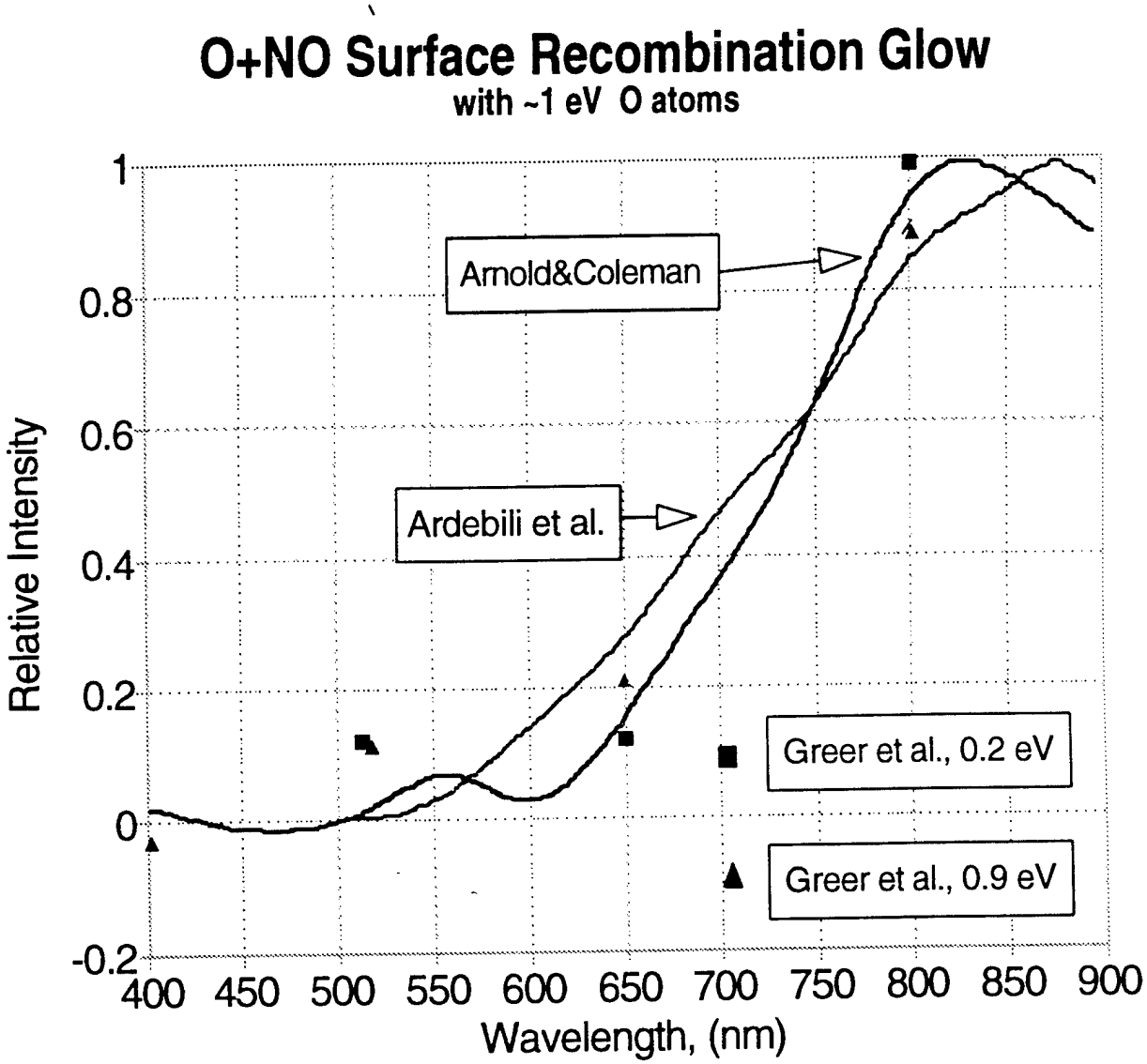
O+NO Surface Recombination Glow
with ~1 eV O atoms
Relative Intensity
Wavelength, (nm)
1
0.8
0.6
0.4
0.2
0
-0.2
400
450
500
550
600
650
700
750
800
850
900
Arnold&Coleman
Ardebili et al.
Greer et al., 0.2 eV
Greer et al., 0.9 eV

NO_2^* CONTINUUM GLOW - 5 eV O-ATOM MEASUREMENTS

T-22564

- LEO velocity simulation with "pure" O beams
- Two studies low flux, low pressure
- Caledonia et al. (1990) pulsed O-atom beam irradiated targets pre-dosed with NO
- Orient et al. (1990) CW O-atom beam with NO gas jet

PSI

PHYSICAL SCIENCES INC.

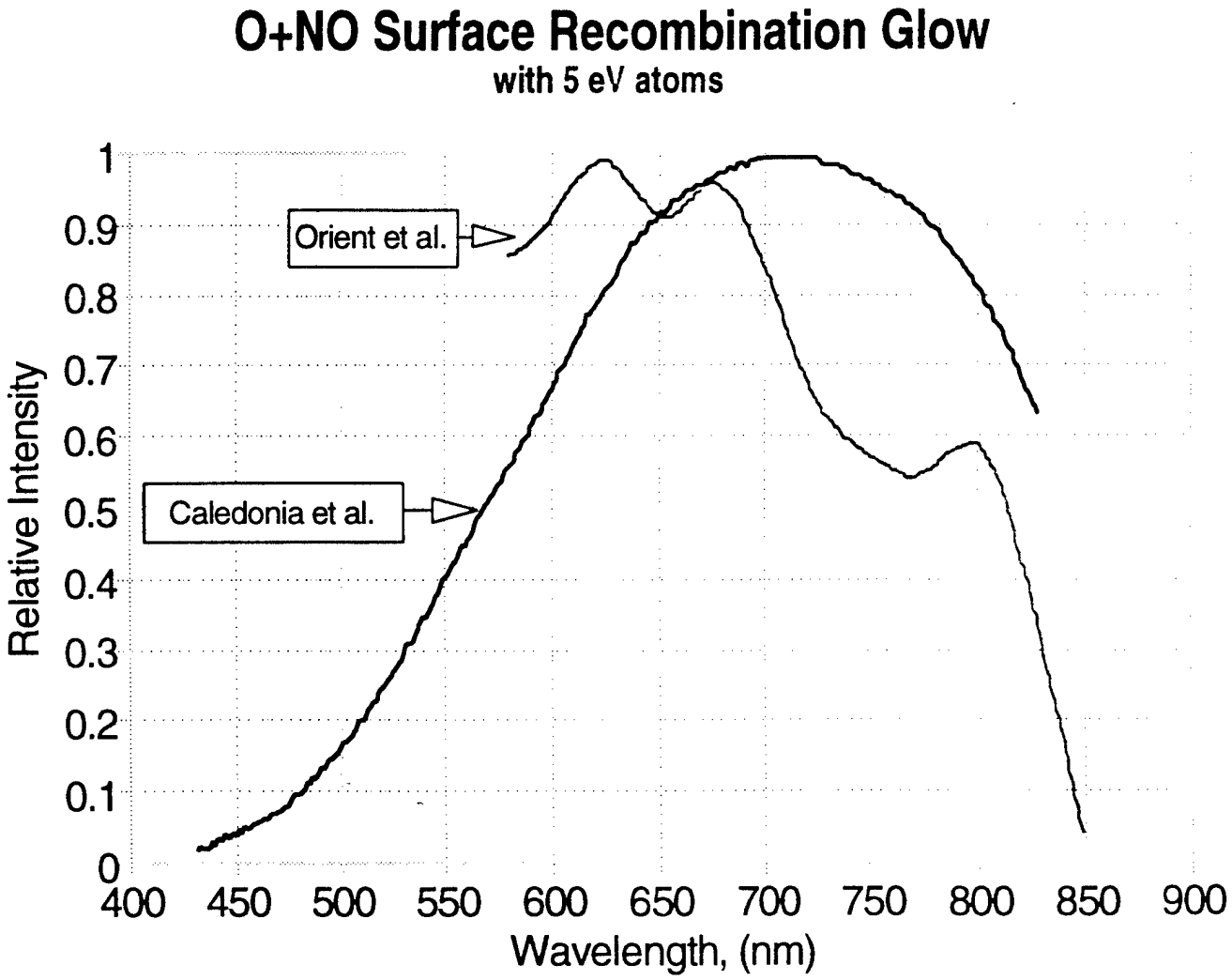
O+NO Surface Recombination Glow
with 5 eV atoms
Orient et al.
Caledonia et al.
Relative Intensity
1
0.9
0.8
0.7
0.6
0.5
0.4
0.3
0.2
0.1
0
400
450
500
550
600
650
700
750
800
850
900
Wavelength, (nm)

TEMPERATURE DEPENDENCE OF O + NO SURFACE GLOW LAB STUDIES, 5 eV O-ATOMS

T-22679

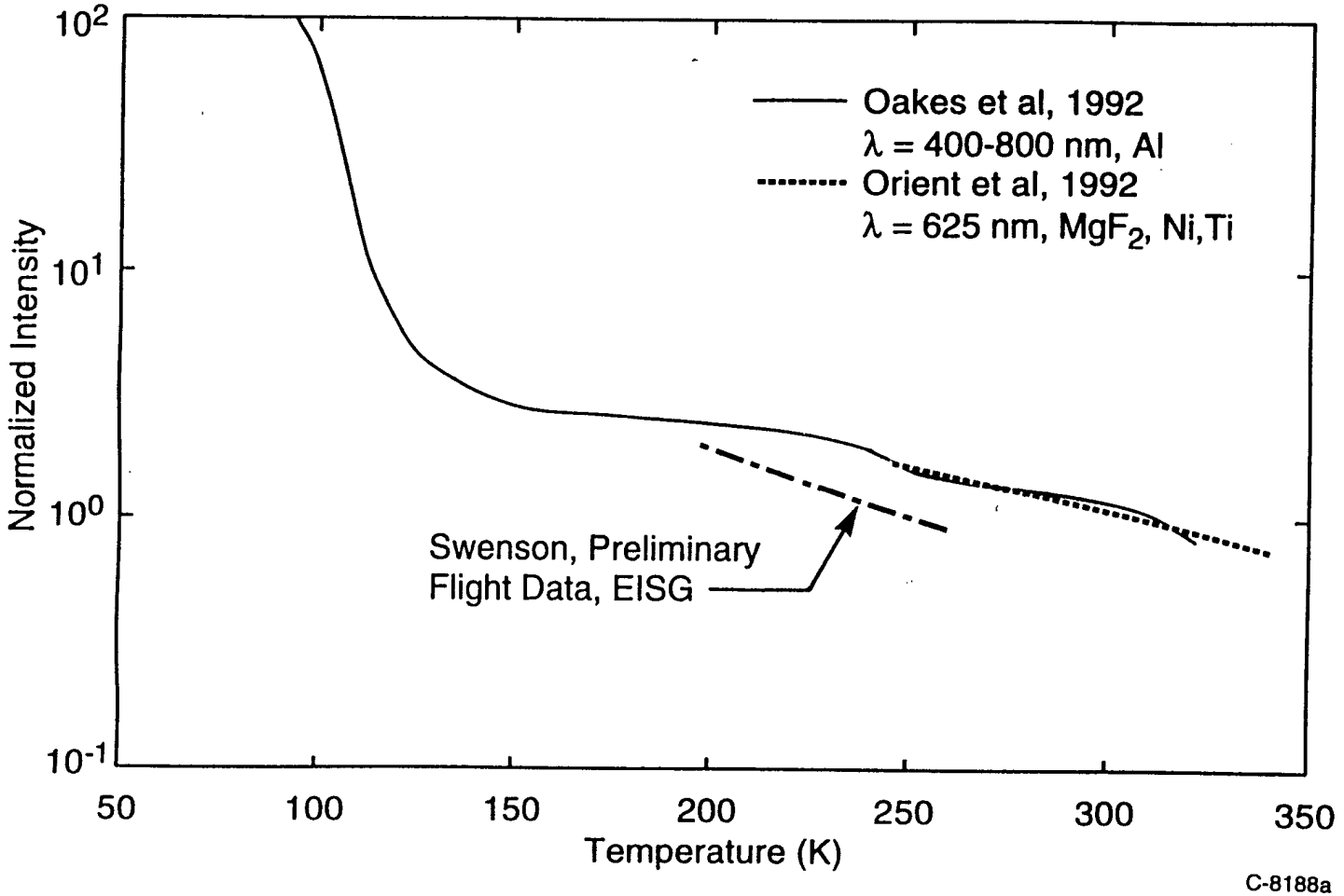

C-8188a

PSI

PHYSICAL SCIENCES INC

UV SURFACE GLOW

T-22566

- No clear ID of source of UV surface glow

- Conflicting lab data on O + NO emissions in the UV
  - — 1 eV studies do not see UV emissions
  - — 5 eV CW studied (Orient et al., 1992) observed UV emissions one-fifth of visible
  - — 5 eV pulsed study (Caledonia et al., 1993) observed no significant UV emissions

PSI

PHYSICAL SCIENCES INC.

GLOW SPECTRA PRODUCED IN COLLISIONS OF 5 eV O-ATOMS WITH MgF_2, Ni + Ti SURFACES WITH ADSORBED NO

Orient et al. (1992)

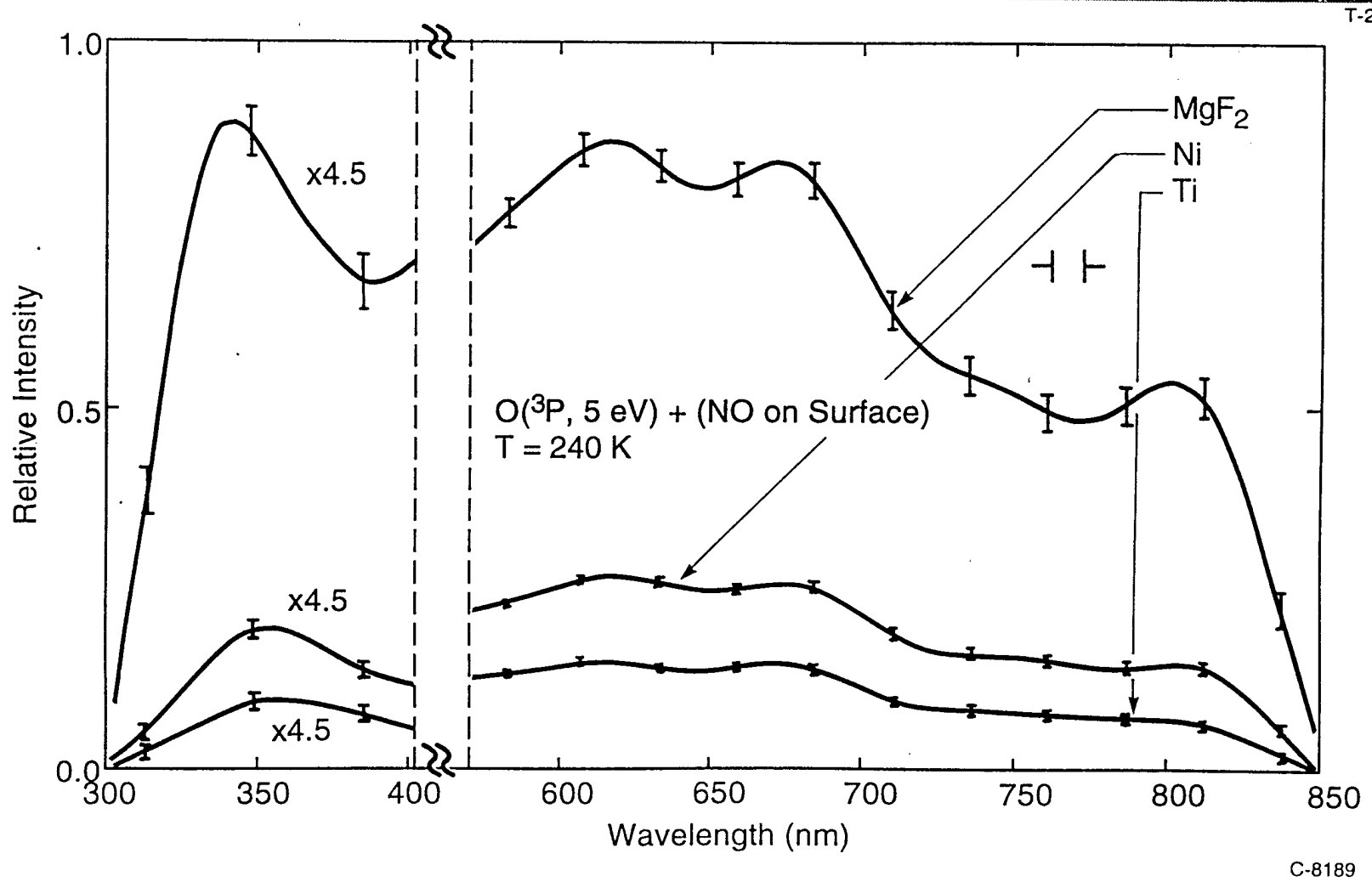

OBSERVED GLOW ABOVE COPPER SURFACE
PULSED O-BEAM, 8 km/s
(integrated over 128 pulses)

T-22568

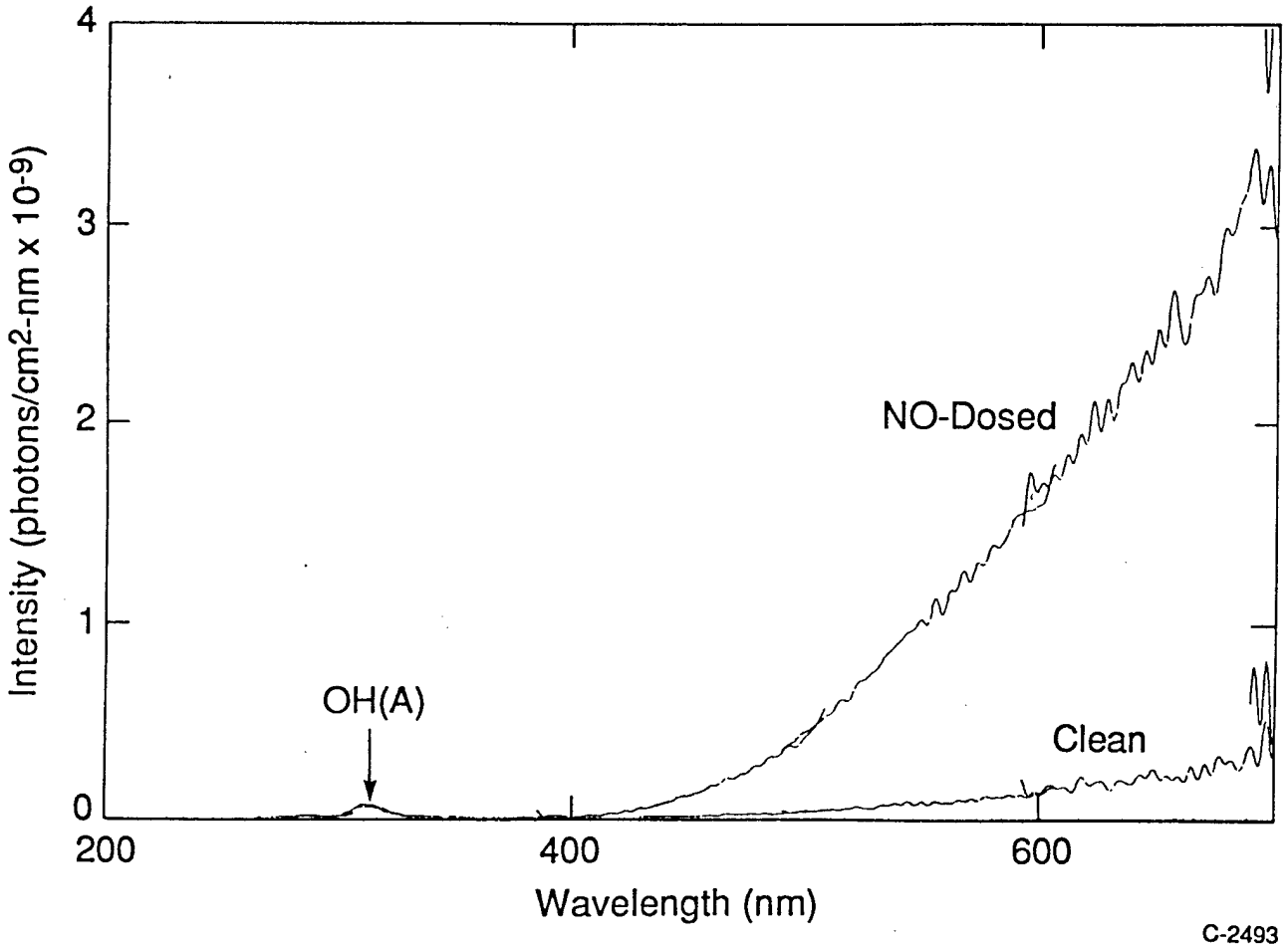

C-2493

PSI

OBSERVED ULTRAVIOLET SIGNATURES, CU SURFACE, O-BEAM, 8 km/s

T-14104

(Integrated Over 128 Pulses)

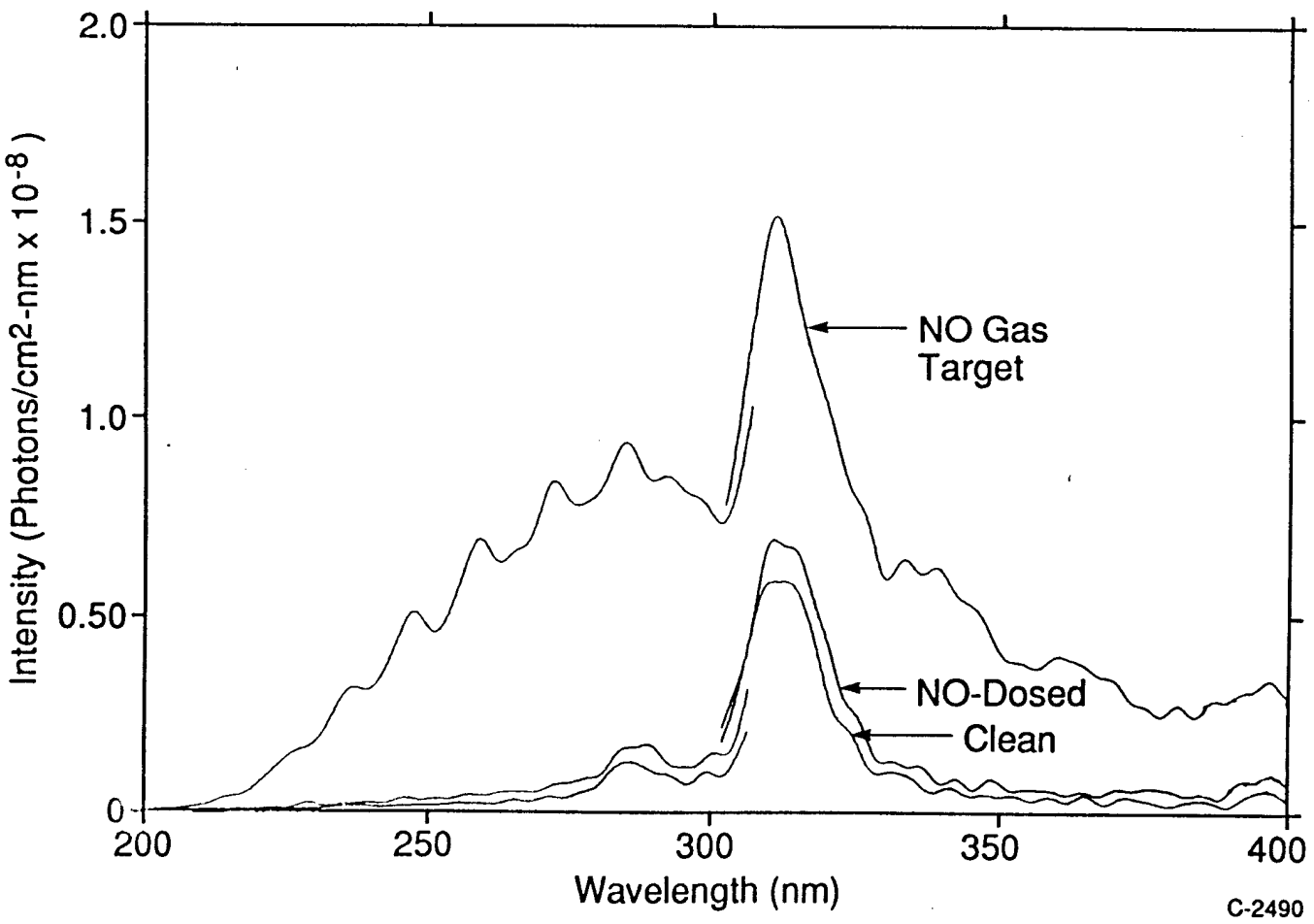

VUV SURFACE GLOW

T-22569

- One preliminary experimental study using PSI's pulsed atom source
  - — 8 km/s N beam, similar flux to O-beam
  - — searched for LBH emissions above surface with VUV diode array spectrometer, none observed

PSI

PHYSICAL SCIENCES INC.

WHERE DOES THE NO COME FROM?

T-22570

Several Suggestions

- Surface recombination of ambient N and O atoms
- N atom formation in ambient surface collisions, e.g., $N_2(\text{fast}) \xrightarrow{S} N + N$
- Reaction between incoming and scattered ambient species, e.g., $\vec{O} + \overleftarrow{N_2} \rightarrow NO + N$

PSI

PHYSICAL SCIENCES INC.

EFFECTIVE EXCITATION CROSS SECTIONS VERSUS O-ATOM VELOCITY

$O + N_2 \rightarrow NO(v,J) + N$

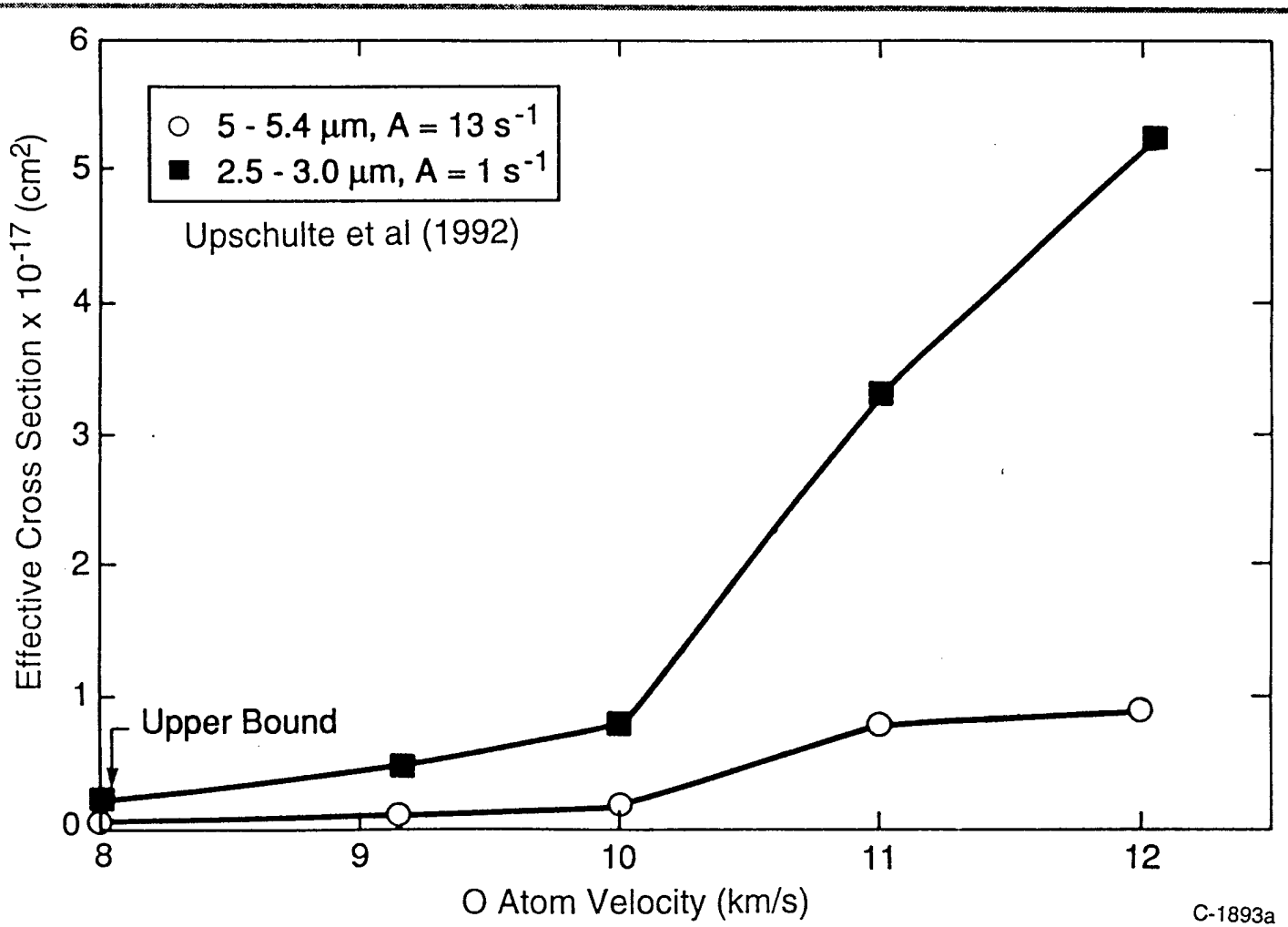

PSI

DETAILED KINETIC MECHANISM

T-22572

- Two limits for surface catalyzed recombination

$$A + B \xrightarrow{S} ? \rightarrow AB(gas)$$

  - Rideal Mechanism: recombination occurs between a surface absorbed species and an incident species
  - Langmuir-Hinshelwood Mechanism: recombination occurs between two surface adsorbed species

PSI

PHYSICAL SCIENCES INC.

SUGGESTED KINETIC PROCESSES FOR THE SHUTTLE GLOW MECHANISM (L-H)

T-19970

Reaction Type	Process	Kinetic Quantity
NO Formation	$\vec{O} + \vec{N}_2 \xrightarrow{\sigma} NO + N$	Cross section
Adsorption	$O(g) \xrightarrow{S_o} O(S)$ $NO(g) \xrightarrow{S_{NO}} NO(S)$	Sticking coefficient
Thermal Desorption	$O(S) \xrightarrow{\tau_o^{-1}} O(g)$ $NO(S) \xrightarrow{\tau_{NO}^{-1}} NO(g)$	Thermal desorption rate
Collisional Desorption	$O(g) + O(S) \xrightarrow{C'_o} 2O(g)$ $\longrightarrow O_2(g)$ $X(g) + O(S) \xrightarrow{C'_x} X(g) + O(g)$ $O(g) + NO(S) \xrightarrow{C_o} O(g) + NO(g)$ $\longrightarrow NO_2(g)$ $X(g) + NO(S) \xrightarrow{C_x} X(g) + NO(g)$	Collisional desorption efficiency
Surface Reaction	$O(S) + NO(S) \xrightarrow{R_{NO_2}} NO_2(g)$ $O(S) + O(S) \xrightarrow{R_{O_2}} O_2(g)$	Reaction rate

PSI

PHYSICAL SCIENCES INC

EXPERIMENT TO STUDY KINETICS OF NO ADSORPTION

T-19972

- Approach
  - — Expose anodized aluminum in vacuum to a background pressure of NO
  - — Use glow to monitor NO surface coverage by pulsing target with 8 km/s O-beam
  - — Vary NO pressure

- Projected kinetics, f = NO surface coverage

$$\frac{df}{dt} = \frac{(NO)}{N_s}\frac{\overline{C}}{4}S_{NO}(1-f) - \frac{f}{\tau_{NO}}$$

whence

$$f = \frac{S_{NO}(NO)\overline{C}/4}{S_{NO}(NO)\overline{C}/4 + \tau_{NO}^{-1}N_S}\left(1 - e^{-\left(\frac{(NO)}{N_S}\frac{\overline{C}}{4}S_{NO} + \tau_{NO}^{-1}\right)t}\right)$$

EXPERIMENTAL APPARATUS

T-8607

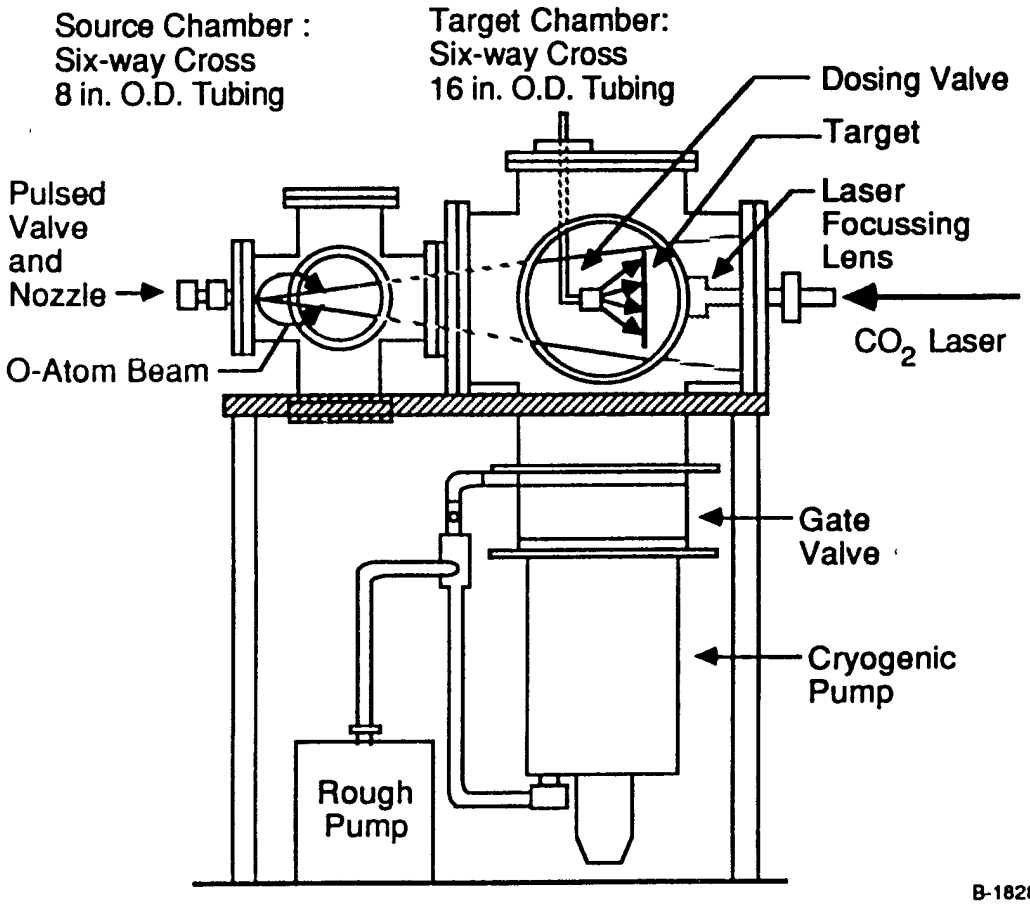

O + NO SURFACE AND GAS GLOW

T-22708

Top: O + NO surface glow

Bottom: O + NO gas glow

Pulse rate = 2 Hz

$P_{NO} = 3.7 \times 10^{-5}$ Torr

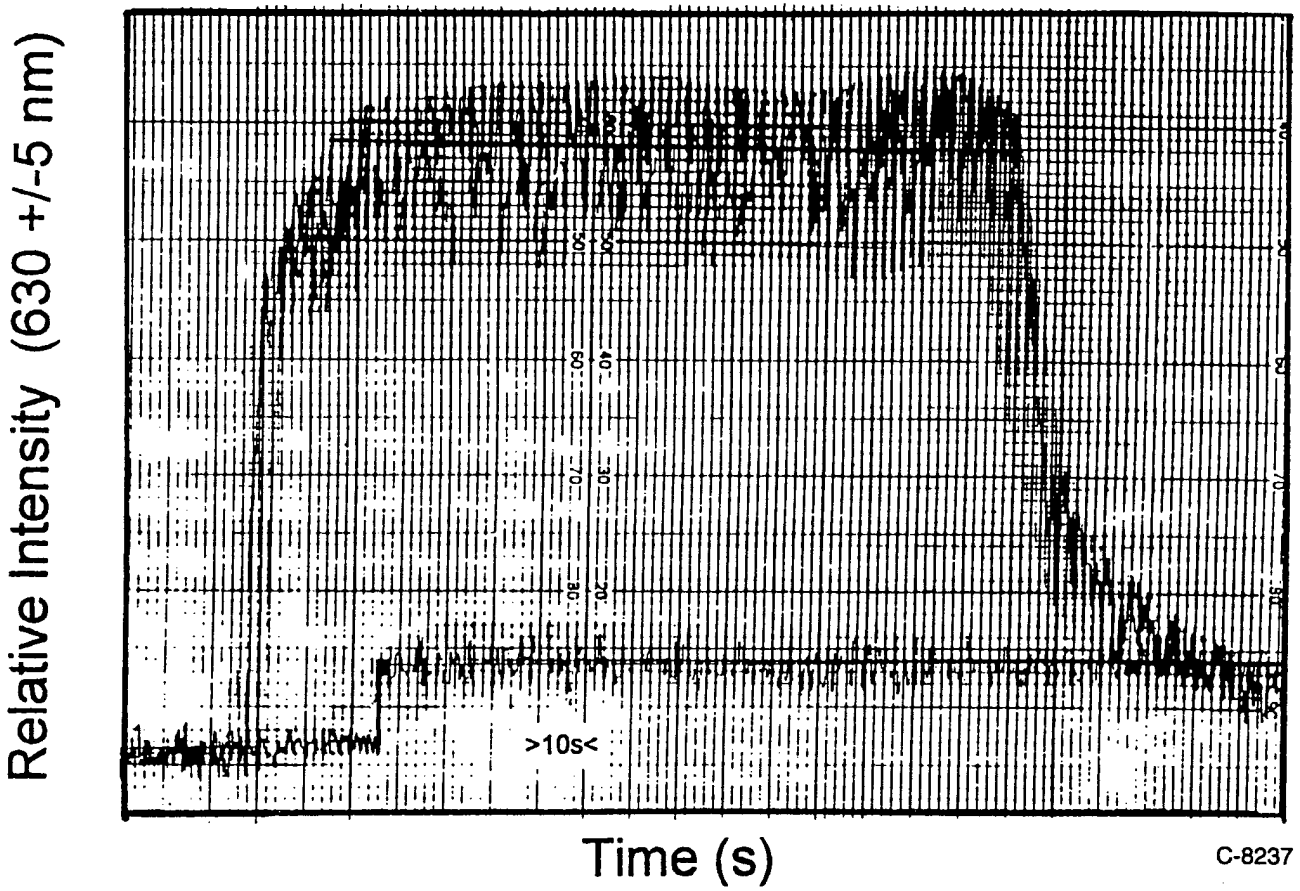

C-8237

PSI

PHYSICAL SCIENCES INC.

SATURATED GLOW INTENSITY VERSUS NO PRESSURE
8 km/s O-atom at 2 Hz, 3.6 x 10^{14}/cm^2, Anodized Al

T-19977

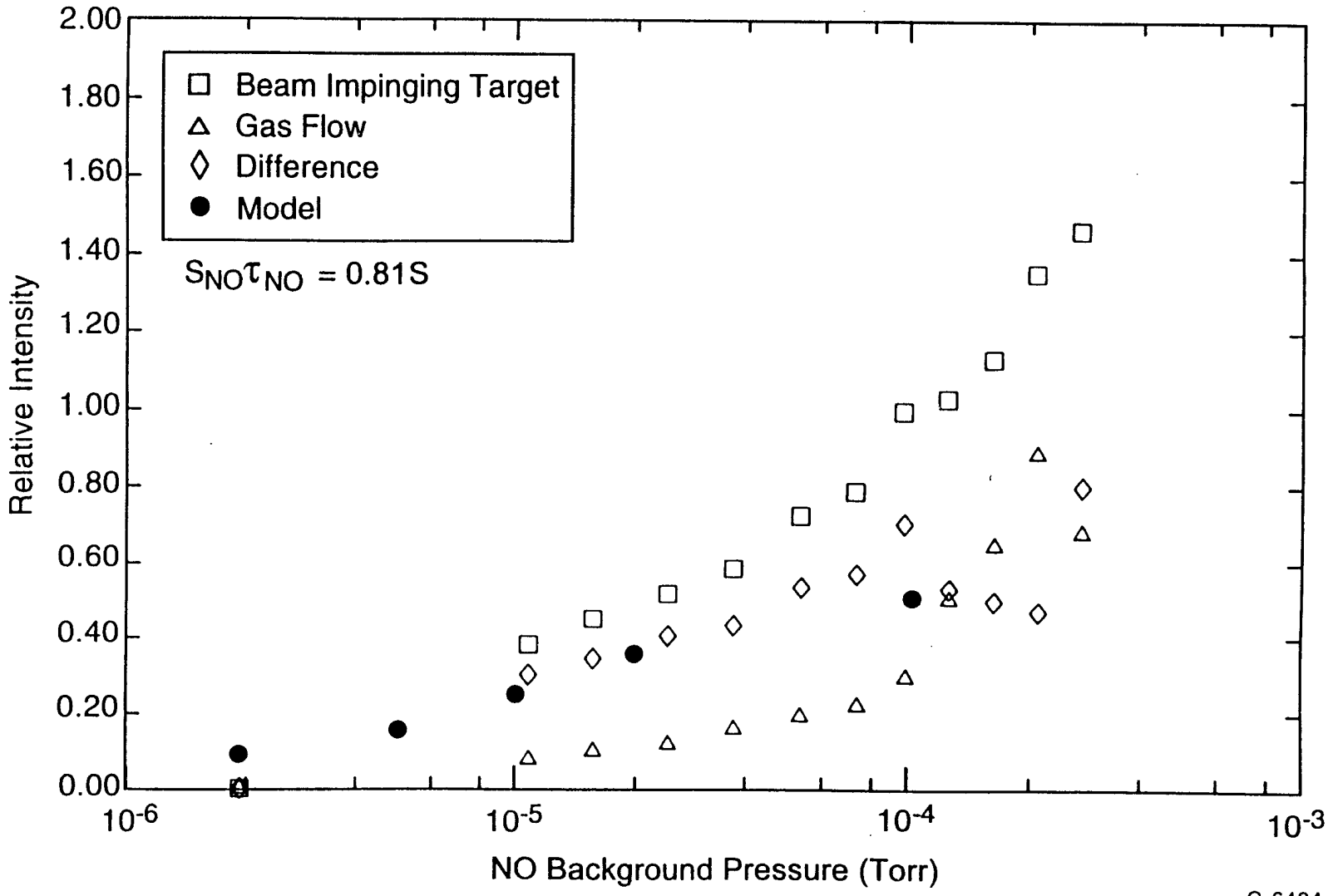

C-6494

NO DOPING STUDIES

T-22873

- Repeatable measurements at NO pressures of 1.4 x 10^{-5}, 2.3 x 10^{-5}, 3.7 x 10^{-5} Torr
- Gas background radiation ~15% of total
- E-fold times varies ~ inversely with pressure
  - — i.e., dominated by coverage, not thermal desorption
  - — 2 to 4.5 s at 2 Hz
  - — 1/2 Hz data unreliable
- Peak intensity varies by only 25% over pressure range
- τ NO < 4 s, => S_{NO} > 0.2, but ....

PSI

Physical Sciences Inc.

NO_2 DOPING STUDIES

T-22874

- Gas glow much stronger than equivalent NO case
  - — could not measure e-fold time to steady state
  - — glow decay after gas termination implies τ long
- Collisional scouring of NO_2 examined
  - — NO_2 removed by O twice as efficiently as NO

PSI

PHYSICAL SCIENCES INC.

NEW HYPOTHESIS FOR MECHANISM (To Be Validated)

T-19979

- Surface adsorbed NO and O form NO_2 on surface which remains adsorbed

- Incoming O atom collides with surface NO_2 in a knock-off or exchange reaction producing gaseous NO_2^*

ADDITIONAL CONFIRMING EVIDENCE FOR HYPOTHESIS

T-19974

- We have measured visible flows produced by 8 km/s O-atom impact on surfaces dosed with NO and with NO_2. **They are spectrally similar.**

- We have found the flow intensity increases strongly with increasing velocity -- unexpected for an L-H mechanism

- Mechanism can be consistent with observed density dependence

STATUS

T-22682

- Experimental observations have led to a new hypothesis for the shuttle glow mechanisms
  - combination Rideal and Langmuir-Hinshelwood
  - hypothesis consistent with ancillary data
  - additional experimental tests/validation of hypothesis required
- Hypothesis to be tested against flight data
  - validated temperature dependence valuable

PSI

PHYSICAL SCIENCES INC.

APPENDIX D

Studies of Visible Glow Mechanisms

Presented at ARO TI Meeting on
Computations of Hypersonic Flows and Radiation
5 December 1994

PSI
PHYSICAL SCIENCES INC.

VG94-233

STUDIES OF VISIBLE GLOW MECHANISMS

G.E. Caledonia
Physical Sciences Inc.
20 New England Business Center
Andover, MA 01810

Presented at ARO TI Meeting on
Computations of Hypersonic Flows and Radiation

5 December 1994

OVERVIEW

T-22561

- Clear Shuttle and Satellite evidence of glows due to surface-catalyzed reactions occurring in low earth orbit

  — $NO + O \xrightarrow{S} NO_2^*$

  $N + N \xrightarrow{S} N_2^*$

  Others ?

- Laboratory studies appropriate to elucidate mechanisms
  - — long history of surface catalyzed glow studies
  - — ability to vary key parameters
  - — simulation always an issue

PSI

PHYSICAL SCIENCES INC.

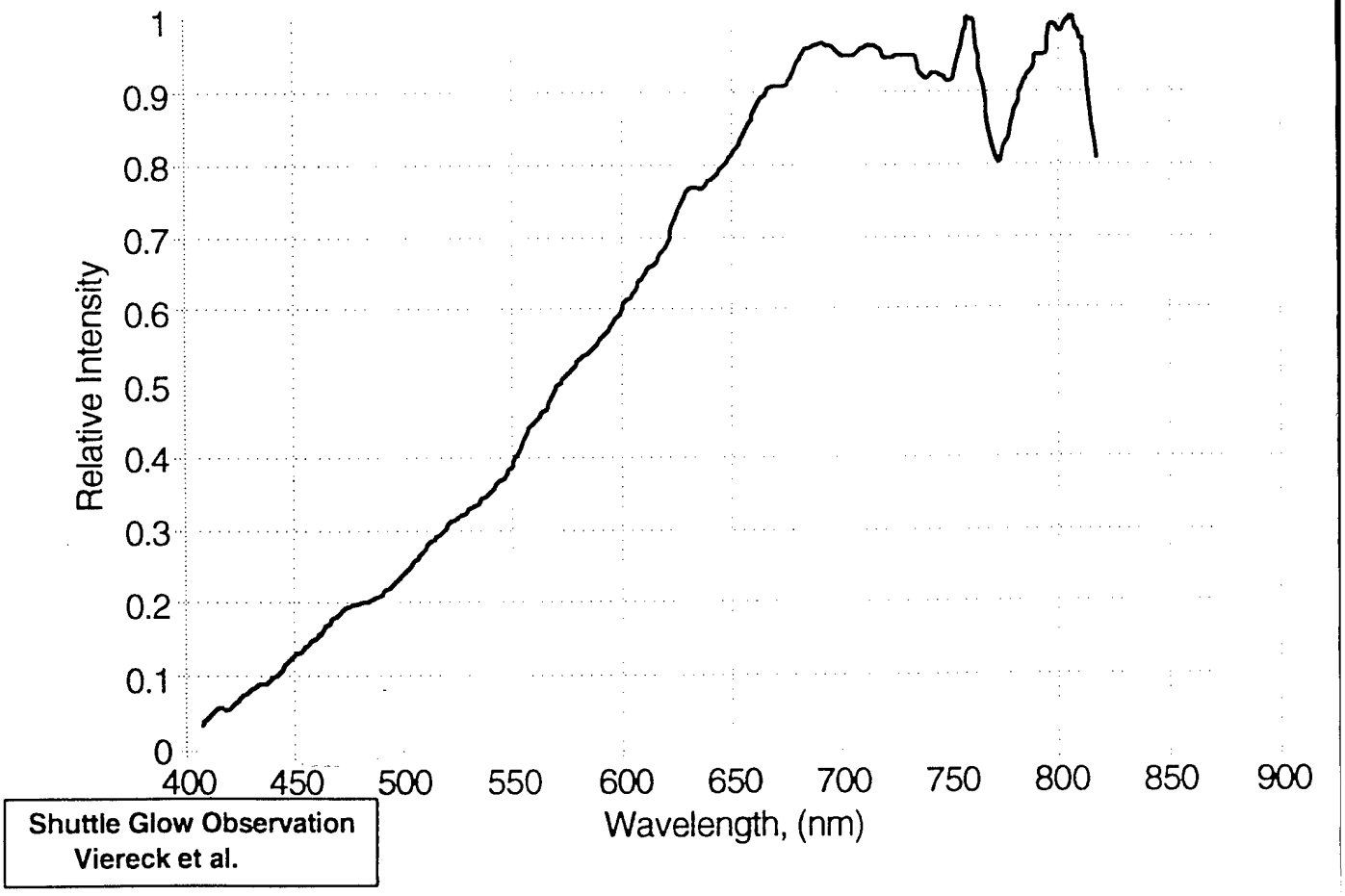
Relative Intensity
1
0.9
0.8
0.7
0.6
0.5
0.4
0.3
0.2
0.1
0
400
450
500
550
600
650
700
750
800
850
900
Wavelength, (nm)
Shuttle Glow Observation
Viereck et al.

NO_2^* CONTINUUM GLOW - THERMAL MEASUREMENTS

T-22562

- $NO + O + M \rightarrow NO_2^* + M$, the air afterglow, a yellow-green emission well studied and understood
- $NO + O \xrightarrow{S} NO_2^*$ produces red shifted continuum emission
  - — several studies since early 1960's
  - — measurements performed at 0.01 to 1 Torr
  - — kinetics confusing, competing processes, e.g.,
    - $NO + O \xrightarrow{S} NO_2^*$
    - $O + O \xrightarrow{S} O_2^*, O_2(A)$

      $O_2(A) + O_2 \rightarrow O_3^* + O$

      $O_3^* + NO \rightarrow NO_2^* + O_2$

PSI

PHYSICAL SCIENCES INC.

Thermal Measurements of O + NO

Recombination Glow

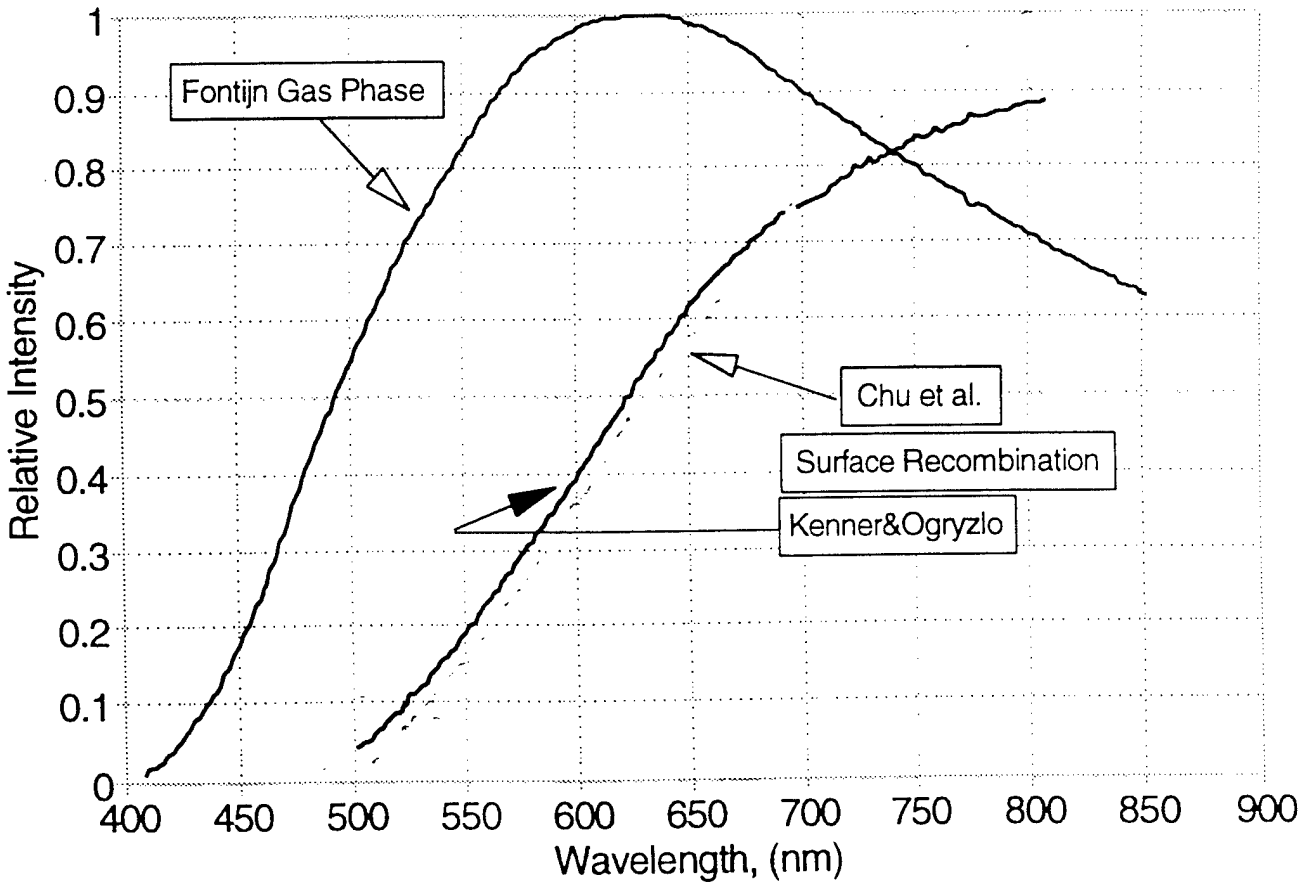

NO_2^* CONTINUUM GLOW - ~ 1 eV O-ATOM MEASUREMENTS

T-22563

- Typical maximum energy for discharge excited O_2/rare gas fast oxygen atom sources
- Directed O-atom source and effluent thermal NO source directed onto target
- Continuous fluxes $\lesssim 3 \times 10^{15}$ cm^{-2} s^{-1} at very low pressure, some V variation
- At least three recent studies in reasonable agreement
  - Arnold + Coleman (1988, 1991)
  - Ardebili et al. (1991)
  - Greer et al. (1993)

PSI
PHYSICAL SCIENCES INC.

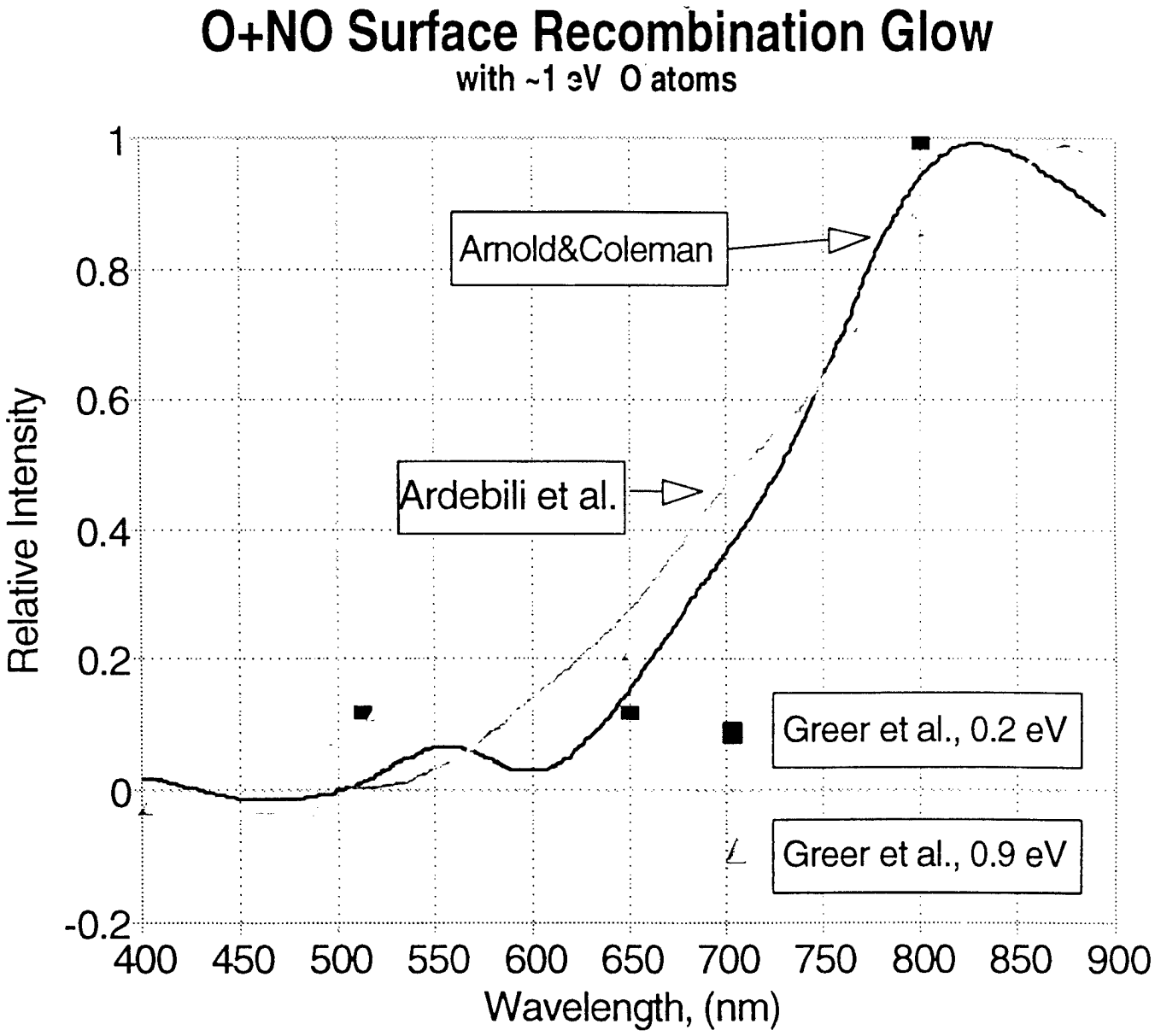
O+NO Surface Recombination Glow
with ~1 eV O atoms
Relative Intensity
1
0.8
0.6
0.4
0.2
0
-0.2
400
450
500
550
600
650
700
750
800
850
900
Wavelength, (nm)
Arnold&Coleman
Ardebili et al.
Greer et al., 0.2 eV
Greer et al., 0.9 eV

NO_2^* CONTINUUM GLOW - 5 eV O-ATOM MEASUREMENTS

T-22564

- LEO velocity simulation with "pure" O beams
- Two studies low flux, low pressure
- Caledonia et al. (1990) pulsed O-atom beam irradiated targets pre-dosed with NO
- Orient et al. (1990) CW O-atom beam with NO gas jet

PSI

PHYSICAL SCIENCES INC

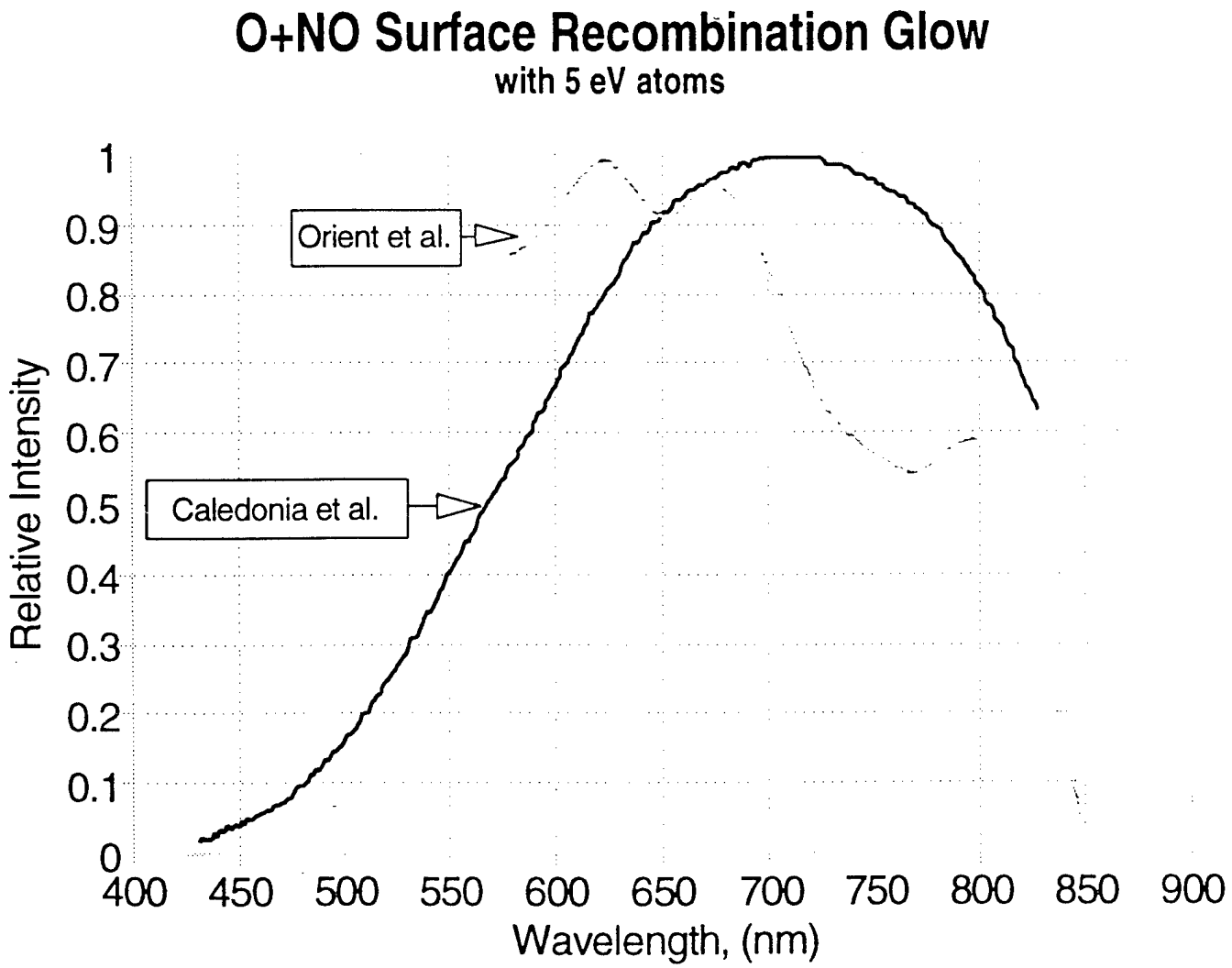
O+NO Surface Recombination Glow
with 5 eV atoms
Relative Intensity
Wavelength, (nm)
Orient et al.
Caledonia et al.
0
0.1
0.2
0.3
0.4
0.5
0.6
0.7
0.8
0.9
1
400
450
500
550
600
650
700
750
800
850
900

TEMPERATURE DEPENDENCE OF O + NO SURFACE GLOW LAB STUDIES, 5 eV O ATOMS

T-22565

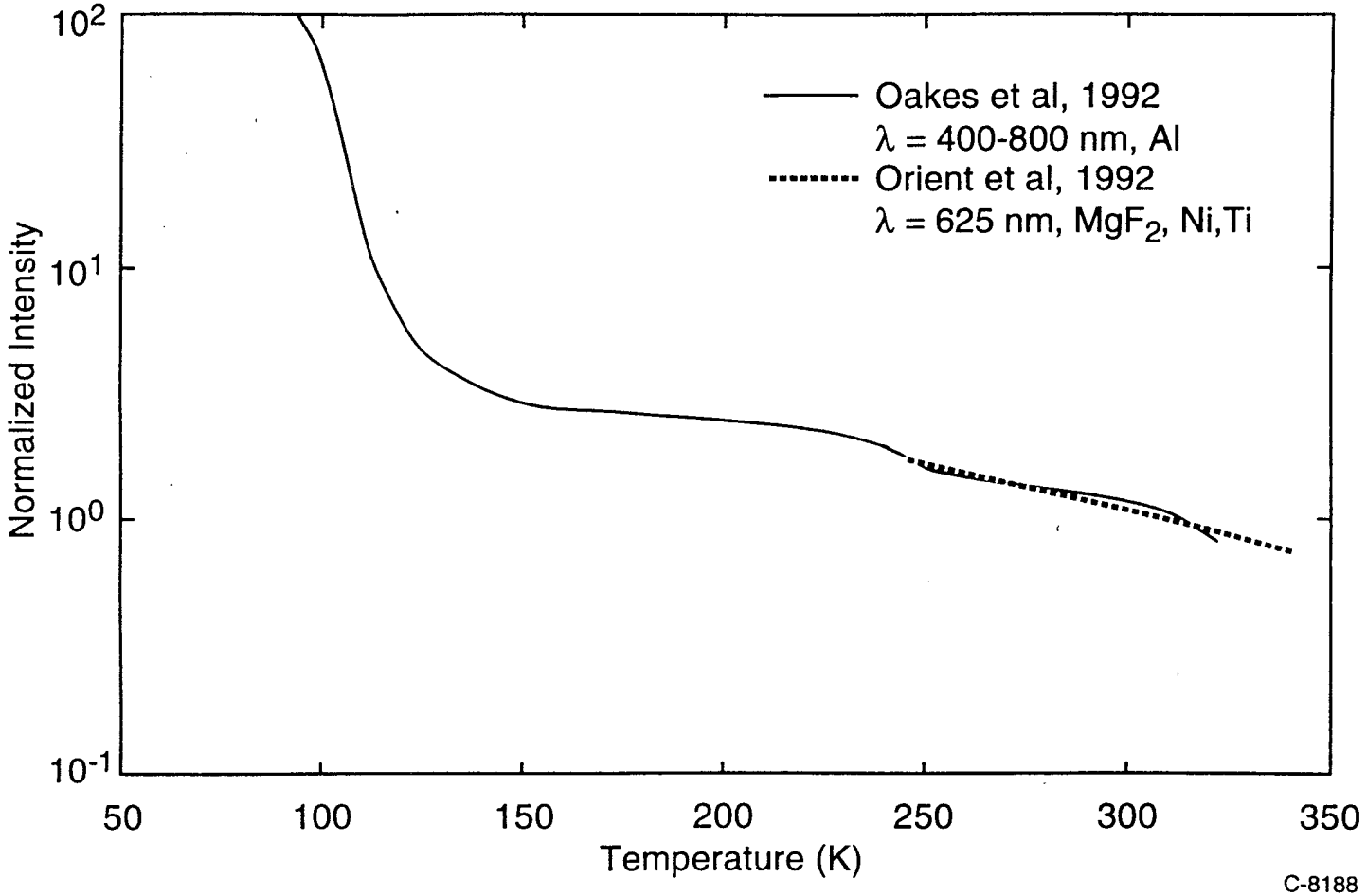

C-8188

PSI

PHYSICAL SCIENCES INC

TEMPERATURE DEPENDENCE OF O + NO SURFACE GLOW LAB STUDIES, 5 eV O-ATOMS

T-22679

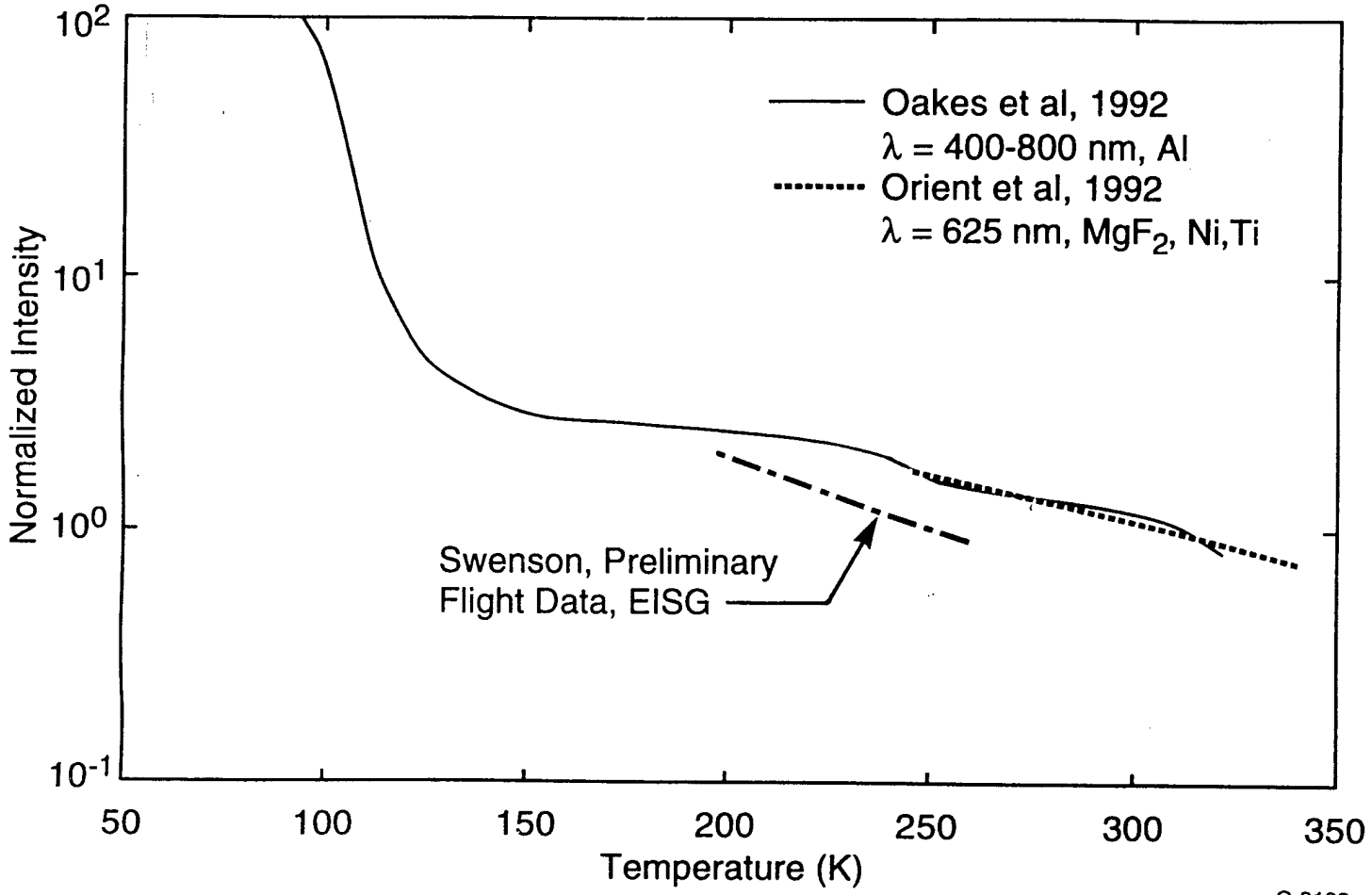

C-8188a

PSI

UV SURFACE GLOW

T-22566

- No clear ID of source of UV surface glow

- Conflicting lab data on O + NO emissions in the UV
  - 1 eV studies do not see UV emissions
  - 5 eV CW studied (Orient et al., 1992) observed UV emissions one-fifth of visible
  - 5 eV pulsed study (Caledonia et al., 1993) observed no significant UV emissions

PSI

PHYSICAL SCIENCES INC.

GLOW SPECTRA PRODUCED IN COLLISIONS OF 5 eV O-ATOMS WITH MgF_2, Ni + Ti SURFACES WITH ADSORBED NO

Orient et al. (1992)

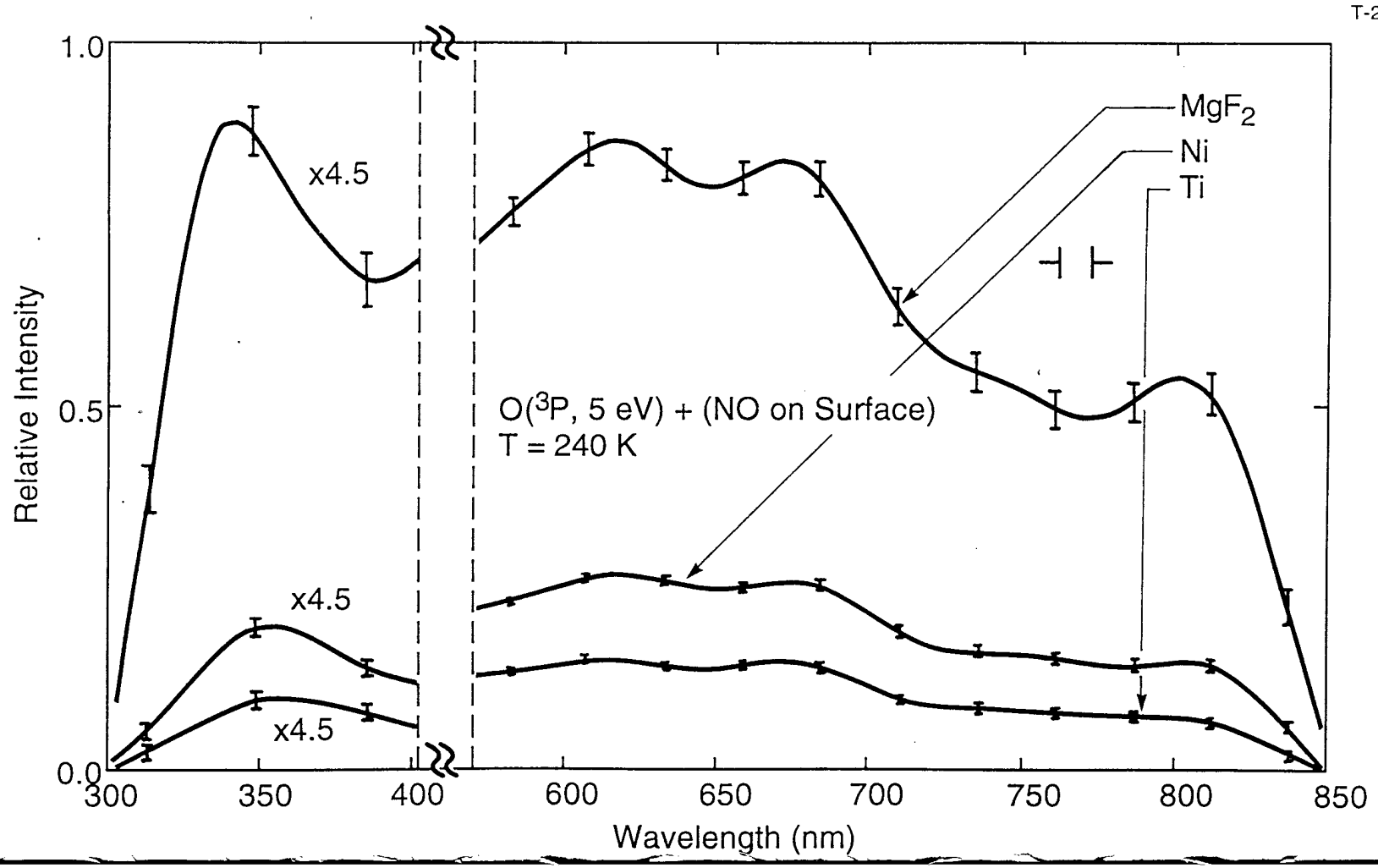

OBSERVED GLOW ABOVE COPPER SURFACE
PULSED O-BEAM, 8 km/s
(integrated over 128 pulses)

T-22568

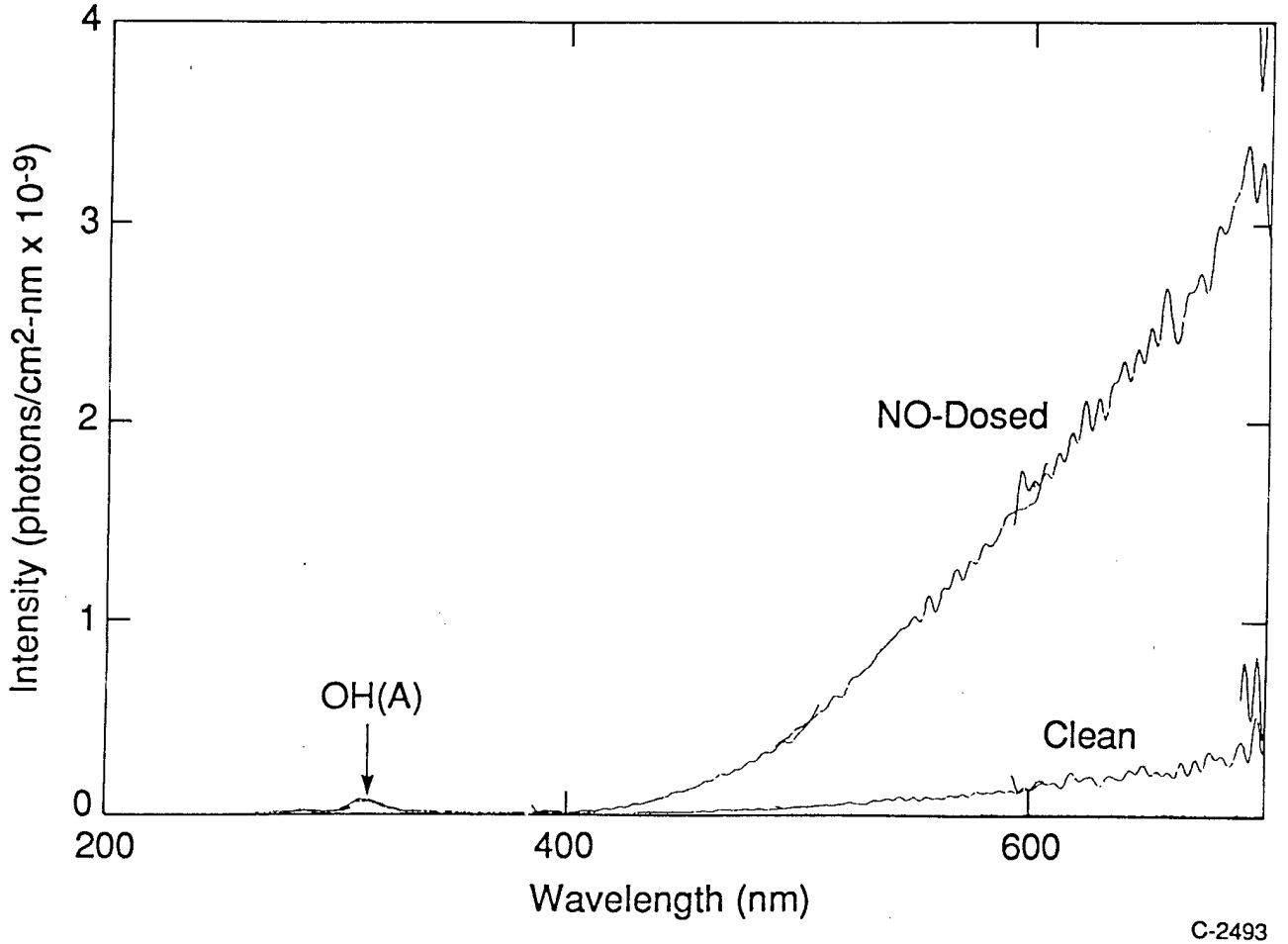

C-2493

PSI

Physical Sciences Inc

OBSERVED ULTRAVIOLET SIGNATURES, CU SURFACE, O-BEAM, 8 km/s

T-14104

(Integrated Over 128 Pulses)

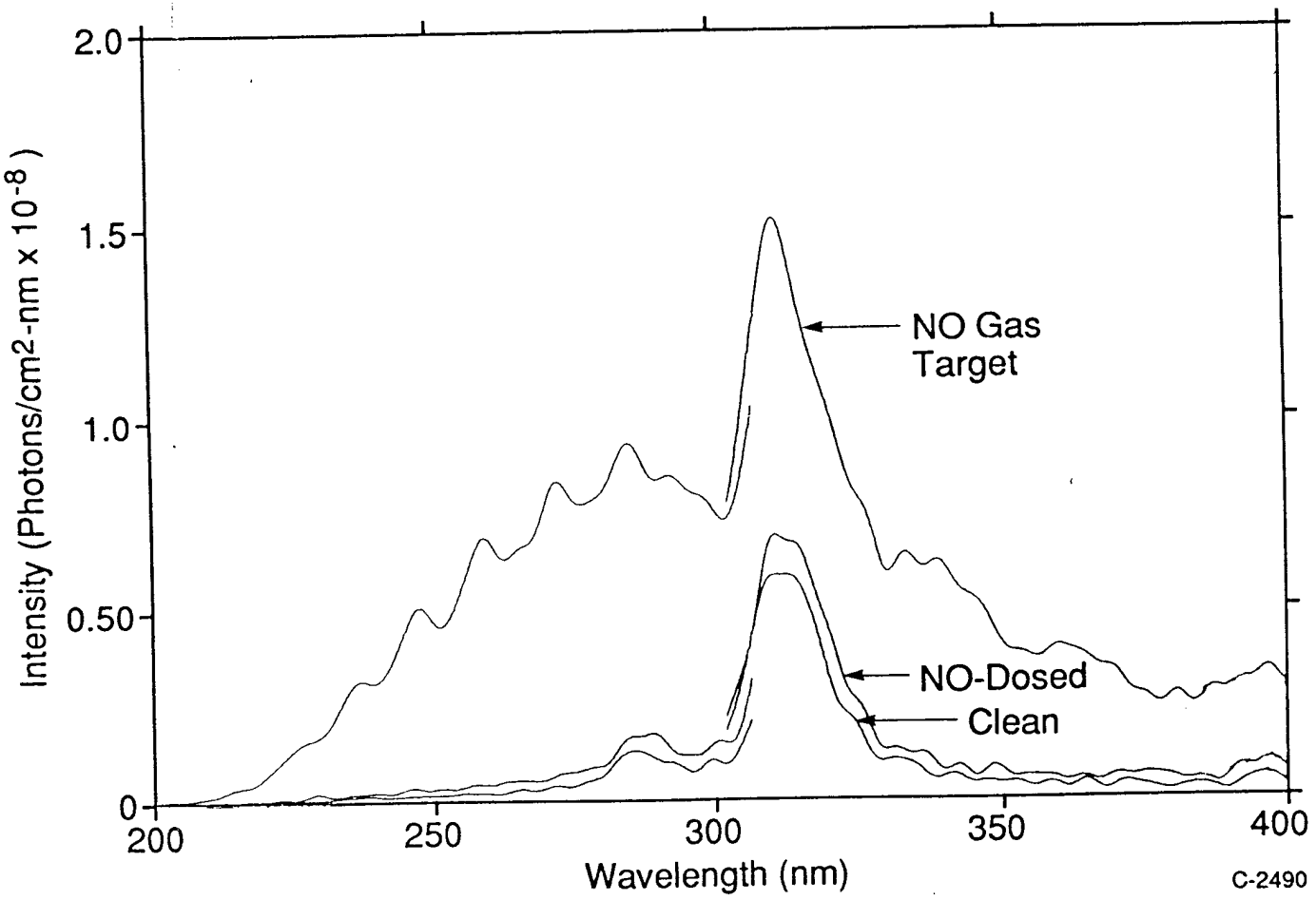

VUV SURFACE GLOW

T-22569

- One preliminary experimental study using PSI's pulsed atom source
  - — 8 km/s N beam, similar flux to O-beam
  - — searched for LBH emissions above surface with VUV diode array spectrometer, none observed

PSI

PHYSICAL SCIENCES INC

WHERE DOES THE NO COME FROM?

T-22570

Several Suggestions

- Surface recombination of ambient N and O atoms
- N atom formation in ambient surface collisions, e.g., $N_2(\text{fast}) \xrightarrow{S} N + N$
- Reaction between incoming and scattered ambient species, e.g., $\vec{O} + \overleftarrow{N_2} \rightarrow NO + N$

PSI

PHYSICAL SCIENCES INC.

EFFECTIVE EXCITATION CROSS SECTIONS VERSUS O-ATOM VELOCITY

$O + N_2 \rightarrow NO(v,J) + N$

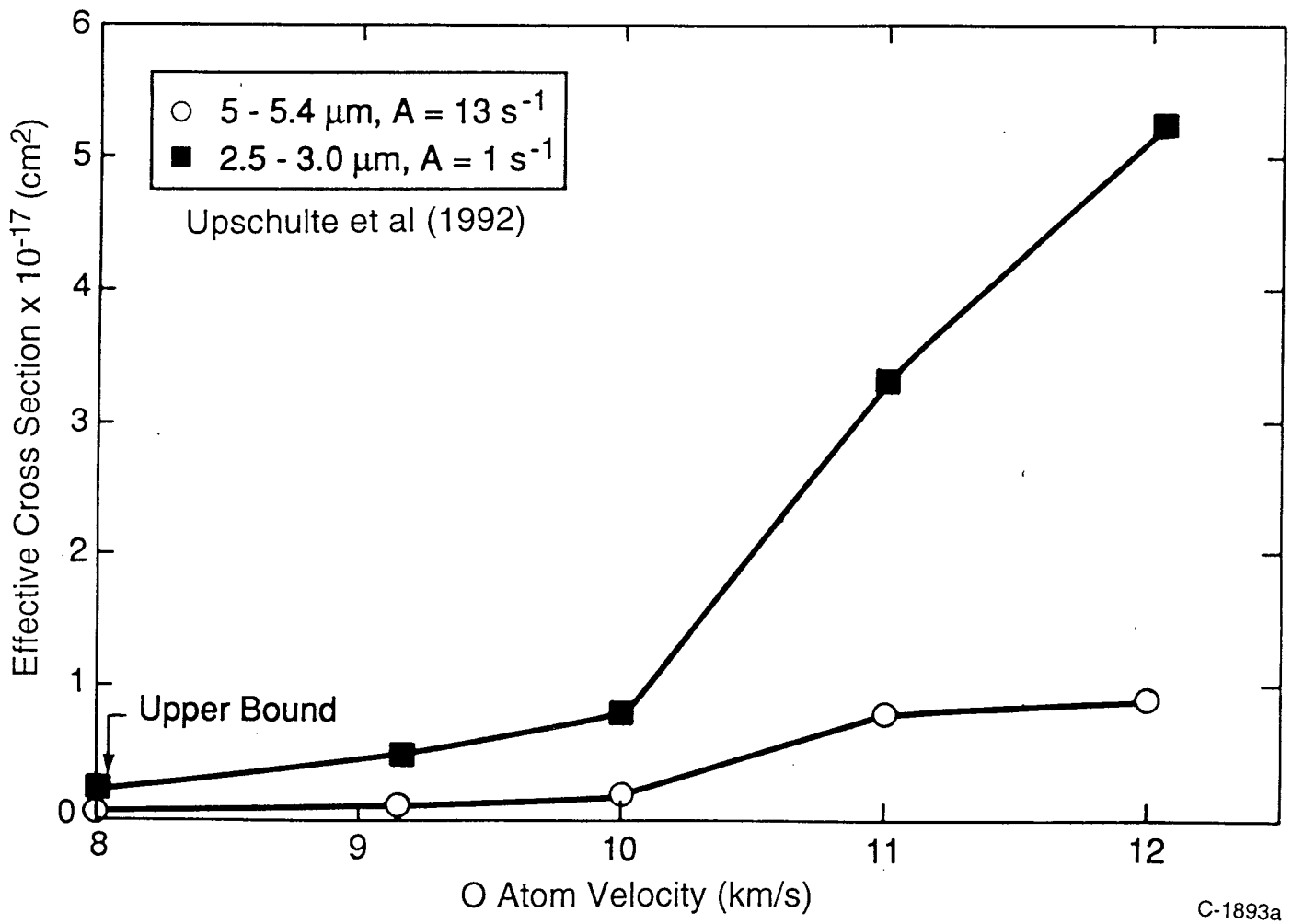

C-1893a

PSI

Physical Sciences Inc

DETAILED KINETIC MECHANISM

T-22572

- Two limits for surface catalyzed recombination

$$A + B \xrightarrow{S} ? \rightarrow AB(gas)$$

  - — Rideal Mechanism: recombination occurs between a surface absorbed species and an incident species
  - — Langmuir-Hinshelwood Mechanism: recombination occurs between two surface adsorbed species

SUGGESTED KINETIC PROCESSES FOR THE SHUTTLE GLOW MECHANISM (L-H)

T-19970

Reaction Type	Process	Kinetic Quantity
NO Formation	$\vec{O} + \vec{N}_2 \xrightarrow{\sigma} NO + N$	Cross section
Adsorption	$O(g) \xrightarrow{S_o} O(S)$ $NO(g) \xrightarrow{S_{NO}} NO(S)$	Sticking coefficient
Thermal Desorption	$O(S) \xrightarrow{\tau_o^{-1}} O(g)$ $NO(S) \xrightarrow{\tau_{NO}^{-1}} NO(g)$	Thermal desorption rate
Collisional Desorption	$O(g) + O(S) \xrightarrow{C'_o} 2O(g)$ $\longrightarrow O_2(g)$ $X(g) + O(S) \xrightarrow{C'_x} X(g) + O(g)$ $O(g) + NO(S) \xrightarrow{C_o} O(g) + NO(g)$ $\longrightarrow NO_2(g)$ $X(g) + NO(S) \xrightarrow{C_x} X(g) + NO(g)$	Collisional desorption efficiency
Surface Reaction	$O(S) + NO(S) \xrightarrow{R_{NO_2}} NO_2(g)$ $O(S) + O(S) \xrightarrow{R_{O_2}} O_2(g)$	Reaction rate

PSI

PHYSICAL SCIENCES INC

MASTER EQUATIONS FOR MONOLAYER COVERAGE

T-19971

- $1 = g_O + g_{NO} + g_{void}$

  F_{NO} = Gaseous NO production rate

  — $dg_{NO}/dt = F_{NO}S_{NO}(1-g_O-g_{NO})/N_S - g_{NO}/\tau_{NO}$
  $-(F_OC_O + F_xC_x)g_{NO}/N_s - g_{NO}g_OR_{NO_2}$

  — $dg_o/dt = F_OS_O(1-g_O-g_{NO})/N_S - g_O/\tau_O$
  $-(F_OC'_O + F_xC'_x)g_O/N_s - g_{NO}g_OR_{NO_2} - g_O^2R_{O_2}$

- Example steady state solution (uncoupled)

$$g_{NO} = \frac{F_{NO}S_{NO}(1-g_O)/N_s}{F_{NO}S_{NO}/N_S + t_{NO}^{-1} + F_OC_O/N_S + F_xC_x/N_S + g_OR_{NO_2}}$$

EXPERIMENT TO STUDY KINETICS OF NO ADSORPTION

T-19972

- Approach
  - — Expose anodized aluminum in vacuum to a background pressure of NO
  - — Use glow to monitor NO surface coverage by pulsing target with 8 km/s O-beam
  - — Vary NO pressure

- Projected kinetics, f = NO surface coverage

$$\frac{df}{dt} = \frac{(NO)\,\bar{C}}{N_S}\frac{}{4} S_{NO}(1-f) - \frac{f}{\tau_{NO}}$$

whence

$$f = \frac{S_{NO}(NO)\bar{C}/4}{S_{NO}(NO)\bar{C}/4 + \tau_{NO}^{-1}N_S}\left(1 - e^{-\left(\frac{(NO)\,\bar{C}}{N_S}\frac{}{4} S_{NO} + \tau_{NO}^{-1}\right)t}\right)$$

EXPERIMENTAL APPARATUS

T-8607

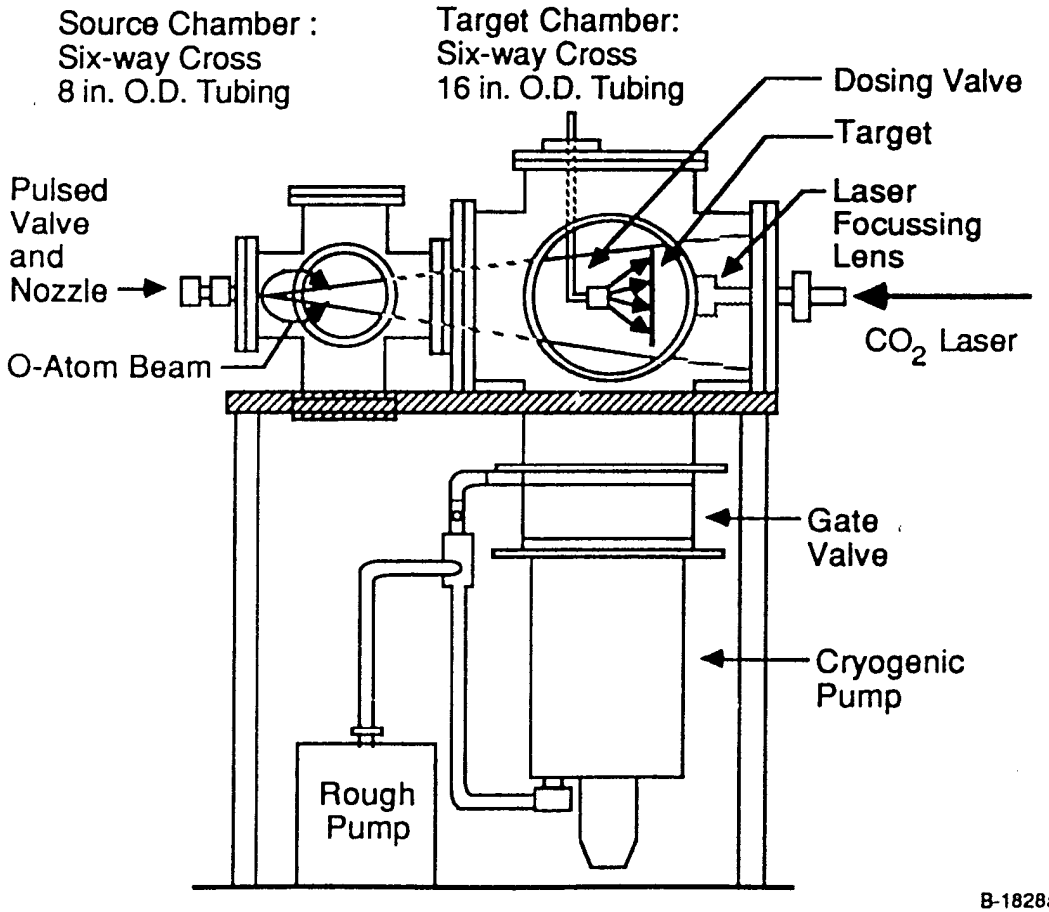

O + NO SURFACE AND GAS GLOW

T-22708

Top: O + NO surface glow
Bottom: O + NO gas glow

Pulse rate = 2 Hz
$P_{NO} = 3.7 \times 10^{-5}$ Torr

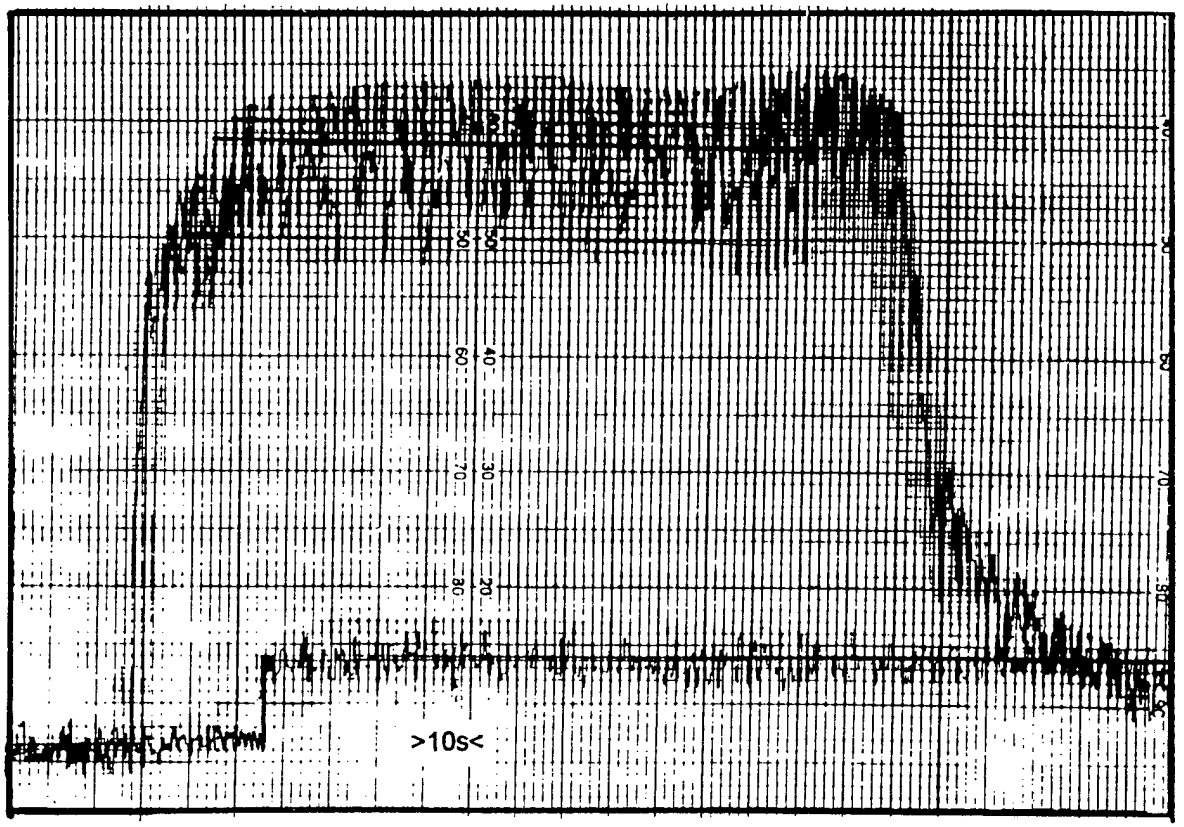

C-8237

PSI
PHYSICAL SCIENCES INC.

SATURATED GLOW INTENSITY VERSUS NO PRESSURE
8 km/s O-atom at 2 Hz, 3.6 x 10^{14}/cm^2, Anodized Al

T-19977

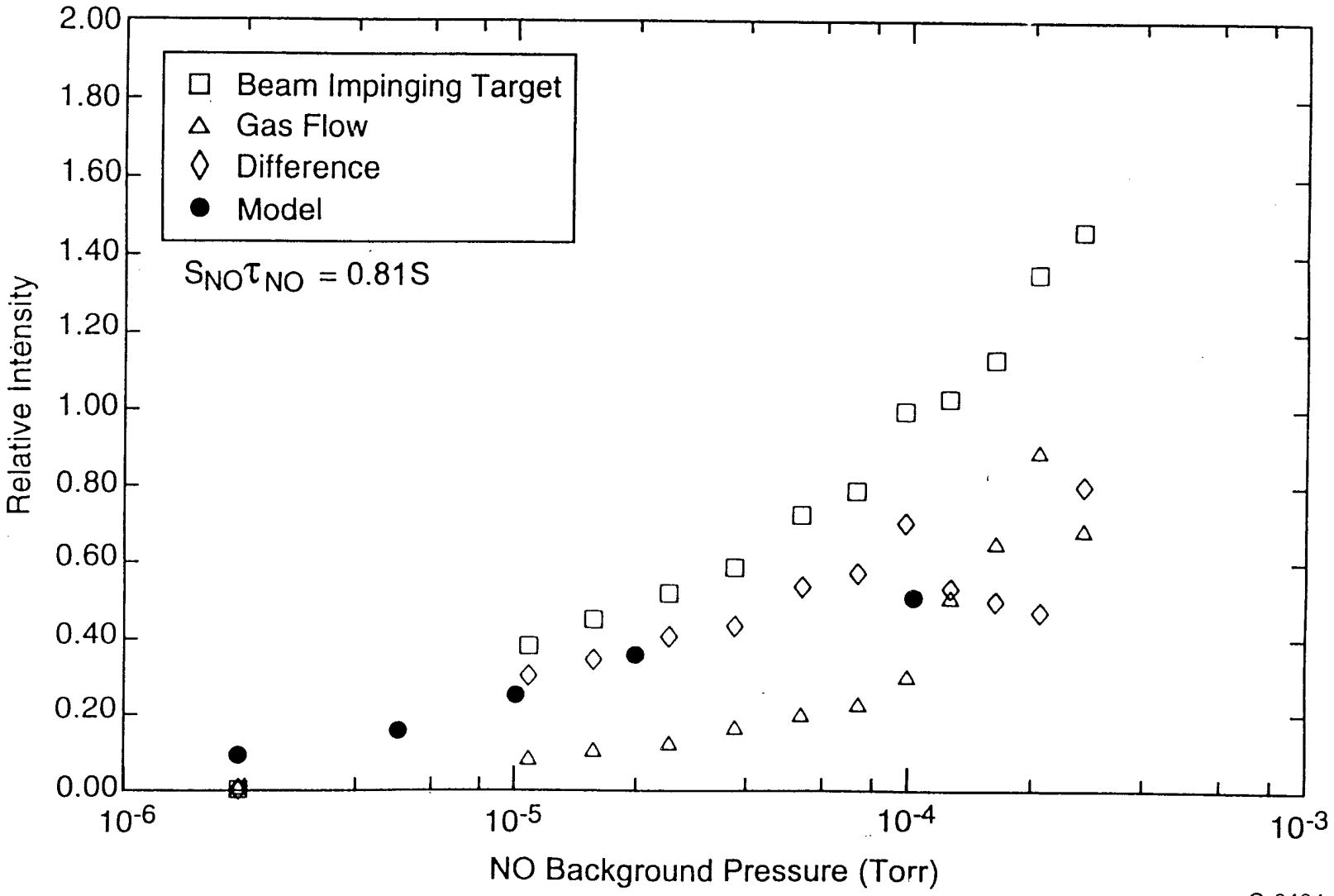

C-6494

NO DOPING STUDIES

T-22873

- Repeatable measurements at NO pressures of 1.4 x 10^{-5}, 2.3 x 10^{-5}, 3.7 x 10^{-5} Torr
- Gas background radiation ~15% of total
- E-fold times varies ~ inversely with pressure
  - — i.e., dominated by coverage, not thermal desorption
  - — 2 to 4.5 s at 2 Hz
  - — 1/2 Hz data unreliable
- Peak intensity varies by only 25% over pressure range
- τ NO < 4 s, => S_{NO} > 0.2, but ....

PSI

PHYSICAL SCIENCES INC

NO_2 DOPING STUDIES

T-22874

- Gas glow much stronger than equivalent NO case
  - — could not measure e-fold time to steady state
  - — glow decay after gas termination implies τ long
- Collisional scouring of NO_2 examined
  - — NO_2 removed by O twice as efficiently as NO

PSI

PHYSICAL SCIENCES INC.

NEW HYPOTHESIS FOR MECHANISM (To Be Validated)

T-19979

- Surface adsorbed NO and O form NO_2 on surface which remains adsorbed

- Incoming O atom collides with surface NO_2 in a knock-off or exchange reaction producing gaseous NO_2^*

ADDITIONAL CONFIRMING EVIDENCE FOR HYPOTHESIS

T-19974

- We have measured visible flows produced by 8 km/s O-atom impact on surfaces dosed with NO and with NO_2. **They are spectrally similar.**

- We have found the flow intensity increases strongly with increasing velocity -- unexpected for an L-H mechanism

- Mechanism can be consistent with observed density dependence

STATUS

T-22682

- Experimental observations have led to a new hypothesis for the shuttle glow mechanisms
  - — combination Rideal and Langmuir-Hinshelwood
  - — hypothesis consistent with ancillary data
  - — additional experimental tests/validation of hypothesis required

- Hypothesis to be tested against flight data
  - — validated temperature dependence valuable

PSI

PHYSICAL SCIENCES INC.

EXPERIMENTAL INVESTIGATION OF SPACECRAFT GLOW (EISG)

T-22573

- Shuttle experiment directed by G. Swenson, LMSC
- Flown on STS-62, March 1994
- Purpose: understanding of physical processes leading to spacecraft glow
  - FUV, visible and IR diagnostics
  - altitude effects examined by stepped circular and elliptical orbits
  - sample temperature effects
  - study effects of N_2 ram release on glow

PSI

PHYSICAL SCIENCES INC.

KEY FINDINGS

T-22574

1. The N_2 LBH bands were not observed in the 1450 to 2000Å region; sensitivity was sufficient to observe then

2. A bright structured glow was observed in the 2200 to 2800Å region
   — related to thruster firing although seen at all times
   — also apparent enhancements in oxygen green and red lines with thruster firings

3. NO_2 glow scales with O-atom concentration from roughly 310 to 220 km but then falls below
   — different from AE observations

4. Visible glow intensity increases 2%/degree between -15, -60° C

5. N_2 blowing above surfaces "quenches" glow
   — thick target

PSI
PHYSICAL SCIENCES INC.

EISG VISIBLE GLOW OBSERVATIONS

T-22576

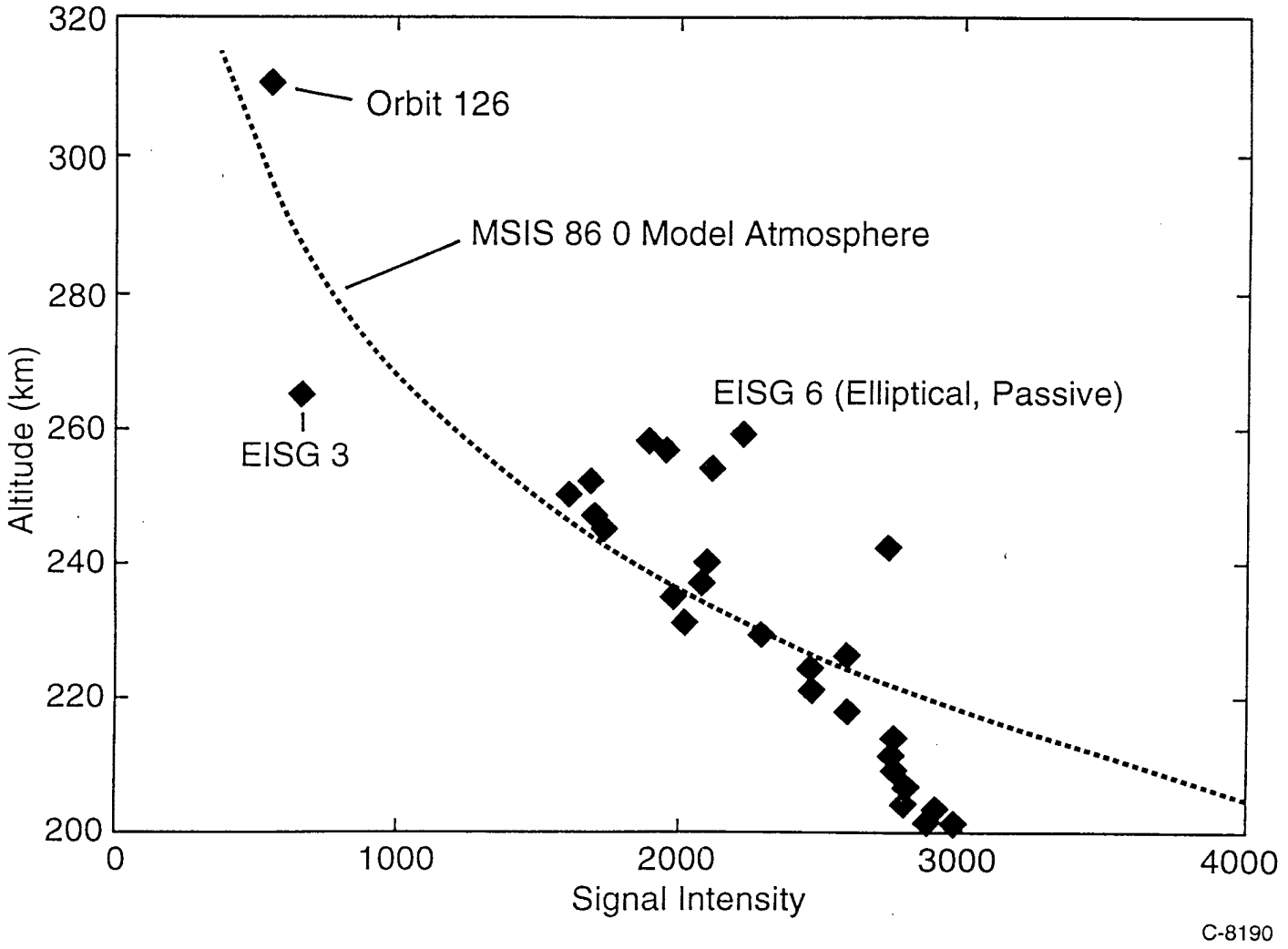

C-8190

EISG FO#7 FAR UV SPECTRUM

T-22575

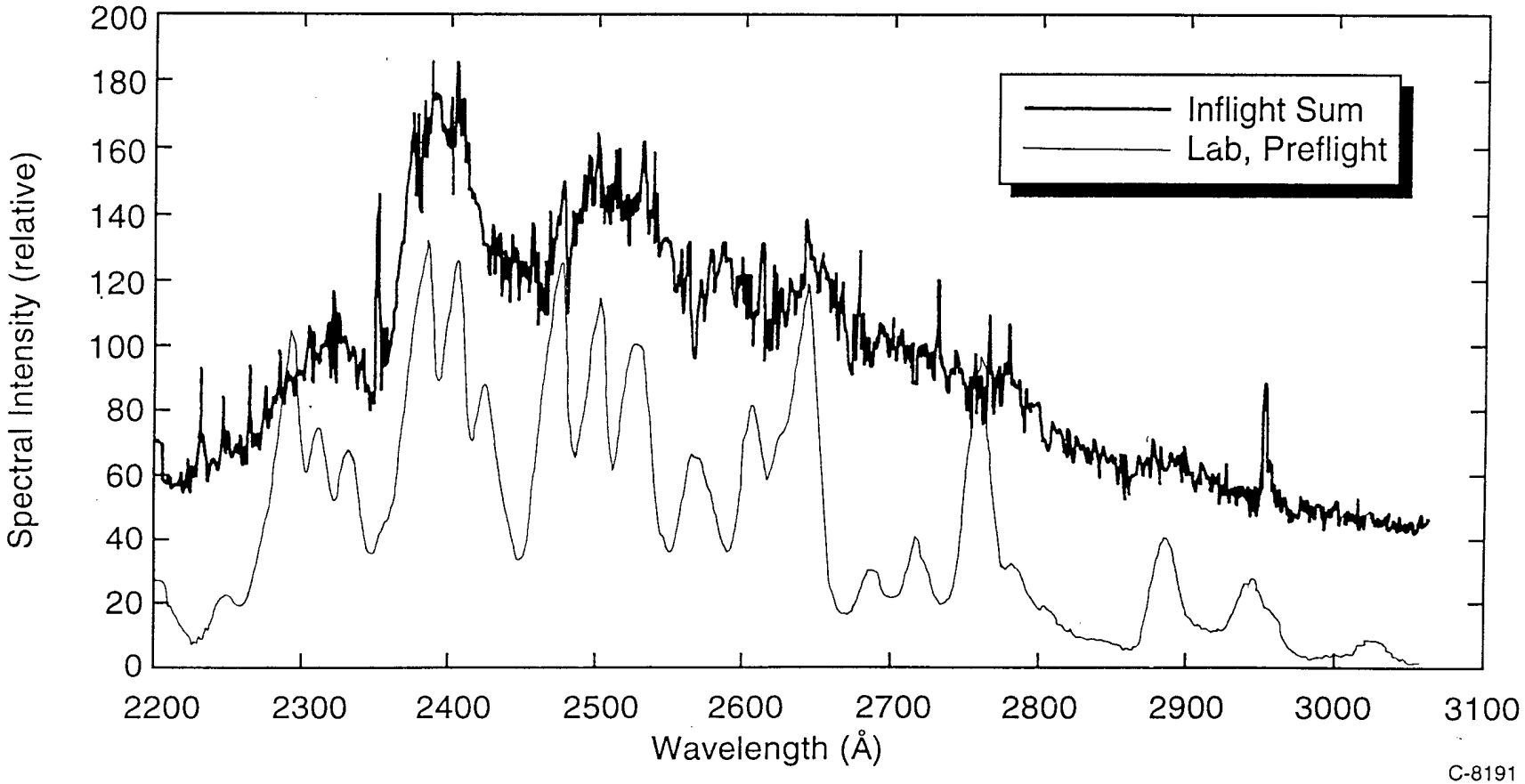

C-8191

CAUTIONS/EISG

T-22624

1. The previous LBH emissions were observed only at 220 km and below on S3-4, a 1 M size satellite

2. The EISG NO_2 glow appears diminished at altitudes below 220 km. Size effect?
   — no diminishment seen on smaller AE

3. If size effect is valid, SKIPPER is more like S3-4 than shuttle

4. The 120 to 200 nm photometer showed signal

PSI
PHYSICAL SCIENCES INC.

APPENDIX E

Visible Shuttle Glow: Gleanings

Presented at ARO TI Meeting
BMDO Missile Signature and Aerothermochemistry Program
22 April 1996

PSI

PHYSICAL SCIENCES INC.

VG96-037

Visible Shuttle Glow: Gleanings

G.E. Caledonia
Physical Sciences Inc.
20 New England Business Center
Andover, MA 01810

Presented at ARO TI Meeting
BMDO Missile Signature and
Aerothermochemistry Program

22 April 1996

Outline

96-1050

- Overview
- Altitude dependence
- N, NO production
- Kinetic model
- Flight predictions
- Temperature dependence

PSI

PHYSICAL SCIENCES INC.

The Visible Shuttle Glow

96-1051

- Broad continuum visible to infrared
- Observed on shuttle, satellites
- Studied in numerous laboratory experiments
- Established to be the result of surface catalyzed $O + NO \rightarrow NO_2^*$
  - — apparent o-atom velocity dependent
  - — material and temperature dependent

PSI

PHYSICAL SCIENCES INC.

Thermal Measurements of O + NO Recombination Glow

96-1052

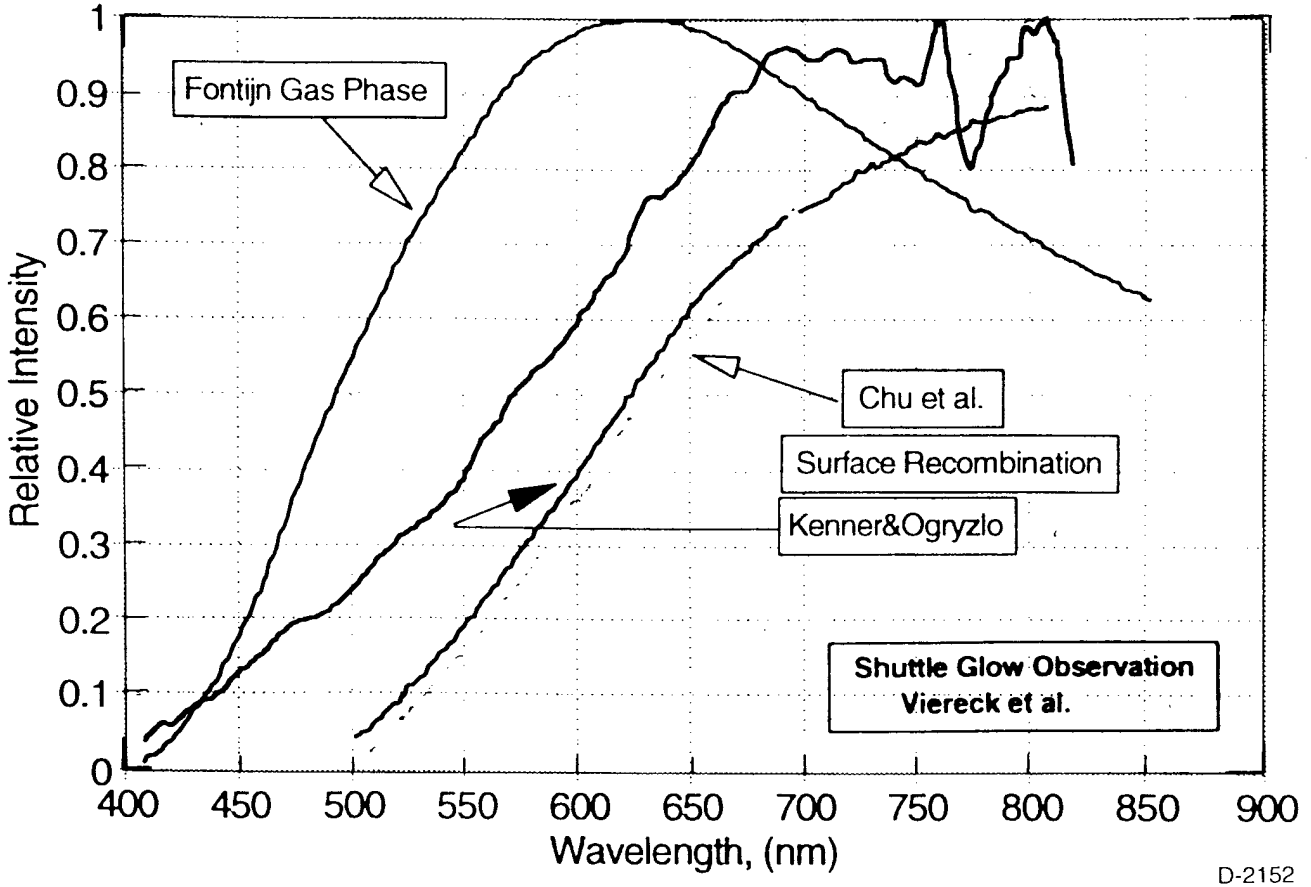

D-2152

PSI

Physical Sciences Inc.

Glow Altitute Dependence

96-1053

- Many flight measurements

- Only two provide altitude variation on same flight
  - — atmosphere explorer (-C, -E)
  - — STS-62, Experimental Investigation of Spacecraft Glow (EISG)

PSI

PHYSICAL SCIENCES INC.

Atmosphere Explorer Glow Data (Yee and Abreu, 1983)

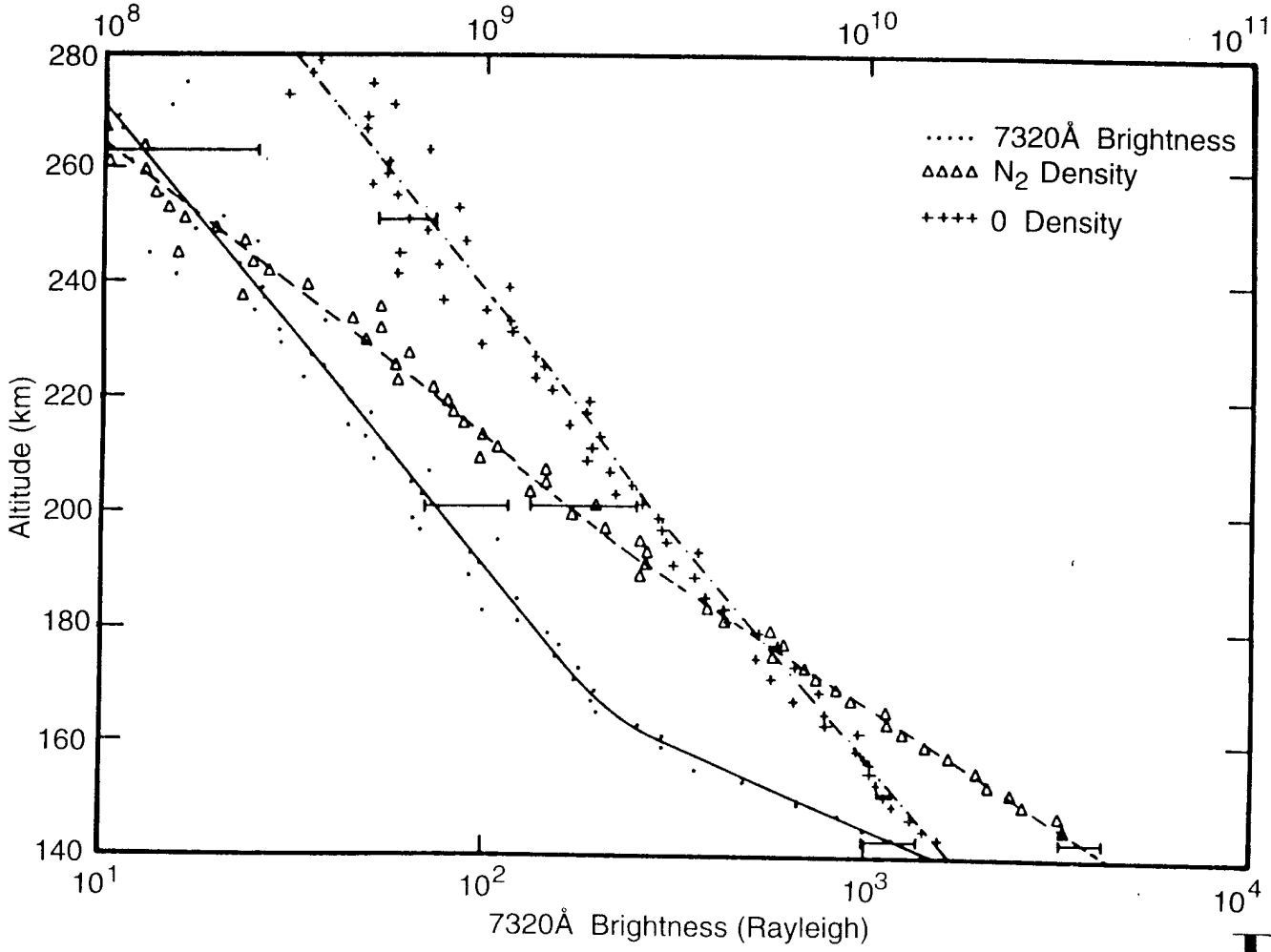

PSI

PHYSICAL SCIENCES INC.

EISG Visible Glow Observations (Swenson et. al., 1995)

96-1055

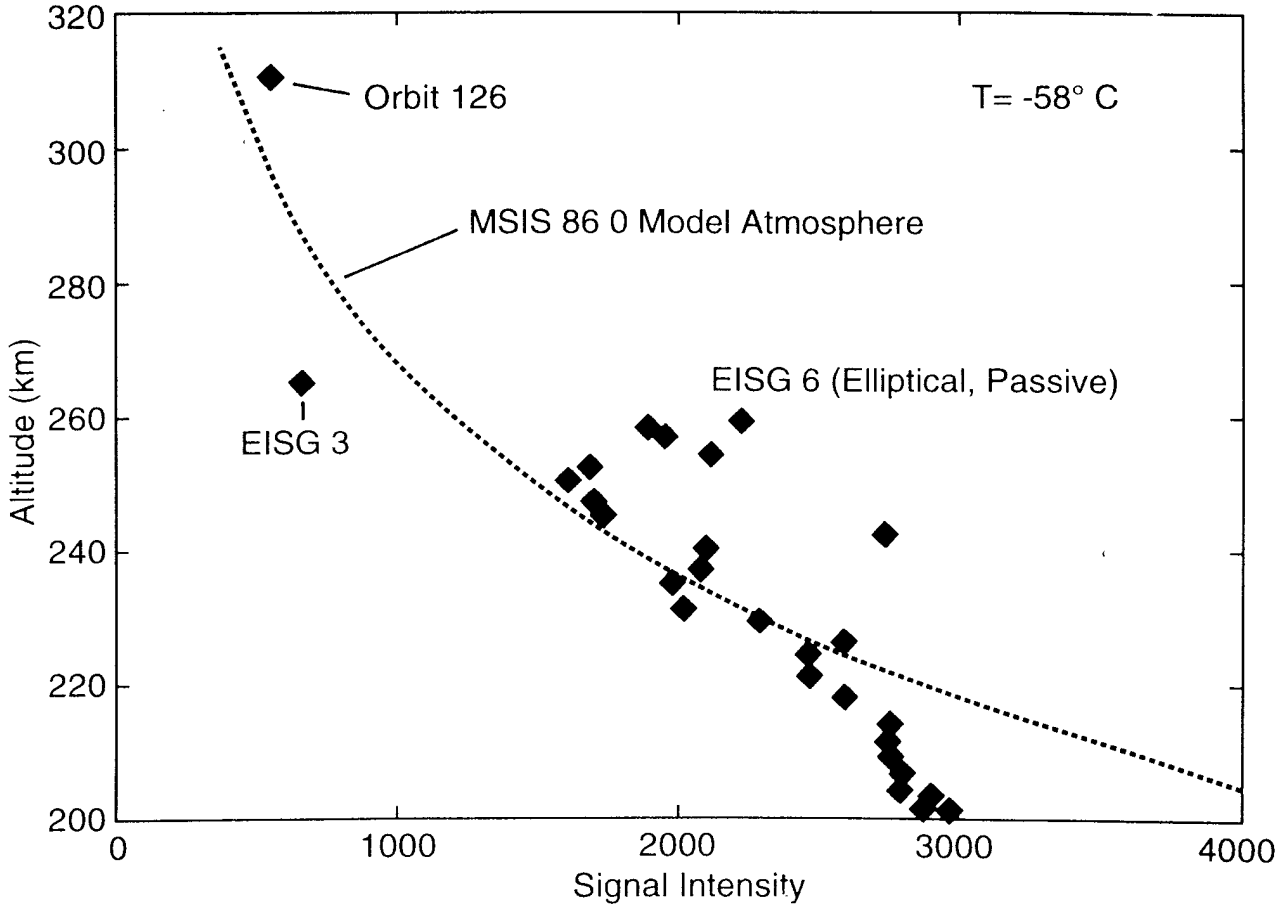

C-8190

PSI

Physical Sciences Inc.

Transition Flow on Space Shuttle-Diffuse Reflection (BIRD, 1990)

96-1056

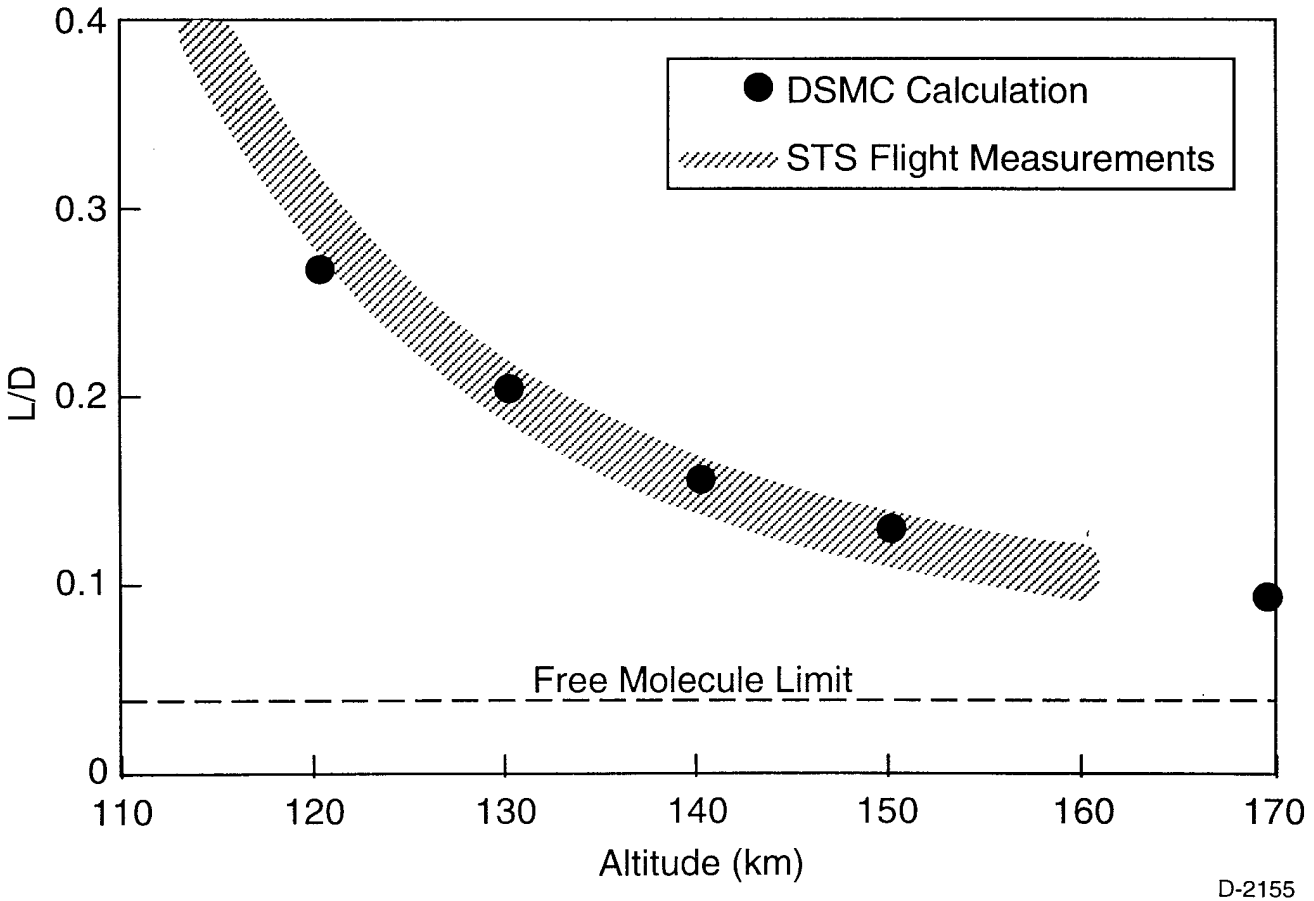

D-2155

- "Transistional regime effects persist to about 300 KM

PSI
PHYSICAL SCIENCES INC.

DSMC Calculations

96-1119

- Dogra + Moss (1991) also predict transition flow effects on shuttle above 200 kM

- EISG data may provide critical clue
  - — AE (and skipper) order of magnitude smaller than shuttle
  - — atmospheric density scale height (e.g. 10) is ~ 60 kM at these altitudes
  - — note surface behavior scales differently than flow behavior

- Estimate flow density buildup modeling critical to glow analysis = need DSMC

- Collaboration with Prof. Ian Boyd, Cornell U.

PSI

PHYSICAL SCIENCES INC.

DSMC Calculations

- One calculation can address several issues

- <u>NO</u> <u>Production</u> <u>Source</u>
  - — $\vec{O} + \vec{N}_2 \rightarrow \underline{NO} + \underline{N}$ gas phase
  - — ambient N (or above) adsorbs followed by
    $$N_S + O_S \rightarrow NO_S$$
  - — ambient NO adsorbs

- NO_2^* formation
  - — $\vec{O} + NO_S \rightarrow NO_2^*$
  - — $\vec{O} + NO_{2S} \rightarrow NO_2^* + O$

PSI

PHYSICAL SCIENCES INC.

DSMC Inputs

- $\vec{O} + \overleftarrow{N}_2 \rightarrow NO + O$
  - — O, N_2 scattered velocity: 1 to 2 km/s
  - — O, N_2 scattering distribution: isotropic
  - — reaction cross section:

V_{rel}, km/s	σ, $cm^2 \times 10^{18}$
8	2
9	4
10	6
11	15

  - — NO velocity, direction: $\vec{V}_{CM}$

- Ambient concentrations O, N, NO, O_2, N_2

- Vehicle dimensions (preliminary calculation for AE)

PSI

PHYSICAL SCIENCES INC.

DSMC Outputs

96-1122

- Surface flux and velocity distribution of O, N, NO
  - — versus altitude
  - — contrasted to free molecular

- These are inputs to a subsidiary surface model
  - — test various kinetic models
  - — adsorption, desorption, chemical reaction, surface coverage, etc.

- Preliminary results to be presented at 31st AIAA Thermophysics Conference

PSI

PHYSICAL SCIENCES INC.

CONCEPTUAL MICRO-VIEW OF ADSORBANT BEHAVIOUR RESULTING IN VISIBLE SHUTTLE GLOW

T-23425

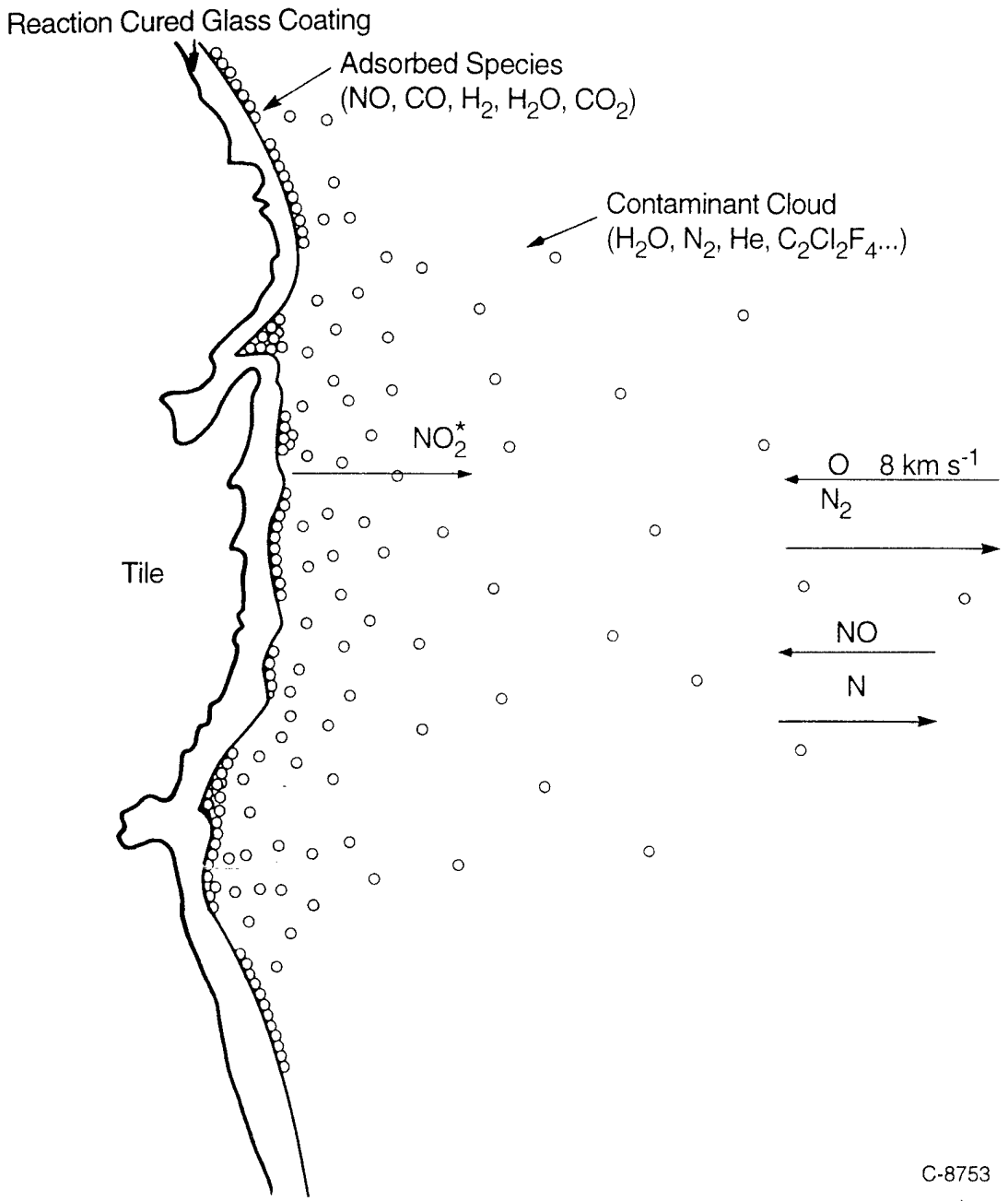

Glow Kinetic Modeling is Complex

96-1123

- e.g., surface kinetics for O + NO

Reaction Type	Process	Kinetic Quantity
Adsorption	$O(g) \longrightarrow O(S)$ $NO(g) \longrightarrow NO(S)$	Sticking coefficient
Thermal Desorption	$O(S) \longrightarrow O(g)$ $NO(S) \longrightarrow NO(g)$	Thermal desorption rate
Collisional desorption or reaction	$O(g) + O(S) \longrightarrow 2O(g)$ $\longrightarrow O_2(g)$ $X(g) + O(S) \longrightarrow X(g) + O(g)$ $O(g) + NO(S) \longrightarrow O(g) + NO(g)$ $\longrightarrow NO_2(g)$ $O(g) + NO_2(S) \rightarrow O(g) + NO_2(g)$ $NO(g) + O(S) \rightarrow NO(g) + O(g)$ $\rightarrow NO_2(g)$ $X(g) + NO(S) \longrightarrow X(g) + NO(g)$	Collisional desorption or reaction efficiency
Surface Reaction	$O(S) + NO(S) \longrightarrow NO_2(g), NO_2(S)$ $O(S) + O(S) \longrightarrow O_2(g), O_2(S)$	Reaction rate

*g ⇒ Gas Phase Species
*S ⇒ Surace Adsorbed Species

T-19970a

- Now add other mechanisms, N, NO_2, etc

PSI
PHYSICAL SCIENCES INC

Skipper Glow Predictions

96-1124

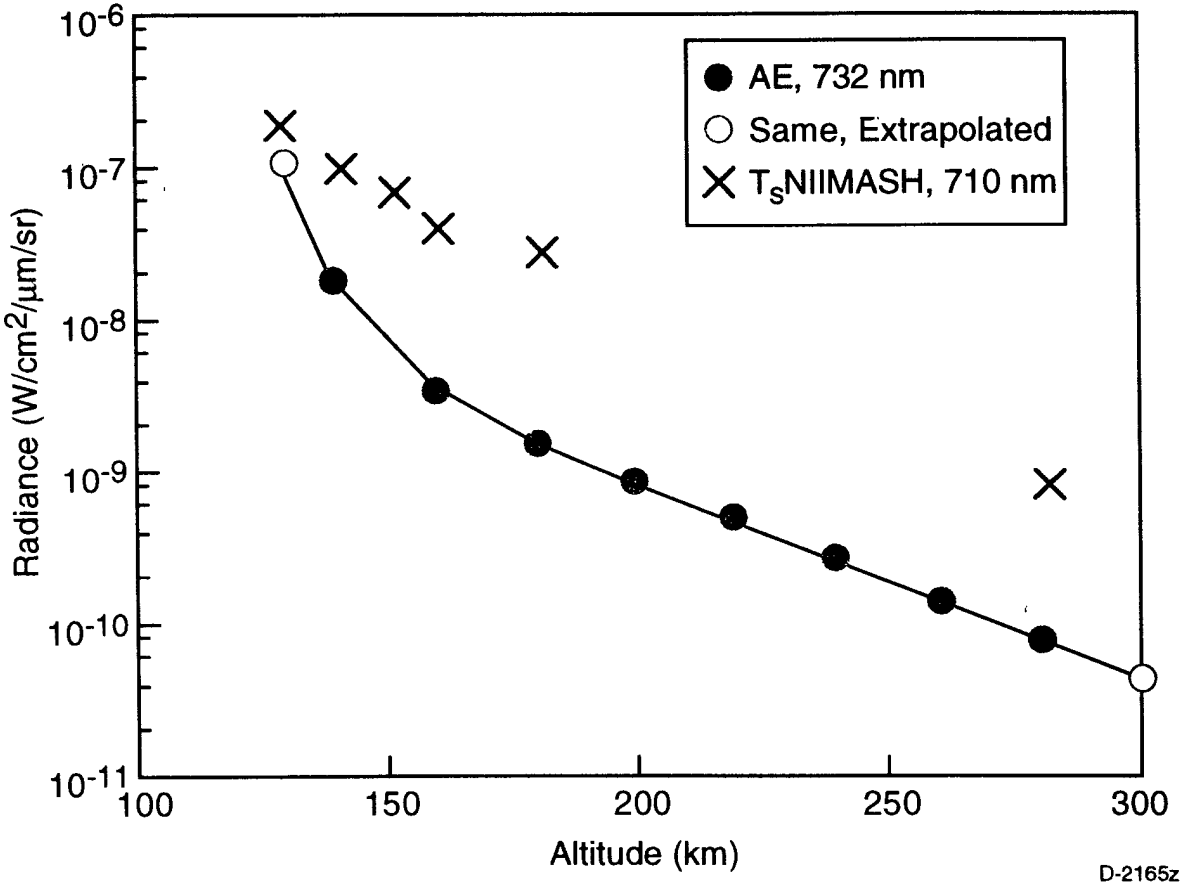

D-2165z

PSI

Physical Sciences Inc.

Glow Temperature Dependence

- Long understood that glow intensity varies inversely with surface temperature
  - assumed α $e^{\Delta E/kT}$
  - ΔE related to surface bond energy
- First estimate (Swenson et. al., 1986) based on disparate shuttle flight data, $\Delta E = 0.14$ eV
- Orient et. al., (1992) Laboratory study, $\Delta E = 0.11$ to 0.12 eV
  - postulated NO•NO bond
- EISG data shows lower ΔE

PSI
PHYSICAL SCIENCES INC.

Glow Data (Orient et. al., 1992)

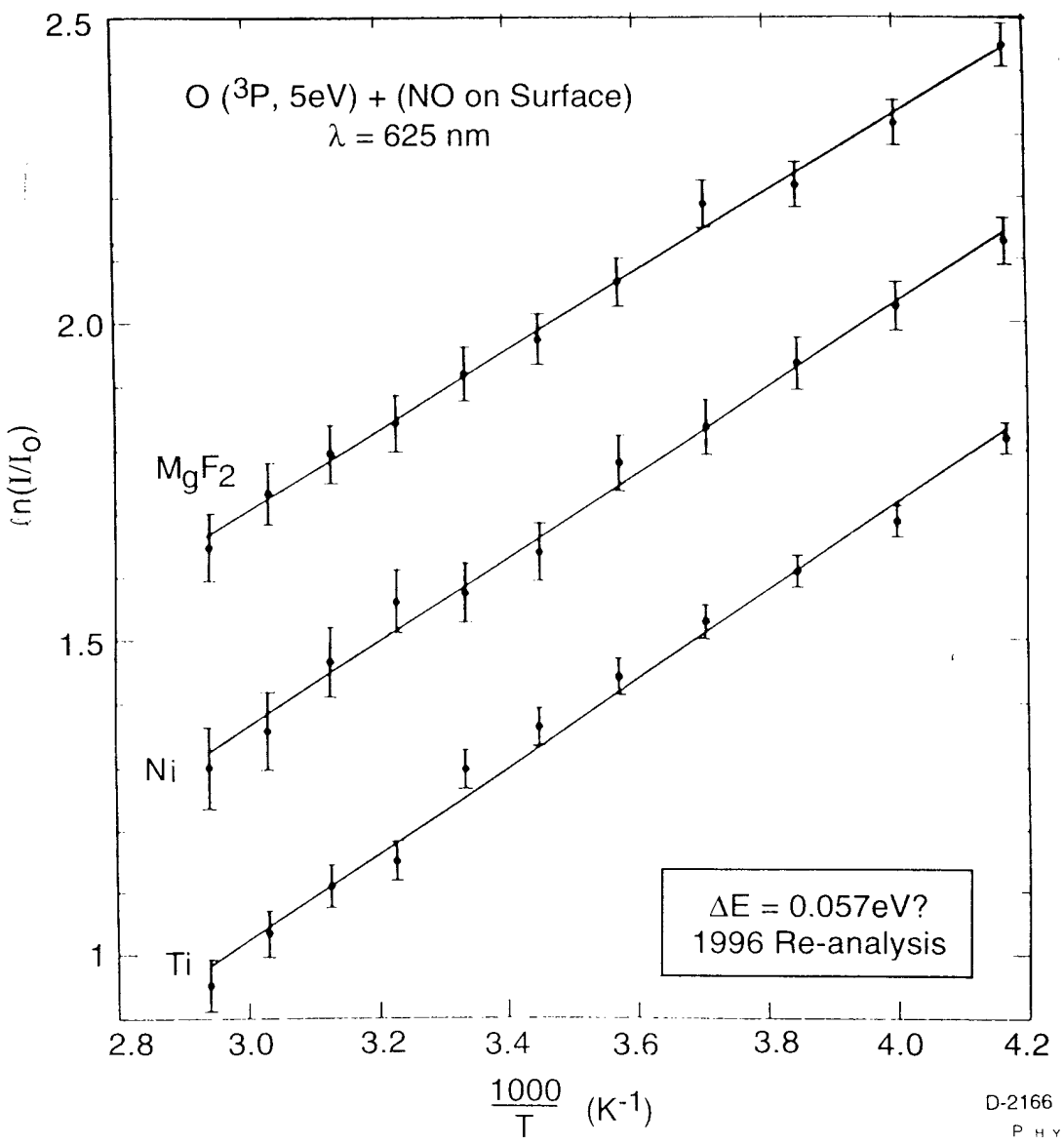

PSI
PHYSICAL SCIENCES INC.

PSI Glow Data vs Temperature (Oakes) (800 nm, aluminum substrate)

96-1147

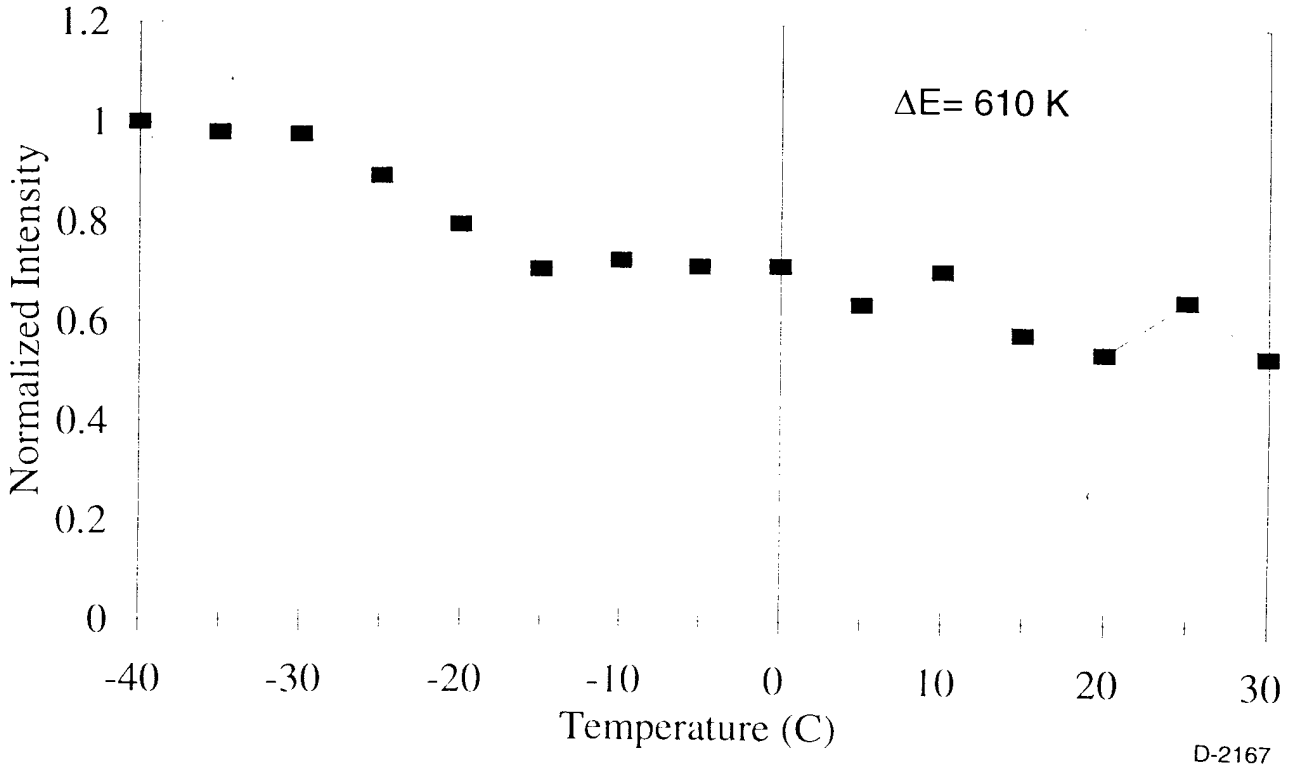

D-2167

PSI

Physical Sciences Inc.

Glow Temperature Dependence

- Most recent analysis of EISG data (Swenson and Rairden, 1996)

  $\Delta E = 0.08$ eV

- Lab data apparently ~ $\Delta E \approx 0.06$ eV

- Still some discrepancy but apparently weaker T dependence than previously thought